U.PORTO

FEUP FACULDADE DE ENGENHARIA
UNIVERSIDADE DO PORTO

Lab to pilot-scale photocatalytic treatment of antibiotics, antibiotic resistant bacteria and antibiotic resistance genes

Thesis submitted in partial fulfillment of the requirements for the degree of Doctor of Philosophy in Chemical and Biological Engineering, at the Faculty of Engineering, University of Porto

Francesco Biancullo

Supervisors:

Prof. Adrián Manuel Tavares da Silva

Prof. Joaquim Luís Bernardes Martins de Faria

Eng. Sérgio Manuel Castro-Silva

SRE CM

LABORATÓRIO ASSOCIADO
LABORATÓRIO DE PROCESSOS DE SEPARAÇÃO E REACÇÃO
LABORATÓRIO DE CATÁLISE E MATERIAIS

A Valentina

Abstract

Antibiotics are needed to fight serious infections. However, due to the human and veterinary abuse of the abovementioned pharmaceuticals, bacteria have developed high rates of antibiotic resistance (AR). Part of the antibiotics not metabolized by the body ends up in urban wastewater treatment plants (UWWTPs) at low concentrations, but exerting a role of stressor and favoring the development of AR. An additional concern is related to the reuse of treated urban wastewater (UWW) for agriculture purpose, making advanced tertiary treatment necessary to produce a good quality effluent.

Among the advanced treatment options of UWW, membrane processes are easily implemented by modular design. Ultrafiltration (UF) is a feasible separation process since it requires low pressure. Microbiological risk in the permeate is mitigated with UF, bacteria and other microorganisms being retained by the small pore size of the membranes (10-100 nm). However, effective antibiotic retention cannot be achieved by this physical separation, an adequate adsorption process (i.e. with activated carbon) or an oxidation process (i.e. O_3, Fenton, H_2O_2/UV, photocatalysis) being necessary. Moreover, biopolymers of effluent organic matter, especially colloidal biopolymers, play a main role as foulants in UWW tertiary treatment with UF. A compact solution combining filtration and oxidation in a single step is a possible solution, photocatalytic membrane reactors (PMRs) being an emerging technology in this field.

Slurry and immobilized catalysts are the most common configurations of PMR applications. The first configuration involves a step where a photocatalyst (usually TiO_2) in suspension is irradiated by UV light. After oxidation by the photocatalytic process (UV/TiO_2), UWW passes through a membrane separation step where the photocatalyst is removed and recirculated to the first step, while the filtrated wastewater (permeate) is released as effluent. The immobilized photocatalyst configuration involves a membrane supporting a fixed photocatalyst layer being irradiated by UV light. Despite the photocatalytic oxidation step is shorter than in the slurry configuration, immobilized PMRs are more feasible for a scale up.

The aim of this PhD project is to develop a PMR for tertiary treatment of urban wastewater (UWW), in an optic of safe water reuse. Particular attention is payed to the efficiency for the removal of antibiotics, antibiotic resistant bacteria and antibiotic resistance genes. Light-emitting diodes (LEDs) are chosen as alternative light source (instead of traditional lamps) in the photocatalytic process involving TiO_2-P25, while ceramic ultrafiltration (UF) membranes (100 nm pore size) are selected for the filtration process.

To achieve the main aim of this study, the first part of the experimental work assesses the efficiency of UVA-LEDs-driven slurry photocatalysis in disinfection and antibiotics removal from secondary UWW in lab scale batch experiments. Azithromycin, trimethoprim, ofloxacin and sulfamethoxazole are selected as antibiotic model pollutants. Different catalyst loads (TiO_2-P25) and UV light configurations (number of LEDs) are tested in secondary UWW spiked with antibiotics. The most efficient condition to degrade antibiotics in spiked UWW is selected to assess the removal of these antibiotics in real concentration and the inactivation of total heterotrophs, *Escherichia coli*, enterococci (including their antibiotic resistant counterpart). Considering the optimized condition, one hour treatment is enough to remove the selected antibiotics under the limit of quantification (LOQ) and to reduce 2-3 log the bacterial load of the selected microbial groups. To simulate a possible storage of treated wastewater before its reuse, the photocatalytic treated water is kept in dark for three days and bacterial regrowth is assessed. A high regrowth rate was observed for total heterotrophs, reaching the bacterial load of UWW before treatment. However, the antibiotic resistant percentage is always lower than the initial value found in raw UWW. Thus, the photocatalytic process is an attractive solution for the treatment of UWW, in particular for the degradation of antibiotics, but it is also concluded that a membrane is needed aiming a more effective disinfection of UWW.

In this context, a pilot PMR is designed and installed with UVA-LEDs and a TiO_2-P25 coated membrane to treat secondary UWW, the concentrate being recirculated in the system. The production of the permeate during UF of UWW is affected by fouling, the original permeance decreasing ca. 98% after 4 h of treatment. Physical cleaning (backwash and backpulse) is not enough to restore the initial permeance of the membrane, a chemical cleaning step with H_2O_2 being necessary. The disinfection performance of the raw ceramic UF membrane is evaluated using microbiological and molecular biology analysis. Total heterotrophs and total coliforms are not found (<LOQ) in the permeate. Molecular biology analysis reveals the presence of 16S rRNA and *intI1*; however, both the genes are close to LOQ. Part of the permeate is stored for one week in dark and potential risk of bacterial regrowth is examined after 7 days. The cultivable method shows no bacterial load in the stored permeate, whereas *intI1* decreases to a value below LOQ and 16S rRNA stabilizes at the value found immediately after filtration.

The same pilot PMR is investigated to treat secondary UWW spiked with ofloxacin, ciprofloxacin and enrofloxacin. The experiments are performed using the raw membrane without light (UF) or with light (UF+UVA), and the TiO_2 coated membrane without light (TiO_2-UF) or with light (TiO_2-UF+UVA). Considering a mass balance of the system, the following removal efficiency is found for all the three antibiotics: UF < UF+UVA < TiO_2-UF < TiO_2-UF+UVA. The removal efficiency obtained after treatment in the PMR ranged from 34% (for ofloxacin) to

62% (for enrofloxacin). Equipment and operating costs of the process are estimated. Moreover, an evaluation of scale up investment to treat 100 m^3 day^{-1} is also performed. However, further optimization of the process is needed (i.e. coating methodologies for immobilization of the photocatalyst on the membrane and photocatalytic contact time) before large scale implementation of this PMR technology.

Resumo

Antibióticos são necessários para combater infeções graves. No entanto, devido ao seu uso excessivo, quer para consumo humano quer veterinário, as bactérias desenvolveram elevadas taxas de resistência a antibióticos. Parte dos antibióticos não metabolizados pelo organismo acaba em estações de tratamento de águas residuais (ETARs). Embora sendo detetados em baixas concentrações, estes compostos favorecem o desenvolvimento de resistência a antibióticos, podendo comprometer a possível reutilização destas águas para fins agrícolas, e tornando cada vez mais necessário um tratamento adequado, como por exemplo, um tratamento terciário avançado.

Entre as diversas opções de tratamentos avançados, os processos de membrana têm sido facilmente implementados devido ao seu desenho modular. A ultrafiltração é um processo de separação viável, uma vez que requer baixa pressão. O risco microbiológico no permeado é mitigado, sendo as bactérias e outros microrganismos retidos pelo tamanho reduzido dos poros das membranas (10-100 nm). Contudo, a retenção eficaz de antibióticos não é possível por esta separação física, sendo necessário um processo de adsorção adequado (i.e., carvão ativado) ou um processo de oxidação (i.e., O_3, processo de Fenton, H_2O_2/UV, fotocatálise). Além disso, biopolímeros de matéria orgânica presentes no efluente, especialmente biopolímeros coloidais, podem levar à incrustação da membrana quando os processos de filtração são aplicados no tratamento terciário de efluentes de águas residuais urbanas. Um módulo compacto combinando filtração e oxidação em uma única etapa é uma possível solução, sendo os reatores de membrana fotocatalítica (PMRs - *photocatalytic membrane reactors*) uma tecnologia emergente. Catalisadores em suspensão e imobilizados são as configurações mais comuns nas aplicações de PMRs. A primeira configuração envolve uma etapa em que um fotocatalisador (geralmente TiO_2) em suspensão é irradiado por radiação UV. Após a o processo fotocatalítico (UV/TiO_2), o efluente passa por uma etapa de separação por membrana onde o fotocatalisador é removido e recirculado para o primeiro passo, e um filtrado (permeado) é gerado. A outra configuração, na qual o fotocatalisador é imobilizado, envolve uma membrana que suporta uma camada de catalisador sendo esta irradiada por radiação UV. Apesar do passo de oxidação ser mais curto do que na configuração em que o catalisador é utilizado em suspensão, os PMRs utilizando fotocatalisadores imobilizados são mais viáveis para um aumento de escala.

O principal objetivo deste projeto de doutoramento consiste no desenvolvimento de um PMR para o tratamento terciário de águas residuais urbanas, que no futuro consiga produzir um efluente com qualidade suficiente para reutilização em diversos fins. É dada especial atenção à eficiência na remoção de antibióticos, bactérias resistentes a antibióticos e genes associados. Para

este efeito, diodos emissores de luz (LEDs) foram escolhidos como fonte de radiação alternativa no processo fotocatalítico envolvendo TiO_2-P25 (em vez de lâmpadas convencionais), enquanto membranas de ultrafiltração (100 nm de tamanho de poro) foram selecionadas para o processo de filtração.

De forma a dar resposta ao objetivo principal deste estudo, a primeira parte do trabalho experimental consistiu em avaliar a eficiência do processo utilizando o fotocatalisador em suspensão e LEDs (UVA) à escala laboratorial, nomeadamente para desinfeção e remoção de antibióticos de águas residuais urbanas. Azitromicina, trimetoprim, ofloxacina e sulfametoxazol foram selecionados como poluentes modelo adicionados a efluentes secundários de ETARs. Diferentes concentrações de catalisador (TiO_2-P25) e número de LEDs foram alvo de estudo. As condições ótimas obtidas foram posteriormente testadas na degradação desses mesmos antibióticos em concentrações reais e na inativação de heterotróficos totais, *Escherichia coli* e enterococci (incluindo resistência a antibióticos). Nestas condições, após 60 min de tratamento, foi possível remover os antibióticos testados para valores inferiores ao limite de quantificação e obter uma redução de aproximadamente 2-3 log da carga microbiológica. De forma a simular um possível armazenamento da água residual tratada antes da sua reutilização, a água tratada pelo processo fotocatalítico foi mantida no escuro durante três dias e o recrescimento bacteriano foi avaliado, verificando-se reativação para os heterotróficos totais para valores próximos dos presentes na água residual antes do tratamento. No entanto, a percentagem de resistência a antibióticos diminui em todos os casos. Assim, o processo fotocatalítico é uma solução atrativa para o tratamento de águas residuais urbanas, em particular para a degradação de antibióticos. Contudo, a filtração por membrana é realmente necessária de forma a obter-se uma desinfeção eficaz.

Neste contexto um PMR à escala piloto, implementando UVA-LEDs e uma membrana revestida com TiO_2-P25, foi desenhado e instalado para o tratamento de águas residuais urbanas, sendo o concentrado recirculado no sistema. A produção do permeado durante o processo de ultrafiltração de águas residuais urbanas é afetada pela incrustação na membrana, ocorrendo uma diminuição acentuada da permeabilidade (aproximadamente 98% após 4 h de tratamento). A limpeza por processos físicos (*backwash* e *backpulse*) não foi suficiente para restaurar a permeabilidade inicial da membrana, sendo necessária uma limpeza química com H_2O_2. O desempenho da membrana cerâmica de ultrafiltração sem catalisador foi avaliada utilizando análises microbiológicas e de biologia molecular. Heterotróficos totais e coliformes totais não foram encontrados (<LQ) no permeado. Através de análises de biologia molecular foi possível verificar a presença de 16S rRNA e *intI1*; no entanto, apresentando valores próximos do LQ. Parte do permeado foi armazenado durante uma semana no escuro e o potencial recrescimento bacteriano

foi estudado após 7 dias. A carga bacteriana cultivável no permeado armazenado manteve-se constante, enquanto que o gene *intI*1 diminuiu para um valor inferior ao LQ e o gene 16S rRNA mantendo um valor próximo ao verificado imediatamente após a filtração.

Uma água residual urbana foi posteriormente contaminada com ofloxacina, ciprofloxacina e enrofloxacina e foram realizadas experiências usando a membrana sem catalisador e sem luz (UF) ou com luz (UF+UVA), e a membrana revestida com TiO_2 sem luz (TiO_2-UF) ou com luz (TiO_2-UF + UVA). Considerando um balanço de massa ao sistema, a eficiência de remoção para os três antibióticos foi a seguinte: UF < UF + UVA < TiO_2-UF < TiO_2-UF + UF. A eficiência de remoção obtida após o tratamento no PMR variou entre 34% (para ofloxacina) e 62% (para enrofloxacina). Os custos de implementação e manutenção foram estimados. Adicionalmente, foi realizada uma avaliação do investimento necessário para o tratamento de 100 m^3 dia^{-1} de águas residuais urbanas. No entanto, o processo deverá ser otimizado (i.e., métodos de imobilização do fotocatalisador na membrana e tempo de contacto no processo fotocatalítico) de forma a ser viável a implementação desta tecnologia à escala real.

Sommario

Gli antibiotici sono necessari per combattere gravi infezioni. Tuttavia, a causa dell'abuso umano e veterinario dei suddetti farmaci, i batteri hanno sviluppato alti tassi di resistenza agli antibiotici. Una parte degli antibiotici non metabolizzati dall'organismo finisce negli impianti di trattamento delle acque reflue urbane in basse concentrazioni, ma esercita un fattore di stress e favorisce lo sviluppo della resistenza antibiotica. Un'ulteriore preoccupazione riguarda il riutilizzo delle acque reflue urbane trattate a fini agricoli, rendendo necessario un trattamento terziario avanzato per produrre un effluente di buona qualità.

Tra le opzioni di trattamenti avanzati della acque reflue urbane, i processi a membrana sono facilmente implementabili mediante l'utilizzo di più moduli. L'ultrafiltrazione è un processo di separazione relativamente economico poiché richiede una bassa pressione di esercizio. Il rischio microbiologico nel permeato è mitigato, poiché i batteri e altri microrganismi vengono trattenuti dalla membrane con pori di piccole dimensioni (10-100 nm). Tuttavia, non è possibile ottenere un'efficace ritenzione degli antibiotici mediante questa separazione fisica, rendendo necessario un adeguato processo di adsorbimento (es. con carbone attivo) o un processo di ossidazione (es. O_3, Fenton, H_2O_2/UV, fotocatalisi). Inoltre, la sostanza organica contenuta nell'effluente, in particolare i biopolimeri colloidali, svolge un ruolo principale nel fouling delle membrane utilizzate nel trattamento terziario di ultrafiltrazione delle acque reflue urbane. Una soluzione tecnologica compatta che combina filtrazione e ossidazione in un'unica fase è rappresentata dai reattori a membrana fotocatalitica. Le configurazioni a catalizzatore in sospensione o immobilizzato rappresentano le più comuni applicazioni dei reattori a membrana fotocatalitica. La prima configurazione prevede una prima fase in cui un fotocatalizzatore (solitamente TiO_2) in sospensione viene irradiato dalla luce UV. Dopo l'ossidazione mediante il processo fotocatalitico (UV/TiO_2), l'acqua reflua passa attraverso una fase di separazione del fotocatalizzatore tramite membrana e conseguente ricircolo nella prima fase di processo, mentre l'acqua filtrata (permeato) viene rilasciata come effluente. La configurazione di fotocatalizzatore immobilizzato invece coinvolge una membrana che supporta uno strato di fotocatalizzatore che viene irradiato dalla luce UV. Nonostante la fase di ossidazione fotocatalitica sia più corta rispetto alla configurazione in sospensione, i reattori a membrana fotocatalitica a configurazione immobilizzata sono più fattibili per l'implementazione a larga scala.

Lo scopo di questo progetto di dottorato è quello di sviluppare un reattore a membrana fotocatalitica per il trattamento terziario delle acque reflue urbane, in un'ottica di riutilizzo dell'acqua trattata. Particolare attenzione è rivolta all'efficacia di rimozione di antibiotici, batteri resistenti agli antibiotici e geni di resistenza antibiotica. I diodi a emissione luminosa (LED) sono

scelti come fonte di luce alternativa (anziché lampade tradizionali) nel processo fotocatalitico che coinvolge TiO_2-P25, mentre le membrane ceramiche di ultrafiltrazione (dimensione dei pori pari a 100 nm) sono selezionate per il processo di filtrazione.

Per raggiungere l'obiettivo principale di questo studio, la prima parte del lavoro sperimentale valuta l'efficienza della fotocatalisi nella disinfezione e la rimozione degli antibiotici da acque reflue secondarie attraverso esperimenti a scala di laboratorio. Azitromicina, trimetoprim, ofloxacina e sulfametossazolo sono selezionati come inquinanti modello di antibiotici e aggiunti nell'acqua reflua urbana. Diverse concentrazioni di catalizzatore (TiO_2-P25) e configurazioni della luce UV (numero di LED) sono testate su acque reflue urbane contaminate da antibiotici. La condizione più efficiente per degradare gli antibiotici in acque reflue contaminate è selezionata per valutare la rimozione di questi antibiotici in concentrazioni reali e per misurare l'inattivazione di eterotrofi totali, *Escherichia coli* ed enterococchi (compresa la loro parte resistente agli antibiotici) nelle acque. Considerando la condizione ottimizzata, un trattamento di un'ora è sufficiente per rimuovere gli antibiotici selezionati al di sotto del limite di quantificazione (LOQ) e per ridurre 2-3 log la carica batterica dei gruppi batterici selezionati. Per simulare un possibile stoccaggio delle acque reflue trattate prima del loro riutilizzo, l'acqua trattata è stata tenuta al buio per tre giorni ed è stata valutata la ricrescita batterica. Gli eterotrofi totali mostrano un alto tasso di ricrescita, raggiungendo il carico batterico dell'acqua reflua prima del trattamento. Tuttavia, la percentuale resistente agli antibiotici è sempre inferiore al valore iniziale trovato nell'acqua reflua secondaria. Pertanto, il processo di fotocatalisi è una soluzione interessante per il trattamento di acque reflue urbane, in particolare per la degradazione degli antibiotici, tuttavia si conclude che è necessario un processo a membrana per una disinfezione più efficace dell'acqua reflua.

In questo contesto, un reattore a membrana fotocatalitica pilota è stato progettato e i LED assieme ad una membrana rivestita di TiO_2-P25 sono stati installati ed utilizzati per il trattamento dell'acqua reflua secondaria. Il concentrato è ricircolato nel sistema. La produzione del permeato durante l'ultrafiltrazione dell'acqua reflua urbana è influenzata da fouling, la permeanza originale diminuisce del 98% dopo 4 ore di processo. La pulizia fisica (controlavaggio e contro-aerazione) non è sufficiente per ripristinare la permeabilità iniziale della membrana, essendo necessaria una pulizia chimica con H_2O_2. Le prestazioni di disinfezione della membrana ceramica ad ultrafiltrazione sono valutate utilizzando analisi microbiologiche e la biologia molecolare. Eterotrofi totali e coliformi totali non sono trovati (<limite di quantificazione) nel permeato. L'analisi di biologia molecolare rivela la presenza di 16S rRNA e *intI1*; comunque, entrambi i geni sono vicini al limite di quantificazione. Una parte del permeato è stoccato per una settimana al buio e il potenziale rischio di ricrescita batterica è esaminato dopo 7 giorni. Il metodo dei

coltivabili non mostra carica batterica nel permeato stoccato. Il gene *intI1* diminuisce fino a un valore inferiore al limite di quantificazione mentre 16S rRNA si stabilizza al valore trovato immediatamente dopo la filtrazione.

L'acqua reflua secondaria viene quindi contaminata da ofloxacina, ciprofloxacina ed enrofloxacina e gli esperimenti vengono eseguiti utilizzando la membrana grezza senza (UF) o con luce (UF+UVA) e la membrana rivestita di TiO_2 senza (TiO_2-UF) o con luce (TiO_2-UF+UVA). Considerando un bilancio di massa del sistema, è stata trovata la seguente efficienza di rimozione per tutti e tre gli antibiotici: UF < UF+UVA < TiO_2-UF < TiO_2-UF+UVA. L'efficienza di rimozione ottenuta dopo il trattamento con il reattore a membrane fotocatalitica varia dal 34% (per l'ofloxacina) al 62% (per l'enrofloxacina). I costi fissi e i costi operativi del processo sono stati stimati. Inoltre, è eseguita anche una valutazione dell'investimento su scala reale per trattare 100 m^3 $giorno^{-1}$ di acqua reflua. Un'ulteriore ottimizzazione del processo (considerando nuove metodologie di immobilizzazione e l'aumento del tempo di contatto fotocatalitico) è necessaria prima dell'implementazione su larga scala della tecnologia delle membrane fotocatalitiche.

Acknowledgements

A special thank to my supervisor prof. Adrián Silva for his strong commitment and precious teachings during all the PhD course.

Thank to my co-supervisor eng. Sérgio Silva, for his technical teachings during the period spent at Adventech and for the fundamental contribution to develop the pilot equipment used for the scientific investigation.

Thank to my co-supervisor prof. Joaquim Faria for his contribution in the scientific discussion and his pearls of wisdom.

Thank to the director of the LCM prof. José Figueredo for giving the access to all the equipments of the laboratories and for his phenomenal Italian speeches.

Thank to prof. Olga Nunes (LEPABE) and prof. Célia Manaia (Universidade Católica Portuguesa), for their advice and contribution regarding microbiological and molecular biology work. Thank to prof. Luigi Rizzo (Università degli Studi di Salerno) for his availability and for supplying materials during my investigation period in Italy.

Thank to dr. Rita Ribeiro for the liquid chromatography analysis, for her scientific explanations and clarifications during the experimental work and the discussion of the results. Thank to my laboratory colleagues Nuno Moreira, dr. Cátia Graça, Ana Gorito, Mariana Miranda, Marta Barbosa, João Sousa, André Torres and all the other members of LCM for their help in the experimental work. Thank to Joana Silva from Universidade Católica Portuguesa for the molecular biology analysis. Thank to my colleagues of Adventech dr. Anabela Nogueira, dr. Nuno Amaral, João Almeida and Inês Inocêncio and the chief eng. Paulo Nunes for their support.

I acknowledge European Union's Horizon 2020 research and innovation programme (Marie Skłodowska-Curie grant agreement No 675530) and Projects NORTE-01-0247-FEDER-033330 (DEPCAT) funded by ERDF/FEDER through NORTE 2020 (Norte Portugal Regional Operational Programme). This work was financially supported by: Associate Laboratory LSRE-LCM - UID/EQU/50020/2019 - funded by national funds through FCT/MCTES (PIDDAC).

Finally, I warmly thank to Antonio, Antonietta, Diletta and Valentina (my special family).

List of Contents

List of Figures

List of Tables

List of abbreviations and symbols

$^{3}EfOM^{*}$	Triplet state exited effluent organic matter
A&ARB&ARBs	Antibiotics, antibiotic resistant bacteria and antibiotic resistance genes
ANOVA	Analysis of variance
AOPs	Advanced oxidation processes
AR	Antibiotic resistance
ARB	Antibiotic resistant bacteria
ARGs	Antibiotic resistance genes
AZT	Azithromycin
BOD	Biological oxygen demand
CAPEX	Capital expenditure
CAS	Conventional actived sludge
C_{cat}	Catalist load
C_{conc}	Concentration in the concentrate
CE	Collision energy
CECs	Contaminants of emerging concerns
C_{feed}	Concentration in the feed
CFUs	Colonies forming units
CFV	Cross flow velocity
CIP	Ciprofloxacin
CLI	Clindamycin
$CO_3^{\bullet-}$	Carbonate radical
COD	Chemical oxygen demand
CPCs	Compound parabolic collectors
C_{perm}	Concentration in the permeate
CXP	Collision cell exit potential
DOC	Dissolved organic carbon
DOM	Dissolved organic matter
DP	Declustering potential
DW	Distilled water
E	Emitted radiant energy
EfOM	Effluent organic matter
ENR	Enrofloxacin
EQS	Environmental quality standards
EU	European Union

E_λ	Emitted radiant energy at given wavelength
FQ	Fluoroquinolone
GO-TiO_2	Graphene oxide doped titanium dioxide
H_2O_2	Hydrogen peroxide
HLB	Hydrophilic-Lipophilic Balanced
$HO^{\bullet}$	Hydroxyl radical
HPLC	High performance liquid chromatography
I_a	Average value of irradiance
IDL	Instrument detection limit
IQL	Instrument quantification limit
I_λ	Spectral intensity of radiation at λ wavelength
k	Pseudo first order reaction rate constant
LBA	Luria Bertani agar
LC	Liquid chromatography
LEDs	Light-emitting diodes
LOD	Limit of detection
LOQ	Limit of quantification
MBR	Membrane bioreactor
MDL	Method detection limit
MeOH	Methanol
m-Ent	m-Enterococcus
m-FC	Fecal coliform agar
MIC	Minimum inhibition concentration
MS	Mass spectrometry
MS/MS	Tandem mass spectrometry
MWCO	Molecular weight cut-off
NI	Negative ionization mode
$O_2^{\bullet-}$	Superoxide radical
O_3	Ozonation
OFL	Ofloxacin
OPEX	Operational expenditure
PAC	Powder activated carbon
PI	Positive ionization mode
PMR	Photocatalytic membrane reactor
PVDF	Polyvinylidene fluoride
qPCR	Quantitative polimerase chain reaction

RO	Reverse osmosis
S&B	Slanetz and Bartley agar
SMX	Sulfamethoxazole
SPE	Solid phase extraction
SUVA	Specific ultraviolet absorbance
TBX	Tryptone bile X-glucuronide agar
TiO_2-P25	Degussa P25 titanium dioxide
TMP	Trimethoprim
TMPR	Transmembrane pressure
TOC	Total organic carbon
TSA	Tryptic soy agar
UF	Ultrafiltration
UHPLC	Ultra-high-performance liquid chromatography
UWW	Urban wastewater
UWWTPs	Urban wastewater treatment plants
β	Specific extinction coefficient
β_λ	Specific extinction coefficient at given wavelength
δ	Thickness of wastewater being irradiated
τ	Optical thickness

Chapter 1. State of the art and thesis outline

This chapter introduces the main topic of the thesis, starting with the problem of water scarcity and the importance to preserve water resources through mitigation actions (such as water reuse). The increasing threat of antibiotic resistance in the aquatic environment is discussed. In particular, the part about the different methods to analyse antibiotic resistance (Section 1.2) is based on the scientific publication that I co-authored: "Antibiotic resistance in wastewater treatment plants: Tackling the black box", Environmental International: 115 (2018) 312–324. Advantages and disadvantages of conventional tertiary treatment and advanced oxidation processes to mitigate the antibiotics pollution and antibiotic resistance risk in urban wastewater is discussed. Particular emphasis is given to the photocatalysis process and photocatalytic membrane reactors. Fundamental and engineering aspects of the abovementioned technologies are presented as the starting point to develop a pilot-scale reactor dealing with advanced treatment of urban wastewater for a safe reuse.

1.1 Water scarcity and water reuse

Water scarcity is one of the main problems that modern human society needs to deal with. Physical water scarcity affects around 1.2 billion people, while 1.6 billion people face economic water shortage. Water scarcity is defined as annual water supply below 1,000 m^3 per person. Moreover, the more human population increases, the higher is the per capita water use. In addition to water scarcity, quality deterioration affects the water resources too. The Strategic Implementation Plan of the European Innovation Partnership on Water considers water reuse as an integrated water management approach to protect the environment (reducing surface/groundwater abstraction) and reduce the cost related to the water supplying (i.e. drinking water treatment or desalination) (EIPW 2012). Urban, recreational, agricultural and industrial uses of treated wastewater are possible water reuse applications. Trends of treated wastewater reuse in agriculture are in escalation either in developed either in developing countries, Cyprus and Israel being the more prominent Mediterranean users of treated UWW in agriculture. However, food contamination by pathogens and accumulation of contaminants of emerging concerns (CECs) and heavy metals in soil, represents a substantial risk to face with. Uptake contaminants by plants and crops hurt the food chain, and it is presently considered as a sever public health problem (Christou et al. 2017a).

So far, national regulations/guidelines are based on conventional parameters (chemical and microbiological) (WHO 2006; California code 2000). Traditional wastewater treatment processes are not able to remove CECs (pharmaceutical, personal care products, among others) and advanced treatment technologies are needed to reach a safe level of water quality before its reuse. Prediction models (empiric and mechanistic) and experimental tests (in vitro and greenhouse) on uptake and metabolism of crops and plants represent the basis for a risk assessment and advance in wastewater reuse regulation (Christou et al. 2017b).

1.2 Antibiotics and antibiotic resistance: Quality standards and detection method

New chemicals recently manufactured soon reach the aquatic environment, and their occurrence (at low concentrations) can be quantified with modern mass spectrometry analytical methods. CECs are a heterogeneous group of chemical compounds with adverse effects on environmental ecosystems. Depending on their properties and structure, CECs can be classified into several categories. Pharmaceuticals (including antibiotics), flame retardants, parabens, bisphenol A, phthalates, personal care products, hormones, illicit drugs, ionic liquids, nanomaterials, disinfection by-products, algal toxins, biocides, pesticide are only some categories of CECs usually found in industrial, hospital and urban wastewater (UWW). No legislation (except the Swiss regulation) exists about the presence of CECs in UWW (Giannakis et al. 2015). The fate

and effects of CECs on environmental water compartments is still under investigation, and further concern is aroused by the possible adverse effect of transformation products (difficult to detect) on the aquatic ecosystem (Richardson and Ternes 2017).

European Commission (EU) since 2000 has focused the attention on this issue, i.e. concerns related with CECs. The first document published to define priority substances harming aquatic ecosystems was the Directive 2000/60/EC. Although no discharge limits were set for most of CECs, EU established in 2008 the Environmental Quality Standards (EQS) by Directive 2008/105/EC. EQS were expressed for each priority substance in terms of annual average value and maximum allowable concentrations, providing protection against long-term and short-term exposure, respectively. Each standard is based on acute and chronic toxicity tests performed on aquatic organisms, also considering accumulation in the ecosystem. The most recent Directive 2013/39/EU identified new priority substances and amended most of the EQS, fixing a deadline for the submission of EQS related to new priority substances (Ribeiro et al. 2015b).

Nowadays, investigation of CECs and TPs in environmental samples involves liquid chromatography (LC) coupled to mass spectrometry (MS). Ultra-High-Performance LC is a very selective and sensitive separation technique involving column filled with packing particles (< 2 μm diameter) at high pressure (until 500 bar). It allows separation of CECs, characterized by a wide range of volatility and polarity, from complex matrices such as UWW. Triple quadrupole in tandem mass spectrometry (MS/MS) is a widely used quantification technique employing multiple reaction monitoring modes. It involves an electrospray ionization source, two mass/charge (m/z) analyzers in series (divided by cell collision) and a detector (electron multiplier). MS/MS analysis is based on the assessment of retention time and m/z values of the parent compound and fragments, the intensity of the signal being directly proportional to the concentration of the target compound.

Antibiotics are frequently found at concentrations ranging from a few ng L^{-1} to μg L^{-1} in many aquatic compartments, namely wastewater influents and effluents, surface water, groundwater and even in drinking water (Barbosa et al. 2016; Carvalho and Santos 2016; Sousa et al. 2018). The use of this class of pharmaceuticals in human and veterinary medicine has triggered the introduction and accumulation of such compounds in the aquatic environment (Verlicchi et al. 2012). Given the potential adverse effects of these contaminants, the European Decisions 2015/495/EU and 2018/840/EU included azithromycin and other antibiotics in the Watch List of environmental concern, which should be monitored in surface waters (Directive 2015, 2018).

Urban wastewater treatment plants (UWWTPs) are considered gateways of antibiotics into the aquatic environment and hot-spots for antibiotic resistance proliferation (Rizzo et al. 2013b;

Karkman et al. 2018; Manaia et al. 2018). The presence of antibiotics, antibiotic resistant bacteria and antibiotic resistant genes (A&ARB&ARGs) in the environment, in particular throughout the urban water cycle and food chain, is considered a severe public health issue. Despite specific physicochemical conditions (i.e. BOD, total N and total P) may affect survival and overgrowth of specific bacterial groups in UWW, antibiotics and heavy metals at low concentration act as stressors on all the bacterial community, promoting the horizontal gene transfer. Moreover, during biomass recirculation, the proliferation of ARB&ARGs is promoted. In this regard, new approaches to reduce A&ARB&ARGs in water and to avoid the negative impacts on the downstream environment are necessary, in particular when the objective is to achieve excellent quality standards for possible reuse of UWW (Ferro et al. 2015; Christou et al. 2017a, 2017b).

Methods to analyse antibiotic resistance in the environment are classified in culture dependent and culture independent. The first method permits to enumerate viable cells (including clinically relevant species); however, only a certain fraction of the bacterial community is cultivable. Moreover, it allows the determination of the minimal inhibitory concentration of antibiotic and the assessment of horizontal gene transfer. The procedures for the analysis are standardised and follow specific guidelines (epidemiological cut-off values). Culture independent methods are based on the analysis of the DNA present in the sample. Quantitative PCR (qPCR) allows to quantifying a specific gene, while metagenomics provides an overview of the bacterial community. Humic acids and dissolved organic matter present in UWW affect the precision of genes quantification in qPCR. Both techniques are expensive (equipment and reagents) and require specific expertise (i.e. bioinformatics).

1.3 Conventional tertiary treatment and AOPs

Conventional UWWTPs are not designed to remove CECs efficiently, whereas standard tertiary treatments as chlorination and UV irradiation have been implemented to disinfect UWW.

Chlorination is a tertiary treatment system involving hypochlorous acid (HClO) or chlorine dioxide (ClO_2) to disinfect UWW. Gas chlorine, sodium and calcium hypochlorite are the main chemicals used in the water to form HClO, while ClO_2 (gas) is usually generated in situ. Not all the HClO and ClO_2 is available to kill microorganisms, the organic matter reacting with the available disinfectant. The main disadvantage of chlorination is the formation of carcinogens disinfection by-products as trihalomethanes (using HClO) or chlorites and chlorates (using ClO_2). HClO and ammonia form chloramines, a less aggressive and more UV-stable disinfectant and with less tendency to form trihalomethanes. Free residual chlorine is the quantity of HClO and hypochlorous ion present in the water and a concentration of 0.2 mg L^{-1} is a technical standard for many countries. Contact tanks with piston flow are a widely used solution guarantying a

specific reaction contact time to inactivate the majority of bacteria. However, chlorination is low effective in controlling antibiotic resistance bacteria regrowth concerning to other non-conventional disinfection processes as H_2O_2/UV (Fiorentino et al. 2015). Moreover, a full-scale study showed an increase in ARGs abundance of secondary UWW after the chlorination process (Liu et al. 2018).

UV irradiation is widely implemented as part of the tertiary treatment (usually after microfiltration) in UWWTPs (Fatta-Kassinos et al. 2011; Michael et al. 2012b). Although the market offers a wide range of UV lamps, medium or low-pressure mercury vapour lamps emitting UVC light are preferred in UWW disinfection due to their germicidal power. Nonetheless, bacterial regrowth after water storage of UV-treated water may disturb the original bacterial community and favour ARB persistence (Rizzo et al. 2013a; Becerra-Castro et al. 2016; Sousa et al. 2017). Moreover, lab- and pilot-scale studies have demonstrated the inefficiency of UVC to remove different antibiotics from aqueous solutions (Abellàn et al. 2009; Kim et al. 2015). Thus, oxidants and/or catalysts (i.e., H_2O_2, $Fe^{2+/3+}$, TiO_2) have been added to attain better treatment performances, these technologies being known as advanced oxidation processes (AOPs).

Consolidated advanced treatments (membrane filtration, ozonation and active carbon) have already been used with success as a tertiary treatment to clean up wastewaters from CECs, including pharmaceutical compounds (Rizzo et al. 2019). Full-scale treatment trains for good quality UWW effluent (adopted in Switzerland and Germany) involves ozonation and powder active carbon (PAC) (Eggen et al. 2014). Bromates and nitrosamines are typical by-products generated during the reaction between ozone and several substances (i.e. dissolved organic carbon) in UWW. Prediction models based on chemical kinetics and water characteristics (ozone dose and reactivity with target CECs, water constituents and presence of by-products precursors) are successfully applied in UWWTP to quantify CECs removal, transformation products and by-products (Lee and Von Gunten 2014).

Advanced treatment technologies are intensive and energy demand systems, based on the generation of powerful oxidant (as hydroxyl radical) for the removal of organic compounds (as CECs), metals and microorganisms. AOPs involve mainly homogeneous light-driven (i.e. H_2O_2/UV and photo-Fenton) and heterogeneous photocatalytic processes (i.e. TiO_2/UV). Despite their high potential in water decontamination, they are not yet implemented in full-scale applications. Several critical aspects should be considered for the efficiency/feasibility of an oxidation process. Reaction kinetics oxidant-CECs is not the only essential parameter, but the reactivity of oxidant to wastewater matrix components should be considered (Ribeiro et al. 2019).

Effluent organic matter, carbonate and nitrate are considered radical scavengers. However, they can promote the generation of other oxidant species such as the carbonate radical. This selective oxidant is effective in CECs removal, especially for those hydrophilic as oxytetracycline (Liu et al. 2015).

1.4 Heterogeneous TiO_2 photocatalysis

When a semiconductor is irradiated by photons with energy equal or higher than the band-gap, electrons from the valence band are promoted to the conduction band, generating electron-hole pairs. In aerated conditions, molecular oxygen is a typical electron acceptor adsorbed on a semiconductor surface, forming the superoxide radical ($O_2^{\bullet -}$). Electron donors in environmental photocatalysis are usually organic molecules or water molecule/hydroxyl ion trapped on the semiconductor surface. In the first case, the organic molecule is directly oxidized, while in the second case, the hydroxyl radical ($HO^{\bullet}$) is formed and reacts without a specific target (indirect photocatalysis of weakly adsorbed pollutant). Organic molecules are converted into intermediates until total mineralization in CO_2 and H_2O. Inorganic contaminants can also react with radicals or photogenerated electrons and holes, being converted in less toxic and less dangerous compounds (Herrmann 1999). Photocatalysis founds application also in water disinfection since $HO^{\bullet}$ damages the cellular membrane and causes injury to DNA (Byrne et al. 2017).

TiO_2 is widely used as a commercial photocatalyst, due to the high chemical stability, low toxicity, resistance to photocorrosion, low cost and high oxidant performance during UV and near-UV/Vis irradiation (band gap of 3.2 eV). TiO_2 with commercial name of Degussa P25 is composed by a mixture of two crystalline phases (anatase and rutile at 4:1 mass ratio) with a specific surface area of ca. 50 $m^2\ g^{-1}$, the diameter particle ranging from 30-90 (single nanoparticle) to 1,000 nm (agglomerated particles) (Salaices et al. 2002). Since the application of commercial TiO_2 is restricted to a narrow range of the light spectrum (from UVC to near UV), a current research issue is to extend the absorption spectra to visible light. Modifications by metal and non-metal doping, forming composites with other oxides or carbon materials are some of the followed strategies (Pastrana-Martinez et al. 2012; Vaiano et al. 2015). However, when dyes are used as a model pollutant in visible light-driven photocatalysis, part of the radiation sensitizes the dye, generating an electron transfer from the pollutant to the catalyst conduction band (Shaham-Waldmann and Paz 2016). For this reason, dyes should be avoided to test the photocatalytic activity of semiconductors that are developed as new photocatalysts (Barbero and Vione 2016).

1.4.1 Engineering insights on photocatalytic processes

Water remediation through photocatalysis involves slurry and immobilized configurations. The main advantage of the immobilized configuration is to avoid a filtration step to separate the catalyst from the treated water. The cost related to keep homogeneous mixing in the reactor is also reduced. However, due to the lower mass transfer, immobilized configurations are less efficient than slurry configurations. Annular photocatalytic reactors are used in the slurry configuration, the radiation field being extensively modelled by several authors (Li Puma et al. 2004, 2010; Li Puma and Brucato 2007; Autin et al. 2013). An annular photocatalytic reactor is composed by a UV lamp in the middle irradiating the catalyst suspension contained in the annulus. The annulus is commonly made of borosilicate glass due to its excellent transmissivity properties. Part of the light is absorbed, and part is scattered by the nanoparticles. The extinction coefficient of TiO_2 is a function of both the effects and should be considered for the determination of optimal catalyst load/annulus diameter. This parameter depends on the particles agglomeration and water matrix. In particular, the higher is the agglomeration of particles (high in UWW without sonication), the lower is the extinction coefficient (Salaices et al. 2002), in UVA range the extinction coefficient varying from 2,000 to 5,000 $m^2\ kg^{-1}$. Optical thickness (τ) is an adimensional parameter considering light irradiation, reactor geometry, catalyst extinction coefficient and catalyst load. Considering scattering albedo of P25 (0.74), the radiation transmission is maximized at $\tau \approx 6$ (Li Puma and Brucato 2007).

Regarding solar photocatalysis in water remediation, compound parabolic concentrators (CPC) are the most used configuration. The principle of operation follows solar thermal applications. Briefly, a reflective surface is used to concentrate the solar radiation on transparent pipes containing catalyst in suspension. For high efficiency, solar rays should be perpendicular to the light collectors. For that reason, solar tracking systems, involving one or more inclination axis, have been reported in the literature. The concentration factor is a parameter considering direct and diffuse light through the semi-angle of acceptance. When CPC is designed to receive all solar incident radiation, the range of acceptance angle is ± 90°. The most used material of the reflecting surface is electropolished anodized aluminium. Catalyst load in solar photocatalytic applications is generally lower than the value used in artificial light-driven reactors (Malato et al. 2009). In both solar and artificial radiation systems, the turbulence regime guarantees a good mixing of catalyst and avoids the settling of nanoparticles. If the catalyst is immobilized on a supporting material, the less restrictive hydraulic regime can be used. However, reactor design is also more complex for immobilized catalysts, since a good compromise between reactor capacity and illuminated surface area is needed. The distances between the light source and the coated surfaces should be minimised.

UV light emitting diodes (LEDs) have received a great deal of attention in the last years in this domain, mainly for water and wastewater treatment, especially due to its ecofriendliness (by replacing mercury) and long-lifetime. In comparison to traditional UV lamps, the electricity is more efficiently converted into light, with the possibility of adjusting the irradiance. Emerging applications include pulsed light in water treatment due to the nearly instantaneous switching of these sources (Xiong and Hu 2013, 2017). UVA-LEDs with emission around 360-390 nm have been selected in different photocatalytic studies (Ferreira et al. 2016; Moreira et al. 2016; Arlos et al. 2017; Cai and Hu 2017; Xiong and Hu 2017; Jallouli et al. 2018). Efforts to optimize the TiO_2 photocatalytic treatment with UV-LEDs, employing model chemical pollutants with or without using a carrier solvent, have been done in the last years (Matafonova and Batoev 2018). Photocatalytic disinfection using TiO_2 and traditional UV lamps has been widely reported (van Grieken et al. 2010; Marugán et al. 2011; Rizzo et al. 2014b), but only a few publications have implemented UVA-LEDs, and they are often limited to *E. coli* (Xiong and Hu 2013; Martín-Sómer et al. 2017).

1.4.2 Photo-assisted treatment of antibiotics

The present work thesis focuses the attention on azithromycin (AZT), trimethoprim (TMP), sulfamethoxazole (SMX), ofloxacin (OFL), ciprofloxacin (CIP) and enrofloxacin (ENR). The first three antibiotics belong to macrolides, diaminopyrimidines and sulfonamides groups, while the last three are classified as fluoroquinolones. **Table 1.1** shows state of the art on the removal of the target antibiotics (selected in the framework of ANSWER project) by photolysis and photocatalysis.

Different antibiotics have been proven more vulnerable to radicals concerning to others. Moreover, oxidation (reacting with hole) or reduction (reacting with electrons) pathways depend on pK_a and molecular structures (Michael et al. 2012b). Matrix effect plays a crucial role in the photodegradation of antibiotics in an aqueous environment. Different water matrices or specific scavengers are considered in the literature to understand the removal pathway of AZT, TMP, OFL and SMX (Klamerth et al. 2009; Hapeshi et al. 2010; Ryan et al. 2010; Sirtori et al. 2010; Miranda-García et al. 2011; Tong et al. 2011; Wammer et al. 2013). The same concentration of antibiotic in different water matrices is obtained by spike condition, the removal efficiency of photolysis and photocatalysis being faithfully assessed. In fact, according to the Langmuir-Hinshelwood kinetic model, the rate constant of CECs increases with initial concentration until reaching a steady state value (Malato et al. 2009). Spike conditions are also used to assess the transformation by-products of target antibiotics during photolysis and photocatalysis. Other authors focused their research on the efficiency of the treatments in antibiotics removal at real

concentrations (Kim et al. 2009; Bernabeu et al. 2011; Prieto-Rodriguez et al. 2012; Moreira et al. 2015, 2016).

Table 1.1. State of the art on the removal of target antibiotics by photolysis and photocatalysis.

Compound	Matrix (location)	Initial concentration	Treatment process	Removal	Reference
Azithromycin	Ultrapure water; Artificial river water (nitrate, humic acids); Natural river water (China)	*20 mg L^{-1}; *20 μg L^{-1}	Simulated solar light (Xe-lamp with filter for λ < 290 nm); or natural sunlight	10% (2 h); 70% (2 h); 70% (8 d)	(Tong et al. 2011)
	Ultrapure water	*2.5-20 mg L^{-1}	Vis light/Metal doped TiO_2 nanorods	100% (2h); 20% (2 h)	(Naraginti et al. 2019)
	Ultrapure water	*10-100 mg L^{-1}	UVC/graphene oxide doped ZnO	100% (2h); 60% (2 h)	(Sayadi et al. 2019)
	River water (Japan)	*10 μg L^{-1}	Simulated solar light	<20% (1 h)	(Hanamoto et al. 2013)
	Nanofiltration concentrate of simulated wastewater	*600 μg L^{-1};	$UV_{254\ nm}$; O_3; and UV/O_3	10%; 100%; and 100%; (0.5 h)	(Liu et al. 2014)
	Secondary urban wastewater (Japan)	100 ng L^{-1}	$UV_{254\ nm}$; and UV/H_2O_2	5%; and 90%	(Kim et al. 2009)
	Secondary urban wastewater (China)	*1 μg L^{-1}	Simulated solar light: (Xe-lamp with filter for λ < 290 nm)	99% (30 h)	(Yan et al. 2017)
	Secondary urban wastewater (Spain)	69 ng L^{-1}	Xe-lamp TiO_2-P25 photocatalysis; Solar TiO_2-P25 photocatalysis (CPC)	No specified	(Prieto-Rodriguez et al. 2012)
	Secondary urban wastewater (Portugal)	140 ng L^{-1}	O_3; TiO_2-P25 photocatalysis (slurry); and TiO_2-P25 photocatalytic O_3	91%; 92%; and 100%	(Moreira et al. 2015)
	Secondary urban wastewater (Portugal)	300-1000 ng L^{-1}	O_3; TiO_2-P25 photocatalysis (immobilized); and TiO_2-P25 photocatalytic O_3	100%; 50%; and 100%	(Moreira et al. 2016)
Trimethoprim	Ultrapure water	*100 mg L^{-1}	Simulated solar light: (Xe-lamp with filter for λ < 290 nm); TiO_2-P25 solar photocatalysis	90% and 90% (3 h)	(Abellàn et al. 2009)
	Ultrapure water	*30 mg L^{-1}	UVA; $UV_{254\ nm}$; Vaccum UV; Vaccum UV/H_2O_2	0%; 20%; 87%; and 96% (2 h)	(Kim et al. 2015)
	Ultrapure water	*200-1000 μg L^{-1}	UVA-LEDs photolysis ; UVA-LEDs/TiO_2-P25 photocatalysis	17%; 100-84%	(Cai and Hu 2017)

Table 1.1. State of the art on the removal of target antibiotics by photolysis and photocatalysis (continued).

Compound	Matrix (location)	Initial concentration	Treatment process	Removal	Reference
Trimethoprim	Ultrapure water; Sea water	*20 mg L^{-1}	Simulated solar light; Simulated solar light/ TiO_2-P25	100% (18 and 23 h); 100% (25 and 75 min)	(Sirtori et al. 2010)
	Ultrapure water; Secondary urban wastewater; River water (USA)	*290 μg L^{-1}	Simulated solar light	41%; 9%; and 16% (3 h)	(Ryan et al. 2010)
	Secondary urban wastewater (Japan)	80 ng L^{-1}	$UV_{254\ nm}$; and UV/H_2O_2	10%; and 100%	(Kim et al. 2009)
	Secondary urban wastewater (China)	*1 μg L^{-1}	Simulated solar light: (Xe-lamp with filter for $\lambda < 290$ nm)	90% (30 h)	(Yan et al. 2017)
	Secondary urban wastewater (Spain)	1.661 μg L^{-1}	Solar TiO_2-P25 photocatalysis (CPC)	70% (8 h)	(Prieto-Rodriguez et al. 2012)
	Secondary urban wastewater (Portugal)	54 ng L^{-1}	O_3; TiO_2-P25 photocatalysis (slurry); and TiO_2-P25 photocatalytic O_3	100%; 100%; and 100%	(Moreira et al. 2015)
	Secondary urban wastewater (Portugal)	0-150 ng L^{-1}	O_3; TiO_2-P25 photocatalysis (immobilized); and TiO_2-P25 photocatalytic O_3	100%; 5%; and 100%	(Moreira et al. 2016)
Ofloxacin	Ultrapure water; Groudwater; Real wastewater (Cyprus)	*10 mg L^{-1}	UVA/TiO_2-P25 photolysis	67%; 29%; and 18% (2 h)	(Hapeshi et al. 2010)
	Ultrapure water	*10 mg L^{-1}	Simulated solar light/ TiO_2-P25	60% (1.50 h)	(Li et al. 2012)
	Ultrapure water; Lake water (USA)	*100 μg L^{-1}	Simulated solar light: (Xe-lamp with filter for $\lambda < 290$ nm)	90%; 99% (5 min)	(Wammer et al. 2013)
	Ultrapure water; Real wastewater (Spain)	*100 μg L^{-1}	Solar photo Fenton	100%; 100%	(Klamerth et al. 2009)
	Ultrapure water; Real wastewater (Spain)	*100 μg L^{-1}	Solar (immobilized) TiO_2-P25 photocatalysis	100%; 100% (2 h)	(Miranda-García et al. 2011)
	River water (Japan)	*50 μg L^{-1}	Simulated solar light	90% (1 h)	(Hanamoto et al. 2013)
	Nanofiltration concentrate of simulated wastewater	*600 μg L^{-1};	$UV_{254\ nm}$; O_3; and UV/O_3	5%; 100%; and 100%; (0,5 h)	(Liu et al. 2014)
	Secondary urban wastewater (Spain)	1,614 μg L^{-1}	Solar TiO_2-P25 photocatalysis (CPC)	84% (8 h)	(Prieto-Rodriguez et al. 2012)
	Secondary urban wastewater (Spain)	203 ng L^{-1}	Solar (immobilized) TiO_2-P25 photocatalysis	77% (6 h)	(Bernabeu et al. 2011)
Sulfamethoxazole	Ultrapure water	*200-1000 μg L^{-1}	UVA-LEDs photolysis ; UVA-LEDs/TiO_2-P25 photocatalysis	16%; 100-69%	(Cai and Hu 2017)

Table 1.1. State of the art on the removal of target antibiotics by photolysis and photocatalysis (continued).

Compound	Matrix (location)	Initial concentration	Treatment process	Removal	Reference
Sulfamethoxazole	Ultrapure water	*30 mg L^{-1}	UVA; $UV_{254\ nm}$; Vaccum UV	9%; 100%; and 100% (2 h)	(Kim et al. 2015)
	Ultrapure water	*100 mg L^{-1}	Simulated solar light: (Xe-lamp with filter for λ < 290 nm); TiO_2-P25 solar photocatalysis	40%; and 80% (3 h)	(Abellàn et al. 2009)
	Ultrapure water; Secondary wastewater (Spain)	*100 μg L^{-1}	Solar (immobilized) TiO_2-P25 photocatalysis	75%; 50% (2 h)	(Miranda-García et al. 2011)
	Ultrapure water; Secondary wastewater (Spain)	*100 μg L^{-1}	Solar photo Fenton	100%; 100%	(Klamerth et al. 2009)
	Ultrapure water; Secondary urban wastewater; River water (USA)	*250 μg L^{-1}	Simulated solar light	87%; 70%; and 72% (3 h)	(Ryan et al. 2010)
	Secondary wastewater (Italy)	*1 mg L^{-1}	Wide spectrum 250 W lamp	100%	(Rizzo et al. 2013a)
	Secondary wastewater (Portugal)	<LOQ	O_3; TiO_2-P25 photocatalysis (slurry); and TiO_2-P25 photocatalytic O_3	-	(Moreira et al. 2015)
	Secondary wastewater (Portugal)	0-1000 ng L^{-1}	O_3; TiO_2-P25 photocatalysis (immobilized); and TiO_2-P25 photocatalytic O_3	100%; 20%; and 100%	(Moreira et al. 2016)
	Secondary urban wastewater (Japan)	200 ng L^{-1}	$UV_{254\ nm}$; and UV/H_2O_2	100%; and 100%	(Kim et al. 2009)
	Secondary urban wastewater (Spain)	*100 μL^{-1}; 1 μg L^{-1}	Xe-lamp TiO_2-P25 photocatalysis; Solar TiO_2-P25 photocatalysis (CPC)	75% (2 h, low C_{P25}); 55% (8 h)	(Prieto-Rodriguez et al. 2012)

* = spiked pollutant; CPC = compound parabolic collectors.

Photodegradation of AZT in real water matrices occurs through indirect photolysis, considering that macrolides do not absorb light >290 nm (Vione et al. 2009). Alkalinity ($CaCO_3$), inorganic ions (nitrate), and dissolved organic matter (humic acids) are parameters enhancing photodegradation of AZT in synthetic water under simulated solar light. The presence of humic acid in artificial freshwater profoundly increases the degradation of AZT (from 16-18% degradation to 73%) under solar photolysis (2 h) (Tong et al. 2011). In more complex water matrices (as secondary UWW), AZT is mainly degraded by triplet states of organic matter ($^3EfOM^*$) under solar photolysis (Yan et al. 2017). Moreover, low removal efficiency (10%) of AZT is reported under UV_{254} radiation in secondary UWW, considering a realistic UV dose

(2768 mJ cm^{-2}) (Kim et al. 2009). The main transformed-product of AZT under solar photolysis is generated by the cleavage of cladinose from the parent compound (Tong et al. 2011). Only a few studies report the removal efficiency of AZT under photocatalysis. In particular, a visible-light/metal-doped TiO_2 nanorods process successfully degraded AZT at different concentrations (2.5-20 mg L^{-1}) (Naraginti et al. 2019), while a UVC/graphene oxide doped ZnO material completely removed AZT (10 mg L^{-1}) under optimized conditions (1 g L^{-1} catalyst load and acidic pH) in two hours (Sayadi et al. 2019). A scavenger study reports $HO^{\bullet}$ as the main oxidant responsible for AZT degradation under photocatalysis, the cleavage of desosamine and cladinose being the main degradation pathway (Naraginti et al. 2019).

The scientific literature reports many environmental studies on TMP and SMX together, and the two antibiotics are often prescribed in conjunction for medical therapy. TMP photodegradation in real water matrices is attributed to hydroxyl/carbonate radicals (Yan et al. 2017). Scavenger studies during TMP and SMX solar photolysis identify effluent organic matter and an inorganic anion (i.e. nitrate) as significant photosensitizers concerning the natural organic matter. Indirect solar photolysis of the two antibiotics in presence of the effluent organic matter (EfOM) can follow two main pathways. The first pathway involves the oxidation though $HO^{\bullet}$ produced by irradiated EfOM and nitrate. The second pathway involves energy transfer from $^{3}EfOM^{*}$ to the substrate, which can switch in triplet excited state and finally in by-product or quenched by oxygen and switch back to the ground state. Electron transfer or H-abstraction by $^{3}EfOM^{*}$ is the other alternative to the second oxidation pathway (Ryan et al. 2010). It is worth to say that ketone intermediates of TMP are photosensitizer of $HO^{\bullet}$; therefore, autocatalytic degradation of TMP can occur under solar photolysis (Sirtori et al. 2010).

Degradation of TMP and SMX by photolysis and photocatalysis in synthetic water is widely reported in the literature. UVC photolysis in DW (ca. 2,000 mJ cm^{-2}) is said to be enough to remove SMX, while only 20% removal is reached for TMP (both antibiotics at 30 mg L^{-1}) (Kim et al. 2015). Comparing the effect of UVC (290-400 nm) radiation and UVC/TiO_2-P25 process, the second treatment has double efficiency in SMX degradation (after 6 h process). However, when no optic filter is used (230-400 nm), photocatalysis has the same effectiveness of UVC (230-400 nm) radiation. SMX is susceptible to direct photolysis by wavelengths below 310 nm. Despite SMX shows no increase of degradation varying the pH under photocatalysis, TOC removal is higher when increasing the pH, the intermediates being influenced (ionic nature). The high aromaticity (SUVA/DOC), and low degradability of the treated solution (BOD/COD) after 6 hours of photocatalytic treatment is due to the presence of by-products with sulfur- and nitrogen-containing aromatic ring (Abellán et al. 2007). Other two studies involving the solar light/TiO_2-P25 process (slurry and immobilized configuration) report high degradation of SMX

(100 µg L^{-1}) in secondary UWW (Miranda-García et al. 2011; Prieto-Rodriguez et al. 2012), the removal of the antibiotic being faster in DW (Miranda-García et al. 2011).

TMP removal from DW by UVC radiation can be described by an exponential function (total removal in 5 h), while a logarithmic function describes the degradation under UVC/TiO_2-P25 (complete degradation in 6 h). In the same study, despite TOC removal is higher in UVC/TiO_2-P25 than in UVC treatment, the aromaticity of the solution increases at the beginning of the process and never reaches the initial value (even after 15 h of treatment). The performance of both methods is influenced by the presence of high transformed products due to the high spiked initial concentration (100 mg L^{-1}) (Abellàn et al. 2009). UVA-LEDs photolysis (UV dose 4,000 mJ cm^{-2}) of SMX and TMP solutions in DW (separately tests) reaches 16 and 17% removal, respectively. When TiO_2-P25 is added (0.05 g L^{-1}), 91 and 78% removal is achieved for SMX, while 93 and 68% removal for TMP (at 5.6 and 7.0 pH, respectively) (Cai and Hu 2017). Oxidation mechanism of TMP during photocatalysis occurs mainly by $HO^{\bullet}$, hydroxylation, demethylation and cleavage being the main mechanism forming TMP intermediates (Sirtori et al. 2010; Cai and Hu 2017). The major degradation pathway of SMX under UVA-LEDs/TiO_2-P25 process involves isoxazole ring opening, hydroxylation and cleavage (Abellán et al. 2007; Cai and Hu 2017). Different results are reported on SMX and TMP removal (in real concentration) from secondary UWW by UVC photolysis and TiO_2-P25 photocatalysis. TMP is found more recalcitrant than SMX under UVC radiation (2,768 mJ cm^{-2}) (Kim et al. 2009) and UVA-LEDs/TiO_2 process (immobilized catalyst) (Moreira et al. 2016). An opposite trend is reported in another study using a solar TiO_2-P25 slurry process (Prieto-Rodriguez et al. 2012).

Other antibiotics considered in the present thesis work are OFL, CIP and ENR (all fluoroquinolones, FQs). This class of antibiotics is susceptible to direct photodegradation under solar light (Ge et al. 2010; Yan et al. 2017). In particular, DOM competes with FQs in absorbing photons, and the effect of reactive species (generated from DOM photoexcitation) in FQs degradation is less significant than direct solar photodegradation. For that reason, FQs degradation is faster in DW than in fresh water under simulated solar photolysis (Ge et al. 2010; Wammer et al. 2013). Photodegradation rate of OFL and ENR in DW is reported to be highly pH dependent. Cationic form (acidic pH) is very stable under solar photolysis, while anionic (basic pH) and zwitterionic (neutral pH) form show similar degradation rate constants (Wammer et al. 2013). An extensive literature is available on FQs degradation through photocatalysis involving commercial (Hapeshi et al. 2010; Miranda-García et al. 2011; Li et al. 2012; Prieto-Rodriguez et al. 2012; Rodríguez et al. 2015) and doped catalysts (Sood et al. 2016; Xie et al. 2017; Kaur et al. 2018; Wang et al. 2019a).

UVA treatment of DW is effective in OFL degradation (ca. 40% removal in 4 h). However, the conversion is not attributed to direct photolysis but to singlet oxygen generated in the aerated condition, conversion of OFL in anoxic condition (N_2) being ca. 5 % (no generation of singlet oxygen) (Hapeshi et al. 2010). In another study, UVA photolysis in the aerated condition is also useful in OFL removal (ca. 15% in 30 min) (Wang et al. 2017). Autocatalytic degradation of OFL under UVA light is also reported in the literature. Singlet oxygen is responsible for producing a cationic radical OFL species and $O_2^{\bullet-}$, their interaction leading to OFL demethylation and formation of H_2O_2 and formaldehyde (Rodríguez et al. 2015). OFL conversion by photocatalysis in DW is reported to be pH dependent and valence band holes (highly produced in low pH) seem to be a primary oxidation pathway of OFL (Hapeshi et al. 2010). Also, under UVA light, OFL excited state can transfer an electron to the catalyst conduction band, generating cationic radical OFL species, while valence band holes can react with oxygen, producing $O_2^{\bullet-}$ (the other main species involved in OFL degradation) (Rodríguez et al. 2015). In a study considering simultaneous degradation of FQs in DW under UVA/TiO_2-P25 process, OFL, CIP and ENR degradation are reported to slightly improving at basic conditions (Li et al. 2012). In secondary UWW, OFL is detected at μg L^{-1}, and few studies report its degradation under solar photocatalysis in slurry (Prieto-Rodriguez et al. 2012) and immobilized configurations (Miranda-García et al. 2011). Both the studies highlight faster degradation of OFL (0.08-0.10 min^{-1} constant rate) with respect to other antibiotics as SMX and TMP.

1.4.3 Photo-assisted inactivation of ARB&ARGs

Biological contaminants as fungi, bacteria and viruses are also inactivated by UVC radiation and photocatalysis. Catalyst type and load (photocatalysis), light intensity and treatment time (both UVC radiation and photocatalysis) are some process parameters influencing the efficiency of disinfection. However, cell wall complexity of microorganisms also plays an important role in the photocatalytic inactivation potential, protozoa, bacterial spores and mycobacteria being the more resistant, followed by viruses, fungi and bacteria. Regarding UVC photolysis, DNA damage represents the main mechanism of bacterial inactivation, the membrane cell being not break (Guo et al. 2013a; Becerra-Castro et al. 2016). Membrane rupture and consequent DNA/RNA damage by oxygen radicals are considered the main bacterial inactivation pathway during photocatalysis. In particular, gram positive bacteria are recognized as a more susceptible microorganism with respect to gram negative bacteria, the first group having a very thick cell wall of peptidoglycan and teichoic acids layers, while the second group showing a first peptidoglycan layer surrounded by lipopolysaccharides and lipoproteins second layer. The osmotic pressure of the water is an important parameter affecting the bacteria vulnerability to photocatalysis, the cell membrane permeability being modified and consequently more susceptible to oxygen radicals. The different

stages of growth phase also have impact on the efficiency of the photocatalytic treatment (Laxma Reddy et al. 2017).

Different approaches to assess the effect of photolysis and photocatalysis on antibiotic resistance are proposed in the literature. Some authors selected a specific ARB and spiked it in sterile water or autoclaved UWW (Rizzo et al. 2013a; Xiong and Hu 2013; Rizzo et al. 2014b; Dunlop et al. 2015; Ferro et al. 2015; Fiorentino et al. 2015; Venieri et al. 2017; Karaolia et al. 2018), while other researchers focused the study on real matrix treatment, considering inactivation of indigenous bacteria and ARGs (Guo et al. 2013a, 2013b; Zhuang et al. 2015; Sousa et al. 2017; Zheng et al. 2017; Moreira et al. 2018). Spiked studies allow the assessment of antibiotic resistance proprieties (and possible modification) of survived bacteria through cultivable methods (MIC, Kirby-Bauer method and E-test), the horizontal gene transfer being another possible mechanism to track (Dunlop et al. 2015; Guo et al. 2015). Considering real matrix, antibiotic resistant and susceptible bacteria are expected to be vulnerable to photocatalysis at the same level. However, after mild treatment, a certain fraction of bacteria can be still viable but not cultivable, storage of water being a good condition for their recovery (Manaia et al. 2018). During storage of treated water, different degree of reactivation and horizontal gene transfer can promote the prevalence of ARB. The post-treatment recovery can be avoided increasing the treatment time (Dunlop et al. 2015; Michael-Kordatou et al. 2018).

Main achievements on ARB&ARGs removal by photolysis and photocatalysis found in the literature are summarized in **Table 1.2**. Solar radiation does not modify any antibiotic resistance proprieties of *E. coli* in UWW (Fiorentino et al. 2015), while artificial UVC radiation (25 mJ cm^{-2} UV dose) has the potential to reduce the resistance to ciprofloxacin of an *E. coli* strain spiked in autoclaved UWW (Rizzo et al. 2013a). Increase of ARB prevalence with respect to total heterotrophs in UVC treated and stored treated UWW is reported in several studies (Guo et al. 2013b, 2013a; Sousa et al. 2017). Moreover, UV radiation is found to increase the prevalence of erythromycin resistant *E. coli* with respect to total *E. coli* (Michael-Kordatou et al. 2015). Realistic UV doses (< 2,000 mJ cm^{-2}) are not effective for a complete removal of ARGs (Zhuang et al. 2015; Sousa et al. 2017; Zheng et al. 2017). However, tetracycline (*tetA*, *tetO*), erythromycin (*ereA*, *ereB*, *ermA* and *ermB*), β-lactam (bla_{TEM}) and fluoroquinolones (*qnrS*) resistant genes are highly reduced in UWW treated by realistic UV doses (Guo et al. 2013b; Sousa et al. 2017). Tetracycline resistant genes (*tetA*, *tetM*, *tetO*, *tetQ* and *tetW*) seem to suffer photolysis more than sulfamethoxazole resistant genes (*sulI*, *sulII*), and the decrease of all the aforementioned ARGs can be described by an exponential function (Zheng et al. 2017). 16S rRNA and class 1 integron-integrase gene (*intI1*) are highly detected in secondary UWW, the typical concentration ranging between 9 and 8 log (gene copies / 100 mL), respectively.

16S rRNA reflects the presence of bacteria (cultivable and not cultivable), while *intI1* carries ARGs cassettes and it is correlated to the horizontal gene transfer. The removal efficiency of the aforementioned two genes by UVC radiation is low (ca. 2 log removal) even considering the high UV dose (ca. 12,000 mJ cm^{-2}) (Zhuang et al. 2015).

TiO_2 photocatalysis has higher potential than UVC radiation alone to inactivate total and antibiotic resistant *E. coli* (Xiong and Hu 2013). Solar driven TiO_2-P25 photocatalysis is found to decrease the prevalence of ARB with respect to total coliforms and total enterococci in treated and 3-days stored treated UWW (Moreira et al. 2018). The same solar driven process, applied on autoclaved UWW spiked with multidrug resistant *E. coli* (Ferro et al. 2015; Fiorentino et al. 2015) and enterococci (Rizzo et al. 2014a), does not seems to change the antibiotic resistance in the survived colonies. The effect of metal doped-TiO_2 photocatalysis on antibiotic resistance change is also investigated in the literature. In particular, nitrogen doped-TiO_2 photocatalysis seems to decrease the ciprofloxacin and cefuroxime resistance of *E. coli* after treatment (Rizzo et al. 2014c). Another study involving cobalt and manganese doped-TiO_2 photocatalysis reports changes of intracellular ARGs and consequent decrease of cefaclor and tetracycline resistance in survived *K. pneumoniae* (Venieri et al. 2017). Few data are available in the scientific literature regarding ARGs removal by photocatalysis. In particular, solar driven graphene oxide-TiO_2 composite and standard TiO_2 photocatalysis have different efficiency in removal of ARGs from secondary UWW (Karaolia et al. 2018; Moreira et al. 2018). 16S rRNA and *intI1* are really hard to remove by solar photocatalysis, while ca. 1 log removal is found for bla_{TEM}, *sul1* and *qrnS* after 3-days storage of treated UWW (Moreira et al. 2018). Ampicillin resistant gene (*ampC*) and *P. aeruginosa* related gene (*ecfX*) are effectively removed by solar driven graphene oxide-TiO_2 composite photocatalysis in 3 h process (Karaolia et al. 2018).

Table 1.2. State of the art on the removal of ARB&ARGs by photolysis and photocatalysis.

ARB&ARG and water matrix (location)	**Antibiotics used to assess the resistance/Kit and procedure to detect the genes**	**Treatment process and main achievements**	**Reference**
E. Coli J-53R; *E. Coli* HT-99. Spike of selected strains (clinical) in DW and autoclaved CAS effluent (United Kingdom).	Rifampicin (100 mg L^{-1}), chloramphenicol (25 mg L^{-1}) in LBA agar. Antibiotics were used only for conjugation tests.	UVA/TiO_2-P25 photocatalysis (immobilized on glass). - 1.5 and 1.0 log reduction (180 min) in DW and UWW; - 3.0 log regrowth after 1 day storage in dark; - Horizontal gene transfer though conjugation after 1 day storage (in LB broth).	(Dunlop et al. 2002)
E. Coli. Spike of selected strains (Spain) in autoclaved CAS effluent (Spain).	Mixture of ampicillin (16 mg L^{-1}), ciprofloxacin (2 mg L^{-1}), tetracycline (8 mg L^{-1}) in TBX agar. Antibiotics were used for the isolation of the strain. **Kirby-Bauer method**: ampicillin (10 mg), ciprofloxacin (5 mg), cefuroxime (30 mg), nitrofurantoin (100 mg), tetracycline (30 mg) and vancomycin (30 mg).	Solar-driven TiO_2-P25 photocatalysis (slurry at low C_{P25}). - 5.5 log reduction reaching LOD (90 min); - No change of antibiotic resistance of survived colonies (at 45 and 90 min).	(Ferro et al. 2015)
E. Coli. Spike of selected strain (Italy) in autoclaved CAS effluent (Spain).	Mixture of ampicillin (16 mg L^{-1}), ciprofloxacin (2 mg L^{-1}), tetracycline (8 mg L^{-1}) in TBX. Antibiotics were used for the isolation of the strain. **Kirby-Bauer method**: ampicillin (10 mg), ciprofloxacin (5 mg), cefuroxime (30 mg), nitrofurantoin (100 mg), tetracycline (30 mg) and vancomycin (30 mg).	Solar radiation and solar-driven TiO_2-P25 photocatalysis (slurry at low C_{P25}). - 5.5 log reduction reaching LOD (7 and 4 h, respectively); - No change of antibiotic resistance of survived colonies.	(Fiorentino et al. 2015)
Heterotrophs. CAS effluent (China).	Cephalexin (16 mg L^{-1}), ciprofloxacin (32 mg L^{-1}), erythromycin (8 mg L^{-1}), gentamicin (16 mg L^{-1}), vancomycin (32 mg L^{-1}), sulfadiazine (512 mg L^{-1}), rifampicin (4 mg L^{-1}), tetracycline (16 mg L^{-1}), chloramphenicol (32 mg L^{-1}) in nutrient agar (beef extract 3 g L^{-1}, peptone 10 g L^{-1}, NaCl 5 g L^{-1} and agar 15 g L^{-1}). Antibiotics were used to measure the ratio of antibiotic resistant and total bacteria.	UVC radiation (10-80 of mJ cm^{-2} UV dose). - Different percentage of resistance (depending on the antibiotics) before the treatment; - Change (increase and decrease) in antibiotic resistance prevalence at different UV doses.	(Guo et al. 2013a)
Heterotrophs. *ereA, ereB, ermA, ermB, tetA, tetB, tetM, tetO.* CAS effluent (China).	Erythromycin (8 mg L^{-1}), tetracycline (16 mg L^{-1}) in nutrient agar. Antibiotics were used to measure the treatment efficiency on resistant and total bacteria. Plasmid from positive control used for standard curves in qPCR.	UVC radiation (10-80 of mJ cm^{-2} UV dose). - Inactivation order: total heterotrophs (80 mJ cm^{-2}) < erythromycin resistant (50 mJ cm^{-2}) < tetracycline resistant (20 mJ cm^{-2}); - Complete ARGs removal (10 mJ cm^{-2}).	(Guo et al. 2013b)

Table 1.2. State of the art on the removal of ARB&ARGs by photolysis and photocatalysis (continued).

ARB&ARG and water matrix (location)	**Antibiotics used to assess the resistance/Kit and procedure to detect the genes**	**Treatment process and main achievements**	**Reference**
E. coli K12 (selected from UWW) and *E. coli* NK 5449 (clinical). Spike of selected strains in synthetic UWW.	Tetracycline (32 mg L^{-1}), rifampicin (160 mg L^{-1}) and nalidixin aicd (50 mg L^{-1}) in LBA agar. Antibiotic were used only for conjugation tests.	UVC radiation (1-40 mJ cm^{-2} UV dose). - Total inactivation of both bacterial strains by UV dose of 40 mJ cm^{-2}; - UV doses below 10 mJ cm^{-2} promote horizontal gene transfer during 1 d storage at 37°C.	(Guo et al. 2015)
E. Coli. 23S rRNA *(enterococci), ampC (enterobacter spp), sul1, ermB, mecA (staphylococcus), ecfX* (*P. aeruginosa*). Spike of selected strain (Cyprus) in MBR effluent (Cyprus).	Sulfamethoxazole, clarithromycin, erythromycin (concentrations not specified) in TBX. Antibiotics were used for the selection of the strain (by MIC) and for the assessment of resistance (after process) by plate count. **Antibiotic susceptibility test dilution (MIC):** sulfamethoxazole, clarithromycin, erythromycin (concentrations not specified). qPCR calibration curve by selected ARB hosting genes and cell-equivalent calculation method.	Solar-driven GO-TiO_2 photocatalysis (slurry). - Different inactivation order between total and resistant strains; - Regrowth (after 1 d storage) decreases at increasing treatment time (no regrowth in 3 h treated sample); - *ampC*, *ecfX* reduced, *ermB*, *sul1*, *23S rRNA* unchanged, using GO- TiO_2; - *ermB* reduced, *sul1*, *ampC*, *ecfX*, *23S rRNA* unchanged, using control TiO_2.	(Karaolia et al. 2018)
E. Coli. MBR effluent (Cyprus).	Erythromycin (100 mg L^{-1}) in TBX. Antibiotics were used to measure the treatment efficiency on resistant and total bacteria.	UVC_{254} radiation (9 W power). - ARB inactivation (90 min for total removal) < total bacteria inactivation (45 min for total removal).	(Michael-Kordatou et al. 2015)
Faecal coliforms, *enterococci*. 16S rRNA, *intI1*, *sul1*, *qnrS*, bla_{CTX-M}, bla_{CTX},. CAS effluent (Spain).	Mixture of tetracycline (16 mg L^{-1}), ciprofloxacin (1 mg L^{-1}) in m-FC and S&B. Antibiotics were used to measure the treatment efficiency on resistant and total bacteria. qPCR standard curves by amplicons of known strains (cloned with InsTAcloneTM PCR Cloning Kit).	Solar-driven GO-TiO_2 and TiO_2-P25 photocatalysis (slurry at low C_{P25}). - Regrowth after 3 days-storage (TiO_2-P25) of treated water; - No regrowth after 3 days-storage, except for total enterococci (GO-TiO_2); - No ARGs reduction immediately after treatment and after storage; - *Proteobacteria* prevalence after storage.	(Moreira et al. 2018)
E. Coli. Spike of selected strains (Italy) in autoclaved water mix (CAS effluent, surface water, 1:9) (Italy).	Mixture of amoxicillin (16-8 mg L^{-1}), ciprofloxacin (2-1 mg L^{-1}), sulfamethoxazole (64-32 mg L^{-1}) in TSA. Antibiotics were used for the isolation of two strains. **E-test (equivalent MIC):** amoxicillin (0.16–256 mg L^{-1}), ciprofloxacin (0.02–32 mg L^{-1}), sulfamethoxazole (0.64– 1024 mg L^{-1}).	Simulated solar light (wide spectrum 250 W lamp with UV filter). - The high resistant strain is faster inactivated (0.4 log removal) than lower resistant strain (0.2 log removal) in 3 h treatment; - The high resistant strain loses the resistance to ciprofloxacin.	(Rizzo et al. 2012)

Table 1.2. State of the art on the removal of ARB&ARGs by photolysis and photocatalysis (continued).

ARB&ARG and water matrix (location)	**Antibiotics used to assess the resistance/Kit and procedure to detect the genes**	**Treatment process and main achievements**	**Reference**
E. Coli. CAS effluent (Italy); Spike of selected strains (Italy) in autoclaved CAS effluent (Italy).	Mixture of amoxicillin (16-8 mg L^{-1}), ciprofloxacin (2-1 mg L^{-1}), sulfamethoxazole (64-32 mg L^{-1}) in TSA. Antibiotics were used for the isolation of two strains. **E-test (equivalent MIC):** amoxicillin (0.16–256 mg L^{-1}), ciprofloxacin (0.02–32 mg L^{-1}), sulfamethoxazole (0.64– 1024 mg L^{-1}).	Wide spectrum 250 W lamp with UV filter (25 mJ cm^{-2} UV dose). - 3 log inactivation of indigenous strain (1 mJ cm^{-2}); - 4 and 6 log removal of high and low resistant strain, respectively; - The high resistant strain loses the resistance to ciprofloxacin (25 mJ cm^{-2}).	(Rizzo et al. 2013a)
Enterococci. Spike of selected strain (Italy) in autoclaved CAS effluent (Italy).	Tetracycline (16 mg L^{-1}) in S&B. Antibiotic was used for the isolation of the strain. **Kirby-Bauer method:** ampicillin (10 mg), ciprofloxacin (5 mg), tetracycline (30 mg), vancomycin (30 mg).	Solar simulated TiO_2-P25 photocatalysis (slurry at low C_{P25}). - Same inactivation rate of total and resistant strain (assays performed separately); - No log reduction in 1 h photolysis control and total inactivation (7 log reduction) in 1 h photocatalysis; - No changes in antibiotic resistance.	(Rizzo et al. 2014a)
E. Coli. Spike of selected strains (Italy) in autoclaved CAS effluent (Italy).	Ciprofloxacin (1 mg L^{-1}), amoxicillin (8 mg L^{-1}), sulfamethoxazole (32 mg L^{-1}) in TSA. Antibiotics were used for the isolation of the strain. **Kirby-Bauer method:** ciprofloxacin (5 mg), cefuroxime (30 mg), tetracycline (30 mg) and vancomycin (30 mg).	Solar simulated TiO_2-PC50, TiO_2-PC100 and N-TiO_2 photocatalysis (slurry at low C). - Faster disinfection with N-TiO_2 photocatalysis; - Total inactivation (7 log removal) after 1 h treatment; - Ciprofloxacin and cefuroxime resistance decreases after treatment.	(Rizzo et al. 2014c)
16S rRNA, *intI1*, *vanA*, bla_{TEM}, *sul1*, *qnrS*. CAS effluent (Portugal)	Standard curves in qPCR by amplicons of known strains (cloned with InsTAcloneTM PCR Cloning Kit).	UV_{254} radiation (30 min). - bla_{TEM} *and qnrS* total removal after treatment, no removal of remaining ARGs; - Increase of ARGs abundance after 3 days-storage in dark.	(Sousa et al. 2017)
Staphylococcus, Acinetobacter and Enterococcus (resistant clinical isolates). Spike of selected strains in DW.	LBA and Mueller Hinton agar with no supplemented antibiotics.	UVA/TiO_2-P25 photocatalysis (slurry at low C_{P25}). - No log reduction after photolysis control (90 min); - Increasing inactivation using higher UV irradiance and catalyst load (0.06-0.12 g L^{-1} and 4-8 W m^{-2} irradiance).	(Tsai et al. 2010)

Table 1.2. State of the art on the removal of ARB&ARGs by photolysis and photocatalysis (continued).

ARB&ARG and water matrix (location)	**Antibiotics used to assess the resistance/Kit and procedure to detect the genes**	**Treatment process and main achievements**	**Reference**
K. pneumoniae (clinical isolates). *tetA, tetM, sul1, bla$_{TEM}$, ampC.* Spike of selected strain (Greece) in autoclaved CAS effluent (Greece).	Nutrient agar with no supplemented antibiotics. **Antibiotic susceptibility test dilution (MIC):** ampicillin (1-256 mg L^{-1}), cefaclor (2-512 mg L^{-1}), sulfamethoxazole (2-128 mg L^{-1}) and tetracycline (2-256 mg L^{-1}). Chemical lysis and phenol/chloroform/isoamyl alcohol. Qualitative PCR followed by DGGE.	Solar-driven TiO_2-P25, metal doped-TiO_2 photocatalysis (immobilized on polymer) and UVC radiation. - Similar rate constant inactivation for UVC and solar-driven metal doped-TiO_2 photocatalysis (0.5 min^{-1}); - Cefaclor and tetracycline resistance change; - ARGs not found in survived colonies: *bla$_{TEM}$* and *tetM* (TiO_2-P25); *sul1*, *tetA*, *bla$_{TEM}$* and *tetM* (metal doped-TiO_2); *sul1*, *tetA*, *bla$_{TEM}$* (UVC radiation).	(Venieri et al. 2017)
E. coli ATCC 700891. Spike of selected strains in DW.	Ampicillin (150 mg L^{-1}), streptomycin (150 mg L^{-1}) in TSA. Antibiotics were used to measure the treatment efficiency on ARB.	UVA-LEDs/TiO_2-P25 photocatalysis (immobilized on glass) and UVC radiation. - Higher inactivation with periodic illumination (using the same UV dose); - UVC treatment (differently from photocatalysis) causes re-growth (4 h storage in light and dark).	(Xiong and Hu 2013)
Heterotrophs. 16S rRNA, *intI1, tetA, tetM, tetO, tetQ, tetW, sulI, sulII.* CAS effluent (China),	Sulfamethoxazole (50 mg L^{-1}) and tetracycline (16 mg L^{-1}) in PCA. Antibiotics were used to measure the treatment efficiency on resistant and total bacteria. Standard curves by plasmid carrying resistance; Results compared with DNase processing.	UVC radiation (80 mJ cm^{-2} UV dose). - Total inactivation (total and resistant bacteria) in 80 min; - Total removal of ARGs not reached; - UVC promotes aptosis mechanism.	(Zheng et al. 2017)
16S rRNA, *intI1, sul1, tetG.* CAS effluent (China),	Plasmid from positive control used for standard curves in qPCR. Applied Biosystems 7500 qPCR detection system.	UV_{254} radiation (12,000 mJ cm^{-2} UV dose). - Partial removal (2.0-2.5 log reduction) of ARGs.	(Zhuang et al. 2015)

LBA: Luria Bertani agar; TBX: tryptone bile X-glucuronide agar; TSA: tryptic soy agar; m-FC: fecal coliform agar; S&B: Slanetz and Bartley agar; DW: distilled water; CAS: conventional active sludge; MBR: Membrane bioreactor; GO-TiO_2: Graphene oxide doped TiO_2.

1.5 Ultrafiltration process

Micro-, Ultra-, Nano-filtration and Reverse Osmosis are pressure-driven separation processes involving different membrane pore sizes and transmembrane pressures (TMPRs). A membrane is composed of a porous support, intermediate layer and active layer (lowest thickness). According to the pore size of the active layer and molecular weight cut off (MWCO), membranes can retain solids, bacteria, colloids, small organic/inorganic molecules and ions. Defect of active layer compromises the membrane selectivity (Issaoui and Limousy 2019). Ultrafiltration (UF) process is characterized by low TMPR (< 3 bar) and pore size membrane ranging from 1 to 100 nm. UF

is applied for surface water disinfection (Arnal et al. 2004; Kim et al. 2008; Guerra et al. 2012), urban wastewater reclamation (Arévalo et al. 2012; Garcia-Ivars et al. 2017), industrial wastewater treatment/recovery (Murić et al. 2014; Dilaver et al. 2018) and food production (Andrade et al. 2015; Li et al. 2018). Hydrophilicity and hydrophobicity proprieties depend on the active material layer and electrostatic interaction depends on the charge of the active surface layer. The pH of the water feed can neutralize the charge (point of zero charge, PZC); for commercial membrane materials such as γAl_2O_3, the PZC value is 8 (Árki et al. 2019). Flat-sheet, tubular (mono-, multi- channel), hollow fiber or spiral wound (reverse osmosis) are common membrane geometries/shapes. Organic polymeric as polyvinylidene fluoride (PVDF) and inorganic ceramic as Al_2O_3, SiC and ZrO are the most used membrane materials in filtration processes (Kang and Cao 2014; Ji et al. 2015). Ceramic membranes have much greater resistance to chemical, thermal and mechanical stress than polymeric membranes. In all the previous cases, the filtration can be run in dead-end or cross-flow mode. In the first case, all the feed flow is converted in permeate (clean water), while in the second case, feed flow passing through the membrane is split in the permeate and concentrate (usually recirculated in the feed tank or further treated by AOPs).

1.5.1 Membrane fouling

Permeate flux decline is often explained by resistance-in-series model. According to that model, total filtration resistance is the sum of membrane resistance itself, concentration polarization, fouling (reversible and irreversible) and foulants adsorption. In cross-flow filtration the reversible fouling is controlled by high tangential shear (generated at a cross-flow velocity value (CFV) around 3-4 m s^{-1}) (Choi et al. 2005). Fouling formation in membrane filtration processes is influenced by membrane pore size and molecular weight of the material present in the feed. In UWW, biopolymers (MW>10 kDa) of EfOM, especially colloidal proteins polysaccharide, play a main role as foulants in UF (Zheng et al. 2009). The nature of biopolymers depends on the specific biological process (MBR, CAS, nitrification, denitrification). Hydrophobic/transphilic neutrals and acids present in EfOM have a negative co-effect with biopolymers, increasing the fouling formation. While reversible fouling is induced by biopolymers with high molecular weight, irreversible fouling is mainly due to humic substances (non-colloidal) (Filloux et al. 2016). On the other hand, the cake layer can improve the rejection of small molecules as CECs. In particular, different rejection efficiencies of pharmaceuticals (1 µg L^{-1} spiked) is found between fine (1-8 nm pore size) UF treated distilled water (DW) and UWW. The study takes into account the matrix feed, membrane MWCO and pH values in the evaluation of intrinsic resistance, irreversible fouling (recovered by chemical cleaning) and reversible fouling (recovered by physical cleaning) (Garcia-Ivars et al. 2017). In DW tests, hydrophobic and

electrostatic interactions play an important role in CECs rejection, while the second barrier separation (fouling) and solute-solute interactions (EfOM-CECs complexes) in UWW can improve the rejection of CECs (especially the neutral compounds).

1.5.2 Oxidation and physicochemical processes combined with separation processes

In UWW tertiary treatment, operating conditions (Choi et al. 2005; Guerra et al. 2012) and cleaning procedures (with/without the use of chemical) (Shi et al. 2014) represent common tools to deal with fouling phenomena. However, a pre-treatment of feed water makes a difference in fouling mechanism (Winter et al. 2016). Before the UF process, an additional pre-treatment can be designed to minimize the biopolymers concentration in the effluent (Zheng et al. 2014). Coagulation, adsorption, UV, AOPs (H_2O_2/UV, O_3) as pre-treatment to UF in drinking water systems (Jeong et al. 2014; Zhang et al. 2015; Yu et al. 2016; Wang et al. 2018) and UWW reclamation (Lehman and Liu 2009; Jeong et al. 2014; Filloux et al. 2016; Winter et al. 2016; Hamid et al. 2017) are successfully applied to reduce the membrane fouling. However, chemical pre-treatment as chlorine leads to a selection of Cl-resistant-bacteria producing more extracellular polymeric substances than normal bacteria, with a negative effect as the fouling of the membrane (Wang et al. 2019b). On the other hand, some researchers have compared the efficiency of UF, considering directly primary UWW. In particular, biologically treated (SBR, CAS) secondary UWW and chemically treated (coagulation) primary UWW, are used as feed in UF processes (Even-Ezra et al. 2011; Delgado Diaz et al. 2012; Zhao et al. 2019). A train process avoiding the secondary treatment can be feasible in the case of space and time limitations. **Table 1.3** describes and resumes the main parameters used in UF studies combining different processes. Membrane fouling in dead-end UF was effectively minimized through the backwashing (optimizing the duration and the number of cycles) (Delgado Diaz et al. 2012). According to the sample characterization performed by Even-Ezra and collaborators (2011), chemically treated primary UWW can present a TOC value three times higher than the DOC (i.e., TOC after 0.22 µm filtration), whereas those values are similar (ca. 15 mg L^{-1}) for secondary treated UWW. Furthermore the particle size distribution of primary UWW after coagulation changes from the average value of 0.07 to 0.30 µm. Due to the higher presence of solids in chemically treated primary UWW, high cross-flow velocity is reported to enhance the permeate flux more than in secondary UWW (Even-Ezra et al. 2011). Low phosphorous concentration and low pH of chemically treated primary UWW favors the reverse osmosis (RO) flux after the UF process, the mineral precipitation being an important parameter favoring the fouling of RO. Coagulation before UF process is implemented not only to reduce the fouling but also to improve the quality of the effluent. For instance, bacteriophage MS2 is used as model pollutant in full-scale urban

wastewater treatment plant and coagulation step before UF process improved the virus removal but only adjusting the pH at 5-6 (Lee et al. 2017).

Table 1.3. State of the art of ultrafiltration process combined with other processes in water remediation application.

Membrane material (pore size/MWCO and surface area)	**Coupling System**	**Matrix/Note**	**TMPR (bar)**	**Specific permeate flux ($L\ m^{-2}\ h^{-1}\ bar^{-1}$)**	**Reference**
Polyethersulfone flatsheet membrane (5-20 kDa, 28 cm^2)	PAC, Al(III) Fe(III) coagulation, GAC post-treatment	**DW and secondary UWW**. CECs (spiked at 0.5 mg L^{-1}) removal	4.0 (CFV= 0.5 m s^{-1})	21 (pure water)	(Acero et al. 2012)
Polymeric hollow fiber membrane (40 nm, 470 cm^2)	H_2O_2/UV	**Secondary UWW**. Dead-end filtration considering DOC, SUVA, turbidity, N and P removal	0.1-0.6 (42 mL min^{-1} feed)	330 (recording TMPR)	(Benito et al. 2017)
Ceramic multichannel tubular membrane (200 nm, 300 cm^2)	Fenton, coagulation ($FeSO_4$), oxidation (H_2O_2)	**Synthetic UWW**. Critical flux test, DOC, TSS removal	1.2 (CFV= 2.0 m s^{-1})	43-255 (sustainable flux)	(Chiu and James 2006)
Polymeric hollow fiber membrane (30 nm, 930 cm^2)	Coagulation by aluminium polychloride	**CAS and primary settled (coagulation) UWW.** Dead-end filtration (recording TMPR), backwashing	0-0.36	2.5-39.0	(Delgado Diaz et al. 2012)
PVDF tubular membrane (25-100 kDa, 43 cm^2)	Coagulation by ferric chloride ($FeCl_3$)	**Secondary UWW from SBR and primary settled UWW.** UF effluent successively treated by RO (12 bar)	1.0 (Re= 620-2,900)	ca. 100 and 500	(Even-Ezra et al. 2011)
PVDF hollow fiber membrane (40 nm-150 kDa, 60 cm^2)	Anion exchange, O_3, H_2O_2/UV	**Secondary UWW.** Dead-end filtration, unified membrane fouling index	<1.0	50-100 x bar	(Filloux et al. 2016)
Ceramic multichannel tubular membrane (1, 5 and 8 kDa/1, 3 and 5 nm, 132 cm^2)	-	**DW and secondary UWW**. CECs (spiked 0.3-1.0 µg L^{-1}) removal. Resistance model	2.0 (300 L h^{-1} feed)	60	(Garcia-Ivars et al. 2017)
γ-Alumina/ZrO_2 tubular membrane (100 nm, 55 cm^2)	O_3 and GAC	**Secondary UWW.** Dead-end filtration, unified membrane fouling index	<1.0 (42 mL min^{-1} feed)	180 x bar	(Hamid et al. 2017)

Table 1.3. State of the art of ultrafiltration process combined with other processes in water remediation application (continued).

Membrane material (pore size/MWCO and surface area)	**Coupling system**	**Matrix/Note**	**TMPR (bar)**	**Specific permeate flux (L m^{-2} h^{-1} bar^{-1})**	**Reference**
Full-scale PVDF hollow fiber membrane (10 nm/150 kDa, 11 m^2)	Coagulation by polyaluminium chloride	**Secondary UWW.** Dead-end filtration, virus removal and pH study	0-2.0	85 x bar	(Lee et al. 2017)
Full-scale ceramic multichannel tubular membrane (100 nm, 25 m^2)	O_3	**Secondary UWW.** Dead-end filtration, NOM removal	0.05-1.50	85-255 x bar	(Lehman and Liu 2009)
Polyamide flatsheet nanofiltration membrane (0.15-0.30 kDa, 75 cm^2)	UV/O_3	**Secondary UWW**. AOP applied only on the concentrate of secondary sludge	4.0	45-35	(Liu et al. 2014)
Ceramic tubular nanofiltration membrane (0.2-0.3 kDa, 3,900 m^2)	O_3	**Secondary UWW.** CAPEX, OPEX analysis and ROSA modelling	5.0 (125 m^3 h^{-1} feed).	25-30 x bar	(Mendret et al. 2019)
α-alumina flatsheet membrane (100 nm, 400 cm^2)	Coagulation polyaluminium chloride	**Primary settled (coagulation) UWW.** Dead-end filtration considering DOC, COD, N removal	0-0.35	42 x bar	(Zhao et al. 2019)

MWCO = Molecular weight cut-off.

Ozonation (O_3) is an effective treatment to degrade colloid NOMs in secondary UWW. For that reason, ozonation as pre-treatment of ceramic UF is implemented in wastewater reuse applications (Lehman and Liu 2009). Due to the relative high cost of the treatment, the ozonation process is feasible only when high quality effluent is required. However, when fouling is reduced, operational cost related to the cleaning mode (backwash with or without chemicals) and pre-coagulation step decreases as well. Lehman and Liu (2009) study shows that the use of the ozonation process (4 mg L^{-1}) on secondary UWW drastically reduces the fouling of UF membrane over four weeks. The pilot system working in dead-end mode (permeate flux of 40 L m^{-2} h^{-1} bar^{-1}) produces a stable TMPR of 3 bar. Biopolymers (40-45 kDa) and humic substances (0.1-5.5 kDa) can be quantified by liquid chromatography coupled with a fluorescence detector. Removal of such substances from secondary UWW are reported in a study comparing

biological active carbon and ozonation as pre-treatment of UF (Hamid et al. 2017). In detail, the UF process cannot remove humic substances due to the large pore size of the membrane, while almost a complete removal of biopolymers can be achieved. On the other hand, ozonation is efficient in the removal of both, reducing reversible and irreversible fouling. However, the DOC content before and after ozonation is similar, meaning that large organic molecules are just break down and not mineralized (Hamid et al. 2017). In another study, a good correlation between fouling phenomena and specific UV absorbance (aromacity indicator) is observed. In this case H_2O_2/UV is selected as pre-treatment of the UF process in order to reduce fouling and operational costs related to the cleaning and maintenance. Despite the TMPR stabilization (dead-end mode setting a flow-rate of 42 mL min^{-1}) is reached in one hour, the main drastic TMPR increase is found in the first 20 min. UV and H_2O_2/UV pre-treatments are reported to extend the filtration operational time before cleaning procedure from 3 min (no pre-treatment) to 9 min (for UV) and to 21 min (for H_2O_2/UV), being 0.2 bar the TMPR starting the cleaning with sodium hypochlorite (Benito et al. 2017). Other AOP (Fenton process) are used as pre-treatment of synthetic UWW before the UF process. In particular, supernatant of Fenton process is filtered by ceramic tubular membrane (200 nm pore size). The maximum TOC removal is reached by Fenton (67%) followed by coagulation with $FeSO_4$ (37%). Critical flux is found to increase from 43 to a value of 258 L m^{-2} h^{-1} by Fenton pre-treatment, critical flux being measured by increasing TMPR until reaching a non-linear relationship with the permeate flux (Chiu and James 2006).

The concentrate destination of pressure-driven processes is an important issue to deal with. Moreover, the recirculation of concentrate in biological compartment can compromise the efficiency of the process (Kappel et al. 2014). Fenton process (Miralles-Cuevas et al. 2017) and ozonation (Liu et al. 2014; Mendret et al. 2019) are used to treat the nanofiltration concentrate. An economic assessment of the ozonation process on nanofiltration concentrate is proposed by Mendret and collaborators (2019). The scheme train proposed by Liu and collaborators (2014) involves the recirculation of O_3 treated-concentrate in secondary treatment compartment. The study shows no residual CECs (antibiotics) in both permeate and concentrate.

1.6 Hybrid technology: photocatalytic membrane reactors

New strategies in fouling control involves the development of a self-cleaning membrane, for instance using photocatalytic oxidation. Photocatalytic membrane reactors (PMRs) technology considers the challenges of increasing the lifetime of the membrane combining oxidation and filtration processes in one step. It results in a cheaper maintenance and lower environmental impact. Moreover, the concentrate quality is improved and the problematics linked to the disposal are reduced. Slurry and immobilized catalysts are the most used configurations in PMR

applications (Ganiyu et al. 2015; Molinari et al. 2017). **Table 1.4** describes and resumes the main parameters used in PMR studies.

Table 1.4. State of the art of PMR in water remediation application.

Material support, geometry (pore size)	**Photocatalyst/ Radiation source**	**Pollutant and Matrix[a]**	**TMPR (bar); Feed (mL min^{-1})**	**Specific permeate flux (L m^{-2} h^{-1} bar^{-1})**	**Reference**
γ-Alumina tubular, D=1 cm L=15 cm (0.005-0.010 μm)	TiO_2 / UVA	Methylene orange	- ; 3	7-12 x bar	(Athanasekou et al. 2012)
γ-Alumina tubular, D=1 cm L=15 cm (0.001-0.010 μm)	GO-TiO_2 / UV-Vis	Methylene blue; Methylene orange	1.15-19.1*; 0.3 (dead-end); 1.5 (cross-flow)	30-40	(Athanasekou et al. 2014)
γ-Alumina tubular, D=1 cm L=15 cm (0.010 μm)	N-TiO_2; GO-TiO_2 / UVA	Methylene blue; Methylene orange	4.6; 3.7	38.2; 34.3	(Athanasekou et al. 2015)
Cellulose, polyamide, anodized alumina disk, D=2.5 cm (0.220 μm)	GO or reduced GO / -	Water vapor and gas permeability	0.001-0.800	50	(Athanasekou et al. 2017)
Alumina and TiO_2 disk, D=2.1 cm (0.100 μm support, 7 nm composite)	TiO_2 / UV_{365}	**Batch**: MC-LR cyanotoxin, *E. coli*; methylene blue, creatinine. **Dead-end**: DOC	2.0 (dead-end); 0.28	6.71	(Choi et al. 2007)
TiO_2 tubular, D=1 cm L=25 cm (0.008 μm)	Slurry TiO_2 / UVC and H_2O_2 / UVC	Oxitetracycline in secondary UWW	1	110 (DW)	(Espíndola et al. 2019)
PVDF disk, D=4.7 cm (0.220 μm)	TiO_2 / UVA	Methylene blue; Ibuprofen; Diclofenac.	2.0 (dead-end)	1.2	(Fischer et al. 2015a)
Polyethersulfone disk, D=4.7 cm (0.450 μm)	TiO_2 nanotubes / UVA	Diclofenac	2.0 (dead-end)	9.6	(Fischer et al. 2015b)
α-Alumina and quarz fiber filter disk, D=5.0 cm (1.0 μm)	TiO_2; N-TiO_2; S-TiO_2 / UVA	Acid Orange 7	0.5 (dead-end); 13	400	(Hatat-Fraile et al. 2017)
Hydrophilic polyethylene fiber module, 500 cm^2 (0.100 μm)	Slurry TiO_2 / UV_{352}	DOC in secondary UWW	0.06-0.12 (dead-end)	200-400	(Ho et al. 2009)
SiC disk, D=3 cm (cut) (0.360 μm)	TiO_2; SiO_2-TiO_2 / UVA	Methylene blue	0.2 (dead-end)	2,100-3,600	(Huertas et al. 2017)

Table 1.4. State of the art of PMR in water remediation application (continued).

Material support, geometry (pore size)	**Photocatalyst/ Radiation source**	**Pollutant and Matrix[a]**	**TMPR (bar); Feed (mL min^{-1})**	**Specific permeate flux (L m^{-2} h^{-1} bar^{-1})**	**Reference**
Hydrophilized polyethylene Hollow fiber, 60 cm^2 (0.400 μm)	TiO_2 / UVA	*E. coli* in secondary UWW	0.020 (dead-end)	50,000	(Jiang et al. 2018)
Cellulose acetate flat-sheet, 27 cm^2 (30 kDa)	Slurry TiO_2 / UVC	UV_{254}, DOC (ultrapure water spiked with humic acid)	1.0	150	(Lee et al. 2002)
Glass fiber filter disk, D=4.7 cm (0.500 μm)	Ag-TiO_2 / Simulated solar light: (Xe-lamp with filter for λ < 290 nm)	Methylene blue; *E.Coli*	7.0 (dead-end)	0.5	(Liu et al. 2012)
γ-Alumina tubular, D=1 cm L=15 cm (0.005 μm)	m-TiO_2 / Vis light	Methylene blue; Methylene orange	2.5	33	(Moustakas et al. 2014)
Polypropylene Hollow fiber, 140 cm^2 (0.200 μm)	Slurry carbon modified TiO_2 / UVA	Methylene blue	1.0	120	(Mozia et al. 2007)
Polypropylene Hollow fiber, 127 cm^2 (0.200 μm)	Slurry TiO_2 / UVA	Acid yellow 36	1.0	120	(Mozia et al. 2009)
Polyethersulfone flat-sheet, 15 cm^2 (10 kDa,)	Slurry TiO_2 / UVC	UV_{254}, DOC in primary and secondary UWW	2.0	50-120	(Mozia et al. 2014)
PES Flat-sheet, 140 cm^2 (15-110 kDa,)	Slurry commercial TiO_2 (including P25) / UVC	Dextrans (5-110 kDa)	1.0-3.0	50-700	(Mozia et al. 2015)
γ-Alumina tubular, D=1 cm L=15 cm (0.005 μm)	TiO_2; Alginate-TiO_2 / UVA	Methylene orange	14.0	6.0	(Papageorgiou et al. 2012)
Cellulose ester disk, D=4.7 cm (0.450 μm)	GO-TiO_2 / UV-Vis	Methylene orange	- (dead-end); 0.25	90 x bar	(Pastrana-Martínez et al. 2015)
Stainless steel fiber disk, D=15 cm (2.0 μm)	TiO_2 nanotubes / UVA	Cimetidine, acetaminophen, sulfamethoxazole, propranolol.	0.001 (dead-end)	10	(Ramasundaram et al. 2013)

Table 1.4. State of the art of PMR in water remediation application (continued).

Material support, geometry (pore size)	**Photocatalyst/ Radiation source**	**Pollutant and Matrix[a]**	**TMPR (bar); Feed (mL min^{-1})**	**Specific permeate flux (L m^{-2} h^{-1} bar^{-1})**	**Reference**
PVDF disk, D=2.5 cm (0.050 μm)	TiO_2 / UV_{254}	ARB&ARGs in secondary UWW	1.4 (dead-end)	875 (PVDF), 1,375 (TiO_2)	(Ren et al. 2018)
γ-Alumina tubular, D=1 cm L=15 cm (0.005-0.010 μm)	TiO_2 / UVA	Methylene blue	14.8-1.5; 2.5-5.0	0.64	(Romanos et al. 2012)
γ-Alumina tubular, D=1 cm L=15 cm (0.005 μm)	TiO_2 / UVA	Methylene blue	14.8;1.5	0.78	(Romanos et al. 2013)
TiO_2 tubular, D=1 cm L=25 cm (0.003 μm / 5 kDa)	UVC Slurry TiO_2 / UVC H_2O_2 / UVC	DOC in secondary UWW	1.0	60-48	(Szymański et al. 2018)
γ-Alumina disk, D=0.47 cm (0.200 μm)	TiO_2 / UV_{365}	Direct black 168	0.5 (dead-end)	82	(Zhang et al. 2006)

[a] = distilled water where not specified.

1.6.1 Slurry systems

Slurry systems have greater efficiency in photocatalysis, the effective surface area being higher than in the immobilized catalyst configuration. However, permeance can be compromised by the accumulation of photocatalyst on the surface (photocatalyst cake layer) generated during the separation/recovery step. Moreover, the catalyst in suspension generates abrasion of membrane, especially at high cross-flow velocity filtration (Mozia et al. 2015; Issaoui and Limousy 2019). The majority of the slurry systems present in the scientific literature involves polymeric membranes due to their low cost and high surface area concerning ceramic membranes. However, since polymeric membranes are highly damaged by oxidants and UV light, the majority of the literature studies investigate slurry systems where UV radiation is not performed in the membrane module. The main configuration adopted by researchers is the batch system, where the concentrate and permeate are recirculated in order to keep constant the catalyst in suspension (Mozia et al. 2009, 2014, 2015; Morawski and Mozia 2016; Szymański et al. 2018; Espíndola et al. 2019). Only few authors report studies of hybrid system in continuous mode (Lee et al. 2002; Ho et al. 2009).

In particular, polymeric hollow fiber submerged membrane modules are used for dead-end filtration of pretreated secondary UWW ($FeCl_3$ coagulation and UVC/TiO_2-P25 photocatalysis) (Ho et al. 2009). No info about catalyst retaining and membrane clogging is given since a settling tank after photocatalysis is reported to remove the majority of the catalyst. Despite pre-coagulation increases the photocatalytic efficiency (during three hours) in DOC removal from 30% (no pre-coagulation) to 80% (pre-coagulation), effluent pH decreases from 7 to 3.5 (lower than the limit of discharge) and turbidity increases from 4 to 12 NTU. However, the critical flux of membrane after photocatalysis process (measured by flux stepping method) is found to increase from 25 to 45 L m^{-2} h^{-1} (Ho et al. 2009). The antifouling effect of phtocatalytic process is found also in the treatment of synthetic water containing humic acids (Lee et al. 2002).

Another study reporting the treatment of secondary UWW by PMR UF (permeate and concentrate recirculation) shows a fouling reduction during six hours operation (40% increase of permeate flow respect to standard UF) (Mozia et al. 2014). The antifouling effect of photocatalytic UF process is the same when using three different catalyst loads (0.5-1.5 g L^{-1}). The water purification is attributed to physical separation, while improvement in water recovery is associated to an increase of hydrophilicity of the membrane, the external surface being covered by a porous TiO_2 layer (Mozia et al. 2014). A study from the same research group reports the effect of sequential UV radiation and UF ceramic monochannel membrane in secondary UWW purification. A 40, 30 and 20% permeate flux decrease is found during six hours of filtration (6 m s^{-1} CFV) coupling the system respectively with UVC, UVC/H_2O_2, UVC/TiO_2. The contribution to DOC removal by TiO_2 adsorption, photolysis, UVC/H_2O_2 and UVC/TiO_2 (without UF) is respectively 20, 20, 58 and 55%. When UV/H_2O_2 and UVC/TiO_2 are combined with UF, both reach 60% removal of DOC from the permeate. However, in five hours of treatment, the ecotoxicity (*T. platyurus* mortality) of the permeate increases with respect to the initial feed for both the combined UF-AOPs (Szymański et al. 2018). The efficiency of PMR in slurry can be measured considering the removal of a model pollutant. Dyes are often chosen as target contaminants due to their easy quantification (Mozia et al. 2007, 2009). However the antibiotic oxytetracycline (spiked at 5 mg L^{-1}) is used as model pollutant in UVC-driven PMR system treating secondary UWW (Espíndola et al. 2019). The treatment time to reach the total removal of the antibiotic is 15 min considering the optimized catalyst load (1.5 g L^{-1}), while a reduction of ca. 50% of DOC in the permeate is achieved after five hours of process. It should be noted that the DOC removal in the spiked UWW is also influenced to the antibiotic mineralization. No significant differences are found in terms of flux deterioration between UVC/UF, UVC/TiO_2/UF and UVC/H_2O_2/UF processes.

1.6.2 Immobilized systems

Despite the immobilized-catalyst technology has high potential implication in water remediation, several operational problems have denied the real scale implementation. In fact, the deposition of photocatalyst on the surface of the membrane decreases the initial pore size, affecting negatively the permeance property. Only in some cases, such as a carbonaceous modified TiO_2, due to its high hydrophilicity, improves the permeance of the photocatalytic membrane with respect to the raw membrane (support). This is attributed to the fact that nanoparticles diameter is smaller than the pore size of the membrane (active layer), the catalyst deposition occurring in the internal part of the membrane (Moustakas et al. 2014). Ceramic membranes represent an ideal material for catalyst immobilization techniques involving calcination and high temperature. Moreover, UV light, strong oxidant as hydroxyl radicals (generated during photocatalysis) and H_2O_2 or acids (used during the cleaning mode) do not damage the membrane material. A configuration of PMRs already patented (Falaras et al. 2010) involves a tubular transparent housing. The filtration is performed from outside to inside of the tubular double-layer photocatalytic membrane. The light irradiation occurs from both outside and inside the membrane (only for monochannel membrane), the UVA-LEDs being used as internal irradiation source (Romanos et al. 2013; Athanasekou et al. 2015). The abovementioned PMR configuration has been tested with synthetic water containing dyes (Papageorgiou et al. 2012; Romanos et al. 2012), and no studies are available in the literature on secondary UWW considering disinfection and antibiotics removal efficiency. The energy consumption considering the light source and the pump is estimated to be comparable with conventional nanofiltration (1 nm pore size). The possibility to reduce the cost related to the light irradiation has been extensively investigated by the development of photocatalysts being activated under solar light. The use of anion and metal doped TiO_2 or carbon composite is an interesting way to achieve a good photocatalytic efficiency using visible light in PMR technology (Athanasekou et al. 2014; Moustakas et al. 2014). However, the difficulties in the development of doped or composite catalysts and the reduced photocatalytic efficiency under visible light with respect to UV light make the industrial implementation a complicated challenge. Several catalyst immobilization methods have been proposed by the literature (Athanasekou et al. 2012; Romanos et al. 2013). In particular, chemical vapour layer-by-layer deposition and nanoparticle growth chemical vapour deposition are reported as efficient methods to immobilize TiO_2 on alumina membranes (Athanasekou et al. 2012). More simple and up-scalable techniques of photocatalyst deposition, as dip-coating in a sol-gel, is used for fabricate composite membranes active in UV and visible light (Athanasekou et al. 2014). However, lower control on catalyst layer formation is achieved. In sol-gels dip coating technique the pore size of the membrane plays an important role in the immobilization of photocatalyst. In particular, 10 nm

is reported to be the optimal pore size membrane to host partially reduced graphene oxide/TiO_2 and bare TiO_2, while 5 and 1 nm pore size can generate sparse deposition of both catalysts via dip coating (Athanasekou et al. 2014).

1.7 Framework of the PhD thesis: the ANSWER project

This PhD thesis is developed in the framework of the Innovative Training Networks (ITN), founded by Marie Skłodowska-Curie grant agreement no. 675530 (ANtibioticS and mobile resistance elements in WastEwater Reuse applications: risks and innovative solutions, ANSWER), in a collaboration between Adventech Lda. (beneficiary of the project) and FEUP.

The ANSWER project (http://www.answer-itn.eu/) hired a total of 15 early stage researchers (ESRs) in 2016, with different scientific backgrounds to achieve specific objectives of the project. ANSWER scientific activities are summarized in technical Working Packages (WPs). ESRs' projects focus the research on antibiotic resistance in urban wastewater field on different point-of-views, relating different science fields (biology, chemistry, engineering, modelling). In order to make uniform, comparable and compatible the research of all the ESRs, specific A&ARB&ARG were selected, based on literature findings and other relevant ongoing projects.

My particular ESR project is related with a WP entitled "innovative technological solution for the removal of antibiotics, antibiotic resistant bacteria and antibiotic resistance genes (A&ARB&ARGs) from UWW", aiming at developing an innovative PMR for the removal of A&ARB&ARGs and the upscale cost analysis of the investigated technologies. Multidisciplinary and inter-sectoral approach is mandatory in order to achieve the main objectives and ANSWER goals. Moreover, ITN recommended that each ESR must be enrolled in a PhD programme to pursue the PhD degree. My contract at Adventech had a duration of three years (02/2016-01/2019). During this period: (i) I have completed the courses of PDEQB – the Doctoral Programme in Chemical and Biological Engineering at FEUP; (ii) I spent the first period at Adventech (8 months), doing bibliographic analysis and designing the PMR; (iii) I did a secondment (6 months) at University of Salerno (Italy) to study the catalyst immobilization techniques and perform preliminary tests with photocatalytic membranes; (iv) I did a research period at FEUP (12 months) and another at Universidade Católica Portuguesa (2 months), performing lab tests and literature analysis on A&ARB&ARGs detection; and (v) finally my last period of contract (8 months) was spent between FEUP and Adventech to perform pilot-scale studies.

Training and dissemination/communication activities were also conducted during the project. Training WP deals with the acquisition of specific skills and tools by the ESRs in order to fulfill the specific individual objectives. For that reason, several training events (TEs) are organized during the entire project lifespan. **Table 1.5** shows the TEs I have participated.

Table 1.5. Topic, place and date of Training Events (TEs) selected during the PhD course.

Main Training Events & Topics	Lead Institution	Date
Summer School: Wastewater reuse practices - case studies; Chemistry and fate of contaminants of emerging concerns and their transformation products in wastewater reuse systems; Bacterial diversity and eco-physiology in water and soil; Risk assessment of antibiotic resistance genes transfer to soil and sludge environments; Dynamics of antibiotic resistance in crop production systems/Uptake of trace elements by crops; Biotic/abiotic factors stimulating horizontal gene transfer in aquatic microbiomes; Advanced wastewater treatment processes currently applied at pilot-scale; Ethics/Bioethics in research.	Spanish National Research Council, **Spain.**	13-23 June 2016
TE-A: Statistics and models for environmental data; Molecular risk characterization; Writing and publishing research. One-day guided tour to urban wastewater treatment plant.	Joint event by Technische Universität Dresden and Karlsruhe Institute of Technology, **Germany**.	12-16 September 2016
TE-D: Wastewater microbiota and the effects of treatment processes; Fostering entrepreneurship - from business models to clients. Field trip: urban wastewater treatment plant.	Joint event by Adventech and Universidade Católica Portuguese, **Portugal.**	5-7 July 2017
TE-E: Wastewater treatment by advanced technologies and risk assessment framework; First ANSWER Workshop "Risk prognosis of environmental and public health aspects of antibiotics, antibiotic resistant bacteria and antibiotic resistance genes".	Joint event by Università di Salerno and Istituto superiore di Sanità, **Italy.**	4-6 September 2017
TE-G: Microbiology in wastewater treatment; Design criteria for wastewater treatment plants; Horizontal resistance gene transfer in soil; Bacterial fingerprinting in wastewater by next generation sequencing.	Joint event by Technische Universität Wien, AGES and WABAG. **Austria**.	26-27 April 2018
TE-H: Environmental/human health risk assessment of antibiotics; Working in academia-policy-business and how to secure a good job; Second ANSWER Workshop "Modelling and risk assessment tools towards sustainable wastewater reuse".	KWR, **Netherlands**.	18-21 June 2018
Final Conference: Presentation of final results and Science Slam for young scientists.	University of Cyprus, **Cyprus**.	9-12 October 2018

Several documents (plans and reports) are filled and updated/modified (every six months) at any stage of the researchers commitment. Training needs, research objectives, research management (i.e. anticipation of journal publications, conference participation, workshop and courses attendance, scientific publications and non-technical divulgation) and long-term career objectives

are discussed. In particular, ANSWER ensures that peer-reviewed scientific papers are published in open access. Participations at conferences, scientific newsletters and non-technical divulgation activities are also mandatory for ESRs during the project. Additional workshops and courses attendance were selected to improve the research skills and enrich my knowledge of the current state of the art. In this framework, I took lectures (and I was also involved in the organization) in the 2nd Summer School on Environmental Applications of AOPs of the European PhD School on AOPs held in Porto in July 2017. **Table 1.6** summarizes my divulgation activities, describing audience details, place and date of the event and dissemination material distributed.

Table 1.6. Description of dissemination/divulgation activities performed so far in the framework of ANSWER.

Type of activity	Date	Short description
School visit	23/11/2016	ANSWER event at "ICS Salvemini" Battipaglia (SA), Italy consisted in 3 lectures (each 20 mins). 50 students (14 year old) were present. Poster, brochures and presentation were developed.
Radio talk	08/02/2017	Conversation (lasted 8 min) on "Radiocastelluccio", a local radio emitting in Salerno province, Italy.
School visit	25/02/2017	40 min presentation at "ICS Gaiter", Caprino Veronese (VR), Italy. 50 students (13 years old) were present. Poster, brochures and presentation were developed.
Articles in newspapers	27/02/2017	Three Italian web newspapers (Sevensalerno, Mezzostampa, Terraoggi) published my press release. An Italian local journalist interviewed me and an article was published (Metropolis).
Cafè scientifique	30/11/2017	One hours talks at "E-learning Café Asprela", Porto. 20 students (25-30 years old) participated actively on the discussion. Leaflets (containing short introduction about ANSWER project and the organizers of the event) were distributed.
School visit	07/12/2017	20 min presentation at "CLIP (the Oporto international school)", Porto. 10 students (16-17 years old) were present and ANSWER brochures were disseminated.

1.8 Objectives and thesis outline

The aim of the PhD thesis is to extend the knowledge on TiO_2-based photocatalysis and photocatalytic ultrafiltration processes as tertiary treatment of urban wastewater (UWW). Special emphasis is given to the presence of antibiotics and antibiotic resistance issue in water. The adopted approach involves lab scale studies, technology scale-up and pilot scale studies. In

particular, photocatalysis involving UVA-LEDs, is first assessed to treat small volumes of UWW and successively implemented in a bigger configuration (adopting ultrafiltration) with higher treatment capacity. The thesis is organized in four chapters. The current chapter provides a state of the art of photolysis and photocatalysis applications in antibiotics removal, as well as antibiotic resistant bacteria and antibiotic resistance genes inactivation in water and wastewater. Moreover, the literature on ultrafiltration (combined with oxidation and physico-chemical processes) and photocatalytic membrane reactor (PMR) process is revised. Considering the lack of information related to the treatment of UWW using PMR (catalyst immobilized configuration), the main operating parameters (i.e. transmembrane pressure, cross-flow velocity, UV irradiance) of different studies on polluted water are considered to aim UWW treatment, considering for the first time antibiotic and antibiotic resistance issue. Chapter 2 describes lab scale studies as starting point for pilot-scale study. For the first time, UVA-LEDs photocatalysis (slurry process) is tested in the treatment of secondary UWW, considering kinetic degradation of antibiotics and implication on indigenous antibiotic resistant bacteria (immediately and after three-days storage). In chapter 3, the main steps to design and realize a PMR (involving TiO_2-P25 coated membrane and UVA-LEDs) to treat UWW are listed. Probes selection, material choices and specific design decision during the development of PMR are discussed and defended. The results obtained by using the developed PMR in UWW treatment are also presented. In particular, the designed pilot equipment is assessed in terms of antibiotic oxidation and bacteria rejection at the same time. Moreover, a basic economic analysis for the evaluation of PMR scale-up feasibility is given. Finally, chapter 4 shows the main conclusions of the work, giving an overview of the results and suggestions for future work.

Chapter 2. Lab scale batch reactor

The aim of the present chapter is to assess the TiO_2-photocatalytic (slurry) process as tertiary treatment of urban wastewater. Simultaneous removal of antibiotics and antibiotic resistant bacteria (ARB) from secondary urban wastewater is presented. Azithromycin, trimethoprim, ofloxacin and sulfamethoxazole were selected as model antibiotics because they represent distinct classes and are among the most used antibiotics to treat human and veterinary infections. The novel aspects of this study include the first evaluation of the antibiotics and ARB removals from real urban wastewaters using UVA-LEDs in the TiO_2-photocatalytic treatment. The scavenging effect of methanol as a carrier solvent in photocatalytic kinetic parameters was also addressed. This chapter is based on the scientific publication "Heterogeneous photocatalysis using UVA-LEDs for the removal of antibiotics and antibiotic resistant bacteria from urban wastewater treatment plant effluents" published on Chemical Engineering Journal 367 (2019) 304–313. In particular, part of antibiotic resistance analysis are carried out during the research period at biotechnology school of "Universidade Católica do Porto".

2.1 Materials and methods

2.1.1 Chemicals and materials

Azithromycin (AZT, CAS number 117772-70-0), trimethoprim (TMP, CAS number 738-70-5), ofloxacin (OFL, CAS number 82419-36-1), sulfamethoxazole (SMX, CAS number 723-46-6), clindamycin (CLI, CAS number 18323-44-9), and deuterated internal standards (azithromycin-d3 and ofloxacin-d3), all with > 98 % purity, were purchased from Sigma-Aldrich. A methanolic stock solution containing AZT, TMP, OFL and SMX (150 mg L^{-1} each) was prepared to be used in the spiked experiments.

TiO_2 (80% anatase, 20% rutile) was supplied by Evonik Degussa GmbH (P25). MeOH and acetonitrile (MS grade) were obtained from VWR International (Fontenay-sous-Bois, France). Ethanol (HPLC grade) was acquired from Fisher Scientific (Leicestershire, UK), whereas formic and sulfuric acid were obtained from Merck (Darmstadt, Germany). Oasis® HLB (Hydrophilic-Lipophilic Balanced) cartridges (150 mg, 6 mL) used for sample preparation, were purchased from Waters (Milford, MA, USA). MilliQ water system provided ultrapure water with resistivity > 18 MΩ cm at 25 °C.

The culture media Tryptone Bile X-Glucuronide Agar (TBX) and Plate Count Agar (PCA) were provided by Sigma-Aldrich, and m-Enterococcus Agar (m-Ent) was supplied by Difco (Maryland, USA).

2.1.2 Wastewater sampling and characterization

Secondary urban wastewater (UWW) was collected at the effluent of the secondary settling tank of an urban wastewater treatment plant (UWWTP) located in Northern Portugal (average monthly flow of 25,707 ± 3,570 m^3 day^{-1}), in three sampling occasions: September-December 2017 (spiked tests), January-March 2018 (non-spiked tests), April-May 2018 (disinfection tests). Wastewater characteristics can be found in **Table 2.1**.

Table 2.1. Wastewater characterization.

Parameter	Value (Mean ± SD)
pH*	7.2 ± 0.2
Conductivity (μS cm^{-1})*	706.9 ± 86.3
Total suspended solids (mg L^{-1})*	33.5 ± 14.7
Volatile suspended solids (mg L^{-1})*	31.4 ± 15.5
Biological oxygen demand (mg L^{-1})*	31.3 ± 23.9
Chemical oxygen demand (mg L^{-1})*	90.3 ± 45.2
Dissolved organic carbon (mg L^{-1})	12.6 ± 4.3

***** = monthly (January 2018) average values provided by the UWWTP manager.

2.1.3 Experimental setup, radiation measurements and absorption-scattering model

The lab-scale batch experiments were run in a 150 mL reactor (5 cm out diameter, 3.8 cm inner diameter and 16.0 cm height at maximum filling, **Figure 2.1a**). Four UV high intensity LEDs (working at 9 W) and the respective heatsink/fan cooling systems (1 W) were placed on four lateral sides of a cubic box containing the annular photocatalytic reactor (**Figure 2.1a**). Each LED (15.5 mm × 23 mm) had a dominant emission line at 381 nm (**Figure 2.1b**) and long service life, with an intensity above 70% after 10,000 h work. The distance between each LED and the reactor was fixed at 3.3 cm (at a height of 10 cm).

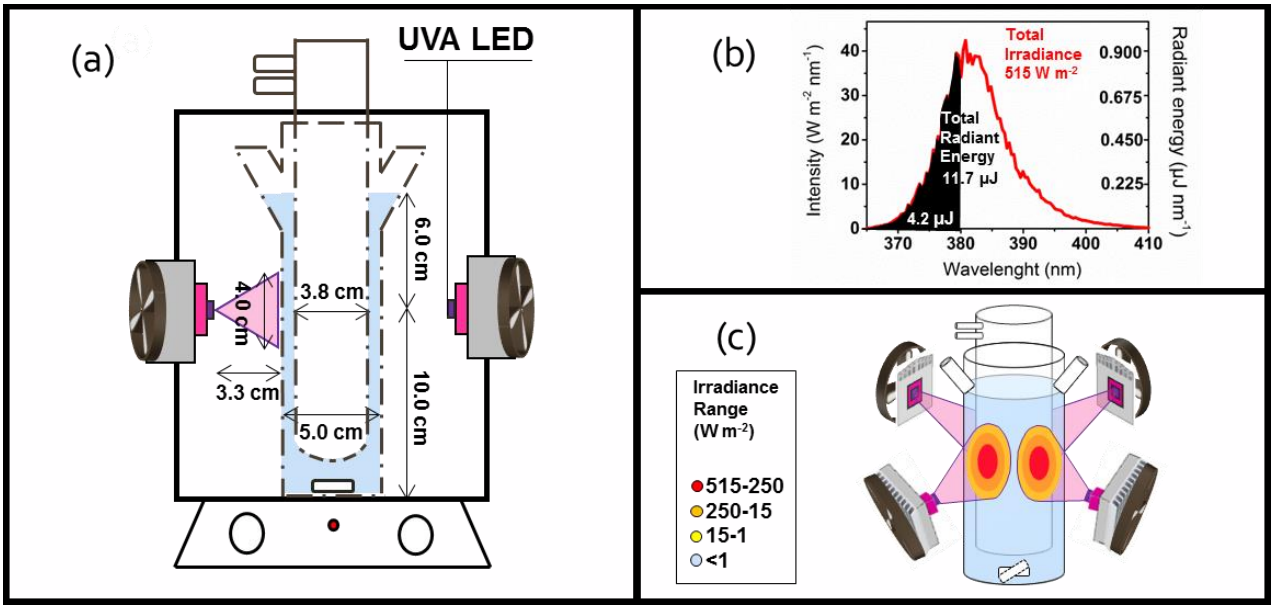

Figure 2.1. Annular photocatalytic reactor used in the experiments (a), LED light spectrum (b) and LED irradiance range (c).

Three main radiation configurations were tested, namely switching on a single LED, two LEDs placed perpendicularly to each other, or the four LEDs (**Figure 2.2a-c**).

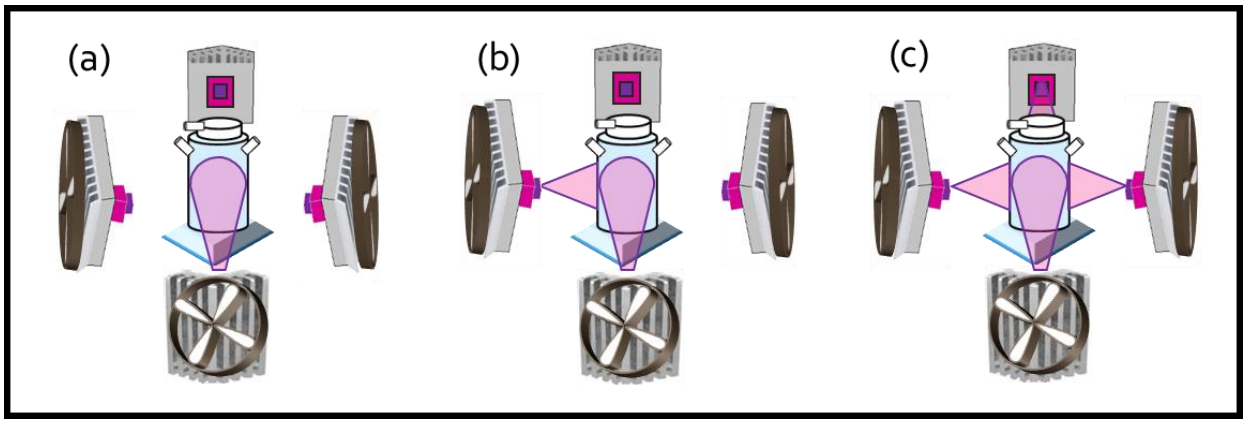

Figure 2.2. Schematic representation of the photocatalytic configurations involving one (a), two (b) and four (c) LEDs.

All the radiation measurements were performed using a spectrometer (Ocean Optics USB2000+) equipped with cosine corrector and the software *Spectra Suit* with the help of my collegue Nuno Moreira (FEUP). The spectral intensity of radiation (W m^{-2} nm^{-1}) and the spectral emitted radiant energy (μJ nm^{-1}) of each LED were measured with the probe at 3.3 cm distance from the LED (i.e., at the reactor wall). The emitted radiant energy (*E*) of a specific wavelength interval was calculated according to **Eq. 2.1**:

$$\boldsymbol{E}\ (\mu\boldsymbol{J}) = \int_{\boldsymbol{\lambda_{min}}}^{\boldsymbol{\lambda_{max}}} \boldsymbol{E_\lambda}\ \boldsymbol{d\lambda} \qquad (\boldsymbol{Eq.\ 2.\ 1})$$

where λ_{min} and λ_{max} define the interval of integration and E_λ is the spectral emitted radiant energy at a given λ.

The total emitted radiant energy is calculated using λ_{min} = 365 nm and λ_{max} = 430 nm in **Eq. 2.1**. The fraction of emitted radiant energy activating TiO_2 is calculated using λ_{min} = 365 nm and λ_{max} = 380 nm in **Eq. 2.1**.

Moreover, the irradiance (W m^{-2}) was recorded by varying the position of the probe in a parallel plane at the same 3.3 cm distance. The UV dose provided by each single LED (in the red zone of **Figure 2.1c**) is given by the time of light exposure multiplied by the average value of irradiance

(considering the irradiated surface). The average value of irradiance (I_a) at the red zone (**Figure 2.1c**) is calculated according to **Eq. 2.2**:

$$\boldsymbol{I_a\ (W\ m^{-2}) = \frac{\int_0^r I_r\ \ A_r\ \ dr}{\int_0^r A_r\ \ dr}} \qquad (\boldsymbol{Eq.\ 2.2})$$

where r is the radius defining the interval of integration of the circle, I_r is the irradiance at position r respect to the centre of the circle, A_r is the circle area function of the radius.
For computational simplicity, the irradiance distribution on external cylindrical surface of the reactor (in the red zone, **Figure 2.1c**) is supposed to be the orthogonal projection of the irradiance measured on the plane. Considering a linear gradient between maximum and minimum irradiance in the red zone (**Figure 2.1c**), I_a is calculated for r = 1 cm.

Optical thickness (τ) at 10 cm of height (central point of red zone, **Figure 2.1c**) is calculated through **Eq. 2.3**:

$$\tau = \delta\ C_{cat}\ \beta \qquad (\boldsymbol{Eq.\ 2.3})$$

where δ is the thickness of wastewater being irradiated, C_{cat} is the catalyst load and β is the spectral average value of extinction coefficient of the photocatalyst (β) at the centre of red zone (**Figure 2.1c**).

Considering a neglected irradiance gradient across the wastewater (low thickness annulus), β is only function of radiation field and specific extinction coefficient values (β_λ) of photocatalyst in water (Salaices et al. 2002; Satuf et al. 2005).

The reactor configuration is modelled as a thin-film annular photoreactor (thickness of annulus, δ = 0.005 m, considering radius and thickness of internal and external walls) but using external light source (Li Puma and Brucato 2007). UVA light absorption of external wall (PYREX®) is negligible and spectral intensity after the external wall is expected to be similar.

2.1.4 Degradation of antibiotics

UWW samples were spiked with the antibiotics following a procedure described elsewhere (Arlos et al. 2017). Briefly, 0.1 mL of the methanolic stock solution (150 mg L^{-1} of each antibiotic) was added to an empty volumetric flask, the residual solvent was evaporated using a nitrogen flow, and 150 mL of UWW were added into the flask, which was stirred and sonicated for 30 s, giving an initial concentration of 100 µg L^{-1} of each antibiotic in the spiked UWW. Dissolved organic carbon (DOC) analyses were performed to confirm MeOH evaporation, based

on the comparison of the values obtained in spiked and non-spiked UWW samples. Similar values were expected, since the contribution of the spiked antibiotics to the DOC content was considered to be negligible (1.9%).

Different TiO_2 loads (0.10, 0.25, 0.50, 1.00, 1.50, and 2.00 g L^{-1}) and number of LEDs (1, 2 and 4 LEDs) were investigated for the removal of antibiotics in spiked UWW, under continuous magnetic stirring and air-sparging (3.5 L min^{-1}). After a 30 min dark adsorption period in the reactor, an aliquot of 15 mL was withdrawn for DOC analysis and the lamp jacked was inserted. Photocatalytic degradation was studied at regular treatment times (0, 15, 30, 60, 120 and 180 min), by withdrawing 1 mL aliquots from the reactor. These aliquots were centrifuged at 13,500 rpm during 10 min, being the supernatant analysed by Ultra-High-Performance Liquid Chromatography with tandem Mass Spectrometry (UHPLC-MS/MS). Photolysis was evaluated during 180 min, using the conditions described above in the absence of TiO_2. For the scavenging study, 75 µL of MeOH was added to the spiked UWW sample (reaching a MeOH concentration of 0.4 g L^{-1}, 0.05% v/v, equivalent to ca. 150 mg L^{-1} of DOC).

Photocatalytic experiments using real non-spiked UWW were carried out with 4 LEDs and 1.00 g L^{-1} of catalyst. Dark adsorption on TiO_2 suspended in UWW was evaluated in 1 L glass bottles covered by aluminum foil. After 24 h of adsorption-desorption equilibrium, a volume of 135 mL of UWW was transferred to the annular reactor, where photocatalytic experiments took place. Different treatment times (0, 5, 10, 15, 30, 60, and 120 min) were tested in distinct assays, since the volume required of filtered treated samples (1.2 µm glass microfiber filters GF/C, 47 mm; Whatman™, UK) for solid phase extraction (SPE) was 100 mL. All assays were performed in triplicate.

2.1.5 Disinfection studies

Disinfection of real UWW was investigated after 60 min of photocatalytic treatment, using wastewater samples collected in different days. Freshly collected secondary UWW was stirred for 30 min in 1 L bottles in the dark (with and without TiO_2) and aliquots of 135 mL were loaded into the annular reactor. The same operating conditions described in section 2.1.4 for the non-spiked experiments were used in disinfection studies (4 LEDs and 1.00 g L^{-1} of catalyst). Control experiments in the absence of catalyst (photolysis) and in the absence of light but with catalyst (dark adsorption) were carried out for the same 60 min. Volumes of 1 or 10 mL were collected after 60 min of photocatalytic treatment. The potential regrowth of bacteria in photocatalytic treated UWW and in respective controls, after 3-day storage in the dark, and at room temperature

(24 °C), was evaluated. Total and antibiotic resistant bacteria were enumerated based on the membrane filtration method.

2.1.6 Analytical methods

The antibiotics were quantified by UHPLC-MS/MS with the help of dr. Rita Ribeiro (FEUP), using a Shimadzu apparatus equipped with a Kinetex™ XB-C18 100 Å column (100 × 2.1 mm i.d.; 1.7 µm particle diameter) supplied by Phenomenex, Inc. (Torrance, CA, USA). Ultrapure water and a mixture of MeOH and acetonitrile (50/50, v/v), both containing formic acid (0.1%, v/v), were used as mobile phase in isocratic mode (20/80 v/v) at a flow rate of 0.3 mL min^{-1}. Column oven and autosampler temperatures were set at 35 and 4 °C, respectively. The injection volume was 20 µL. For non-spiked experiments, the samples were previously concentrated and cleaned-up by SPE before UHPLC-MS/MS analysis, by using OASIS® HLB cartridges to extract the target antibiotics from 100 mL of real UWW (Ribeiro et al. 2015a). Briefly, the samples were acidified to pH 3 using sulfuric acid and supplemented with 20 µL of a solution containing 5 mg L^{-1} of each deuterated internal standard, consisting of azithromycin-d3 and ofloxacin-d3. The acidified samples were passed through the cartridges at a constant flow of 10 mL min^{-1}, previously conditioned with ethanol and ultrapure water (4 mL each). After the washing step with 4 mL of ultrapure water and subsequent drying, 4 mL ethanol were used as elution solvent and the eluate was collected in glass tubes. The extracted solution was dried in a Centrivap Concentrator® device (LABCONCO® Corporation, Kansas City, MO, USA), during 120 min at 45 °C. The dried extracts were dissolved in 250 µL of ethanol and the resulting solution was filtered through 0.22 µm polytetrafluoroethylene syringe filters (Membrane Solutions, Kent, WA, USA), and further analysed by UHPLC-MS/MS (conditions in **Tables 2.2 and 2.3**).

Table 2.2. Selected reaction monitoring (SRM) instrument parameters for tandem mass spectrometry analysis of target analytes.

Analyte	ESI mode (NI or PI)	Precursor ion (m/z)	Quantification (SRM1)				Confirmation (SRM2)				Ion ratio
			Product Ion	DP (V)	CE (V)	CXP (V)	Product Ion	DP (V)	CE (V)	CXP (V)	
AZT	PI	749.40	158.15	-36.0	-52.0	-13.0	591.35	-36.0	-47.0	-21.0	1.02
CLI	PI	425.00	126.15	-20.0	-30.0	-23.0	377.10	-20.0	-21.0	-25.0	33.3
OFL	PI	362.00	318.15	-28.0	-19.0	-21.0	261.15	-28.0	-29.0	-26.0	1.56
SMX	NI	252.00	156.00	12.0	15.0	29.0	92.05	12.0	27.0	17.0	7.65
TMP	PI	290.50	230.00	-30.0	-24.0	-24.0	123.05	-30.0	-26.0	-21.0	1.23

NI, negative ionization mode; PI, positive ionization mode; DP, declustering potential; CE, collision energy; CXP, collision cell exit potential.

The DOC of samples was measured before the experiments by using a Shimadzu TOC-L analyzer.

Table 2.3. Retention time, range, instrument and method detection and quantification limits, extraction recovery, accuracy and precision of analysis for each target analyte.

Analyte	Retention time (min)	Range (ng L^{-1})	IDL (µg L^{-1})	IQL (µg L^{-1})	MDL (ng L^{-1})	Recovery (%)	Accuracy (%)	Intra-batch precision (RSD, %)
AZT	0.945	0.44 – 100	0.30	0.88	0.15	69.1-78.8	91.2-117	< 5.6%
CLI	0.876	0.48 – 100	0.32	0.96	0.16	72.9-80.5	85.2-101	<11%
OFL	0.834	3.07 – 100	1.42	4.32	1.01	61.7-67.2	88.0-112	<8.6%
SMX	0.970	0.55 – 100	0.09	0.27	0.18	28.4-32.0	89.9-108	< 8.9%
TMP	0.801	1.23 – 100	0.72	2.19	0.41	38.1-47.4	92.0-107	< 3.6%

IDL is the instrument detection limit; IQL, instrument quantification limit; MDL, method detection limit.

2.1.7 Bacterial count

The culture medium PCA (for total heterotrophs), and the selective media m-Ent (for enterococci) and TBX (for *E. coli*), supplemented or not with antibiotics, were used for the enumeration of resistant and total bacteria, respectively, by the membrane filtration method as described elsewhere (Novo et al. 2013). Antibiotics were sterilized by filtration (0.22 µm

porosity) prior to addition to the sterilized culture media. AZT (stock solution prepared in ethanol) was added to TBX to reach a concentration of 32 mg L^{-1}; OFL (stock solution prepared in distilled water adding dropwise 4 g L^{-1} NaOH until total dissolution) was added to m-Ent for a final concentration of 4 mg L^{-1}; and SMX (stock solution prepared in distilled water adding dropwise 100 g L^{-1} NaOH until total dissolution) was added to PCA to reach a concentration of 512 mg L^{-1}. The selected concentrations were in accordance with epidemiological cut-off values (CLSI 2016).

Samples or serial 10-fold dilutions were filtrated through cellulose nitrate membrane filters (0.22 µm porosity, Biotech, Germany), which were placed on the respective culture medium and incubated at temperature and time, as follows: 30 °C and 24 h for PCA and PCA+SMX; 37 °C and 24 h for TBX and TBX+AZT; and 37 °C and 48 h for m-Ent and m-Ent+OFL. All assays were performed in triplicate. The ratio between the number of colony forming units (CFU) on antibiotic supplemented and non-supplemented media was used as an indicator of the resistance percentage.

2.1.8 Statistical analysis

CFU (log value) of total bacteria, resistant bacteria and their ratio, corresponding to each experiment or control were compared by single factor analysis of variance (ANOVA), followed by post-hoc Tukey's test using the software SPSS (Version 25.0 for Windows). The significance level was set to 0.05.

2.2 Results and discussion

2.2.1 Photodegradation of antibiotics

The degradation efficiencies by UVA of the antibiotics spiked in UWW, in the absence of MeOH and using 4 LEDs, revealed the following resilience order: TMP ≈ SMX > AZT > OFL (**Figure 2.3a**). Owing to the low absorbance above 290 nm wavelength (Vione et al. 2009; Ge et al. 2010; Hanamoto et al. 2013), many antibiotics are recalcitrant to photolysis (i.e., macrolides, sulfonamides and pyrimidine). However, real matrices can play an important role on their indirect photodegradation, exceptions being found in some cases as fluoroquinolones, which are reported to be more susceptible to UV photolysis in pure water than in UWW (Hanamoto et al. 2013; Wammer et al. 2013). Thus, indirect photolysis can take place by means of some inorganic species and/or the effluent organic matter (EfOM) present in UWW, as well as by its excited

triplet state (^{3}EfOM*) (Ryan et al. 2010). For instance, degradation of the zwitterionic form of OFL at pH 7.7 was reported under solar light (Wammer et al. 2013), the natural dissolved organic matter and OFL being suggested to compete for absorption of photons, as fluoroquinolones in general (Ge et al. 2010). In contrast, $HO^{\bullet}/CO_3^{\bullet-}$ radicals were proposed as the main species involved in the mechanism of TMP photodegradation in secondary UWW under solar light, whereas ^{3}EfOM* was responsible for the AZT elimination (Yan et al. 2017). Another study has also reported that natural organic matter (humic acids) favours the degradation of AZT under solar photolysis in certain conditions (Tong et al. 2011).

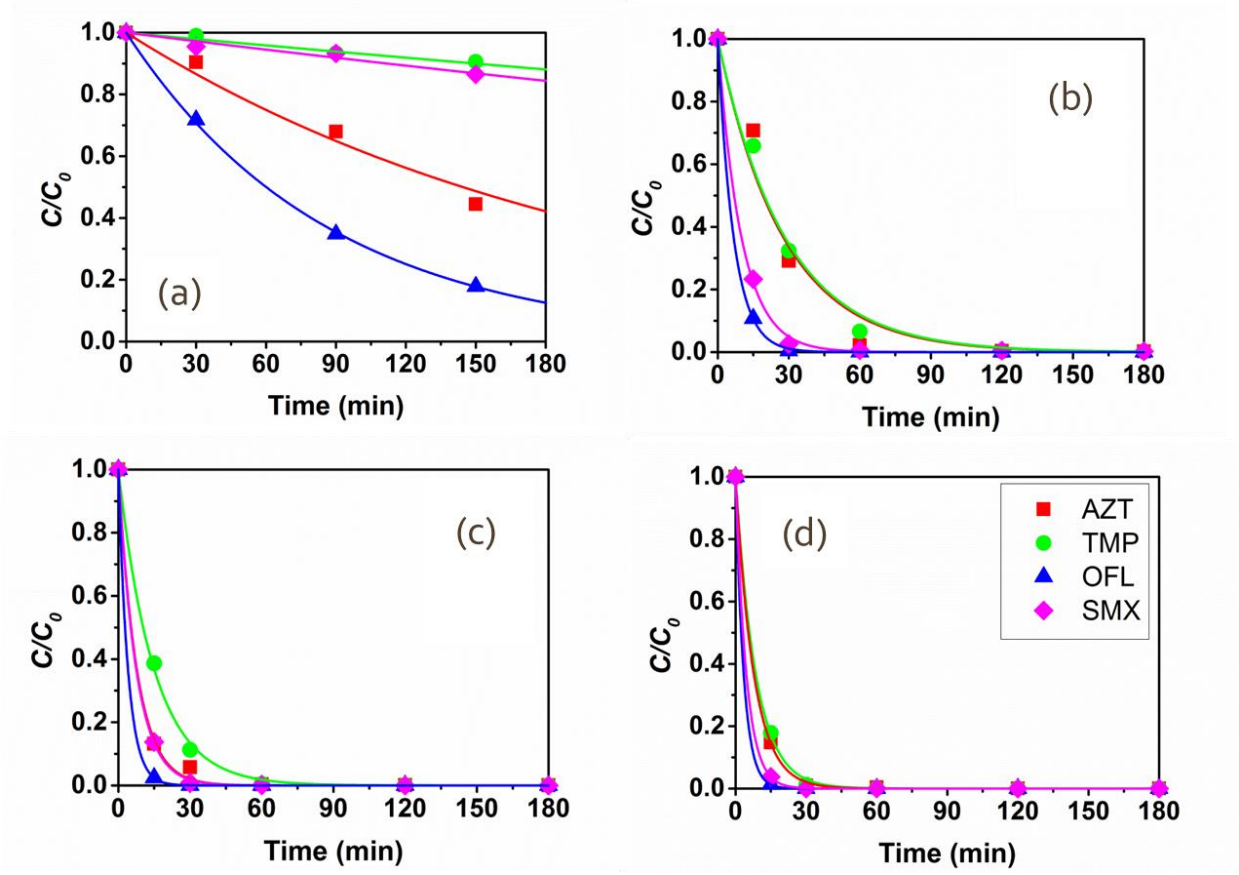

Figure 2.3. Removal efficiencies of AZT, TMP, OFL and SMX spiked in UWW (100 µg L^{-1} without MeOH) by using 4 LEDs without catalyst (a) and 1 (b), 2 (c) and 4 LEDs (d) in photocatalytic experiments (catalyst load set at 1.00 g L^{-1}).

Regarding the effect of MeOH on photolysis (**Table 2.4**, **Figure 2.4**), this solvent (0.05% v/v) did not markedly disturb the above mentioned order of resilience for these antibiotics (TMP > SMX > AZT ≈ OFL), but affected the values of the respective apparent first-order reaction rate

constants (k): k_{OFL} increased slightly, k_{AZT} and k_{SMX} increased 2.5 and 9 times, respectively, whereas k_{TMP} decreased 7 times.

Table 2.4. Apparent first-order reaction rate constant (k), as function of optical thickness and catalyst load, considering different number of LEDs in different matrices.

Matrix	Optical thickness (-)	Catalyst load (g L^{-1})	k x 10^3 (min^{-1})											
			1 LED				2 LEDs				4 LEDs			
			AZT	TMP	OFL	SMX	AZT	TMP	OFL	SMX	AZT	TMP	OFL	SMX
Spiked WW (w/o MeOH)	0.00	0.00									4.8	0.7	11.5	0.9
	0.97	0.10									29.2	14.3	47.5	25.5
	2.43	0.25									56.8	38.0	108.7	75.7
	4.86	0.50									67.6	56.9	180.2	105.0
	9.73	1.00	36.3	35.4	149.7	100.3	129.8	66.8	248.5	133.6	129.1	117.1	290.5	212.6
Spiked WW (MeOH)	0.00	0.00	4.8	0.3	3.8	1.3	3.5	0.5	5.7	3.6	12.0	0.1	13.0	8.1
	0.97	0.10	a	a	a	a	13.6	2.2	21.6	9.7	13.3	5.2	41.6	14.1
	2.43	0.25	6.6	3.4	29.4	17.0	10.9	5.7	39.7	19.1	26.4	8.9	69.8	34.4
	4.86	0.50	12.7	4.7	45.1	27.0	18.8	7.6	82.2	48.1	18.3	14.3	111.8	53.5
	9.73	1.00	15.4	7.9	76.5	53.7	32.5	13.4	171.1	83.1	67.0	23.5	269.6	144.4
	14.59	1.50	27.4	11.7	126.6	100.2	45.8	20.6	211.8	178.8	66.0	29.0	264.3	b
	19.46	2.00	19.6	11.5	135.2	104.0	57.6	17.9	273.7	228.8	43.6	33.4	301.9	b
Actual WW	9.73	1.00									64.6[d]	128.2[d]	363.7[d]	c

a, data not significant; b, lack of data (removal) between 0 and 5 min; c, initial concentration below the limit of quantification; d, k obtained by $C/C_0 = e^{-kt}$ (C_0 is different for each antibiotic).

Because the degradation rate of AZT and SMX is much higher in UWW with MeOH (**Figure 2.4**) than in UWW (**Figure 2.3a**), it seems that MeOH promotes ^{3}EfOM* in UVA photolysis. On the other hand, TMP was the most resilient to UVA photolysis, but in the presence of MeOH its degradation is even slower. MeOH did not remarkably modify the rate in the case of OFL. Accordingly, scavenging studies have already revealed that singlet oxygen is the main reactive oxygen species responsible for the degradation of OFL (Hapeshi et al. 2010), and of most fluoroquinolones, such as levofloxacin, gatifloxacin, difloxacin and balofloxacin (Ge et al. 2010), suggesting also that the ^{3}EfOM* degradation pathway is not dominant. In fact, photo-oxidation resulting from reactive oxygen species photochemically generated from the oxygen dissolved in the reaction mixture was already shown in a previous study (Hapeshi et al. 2010).

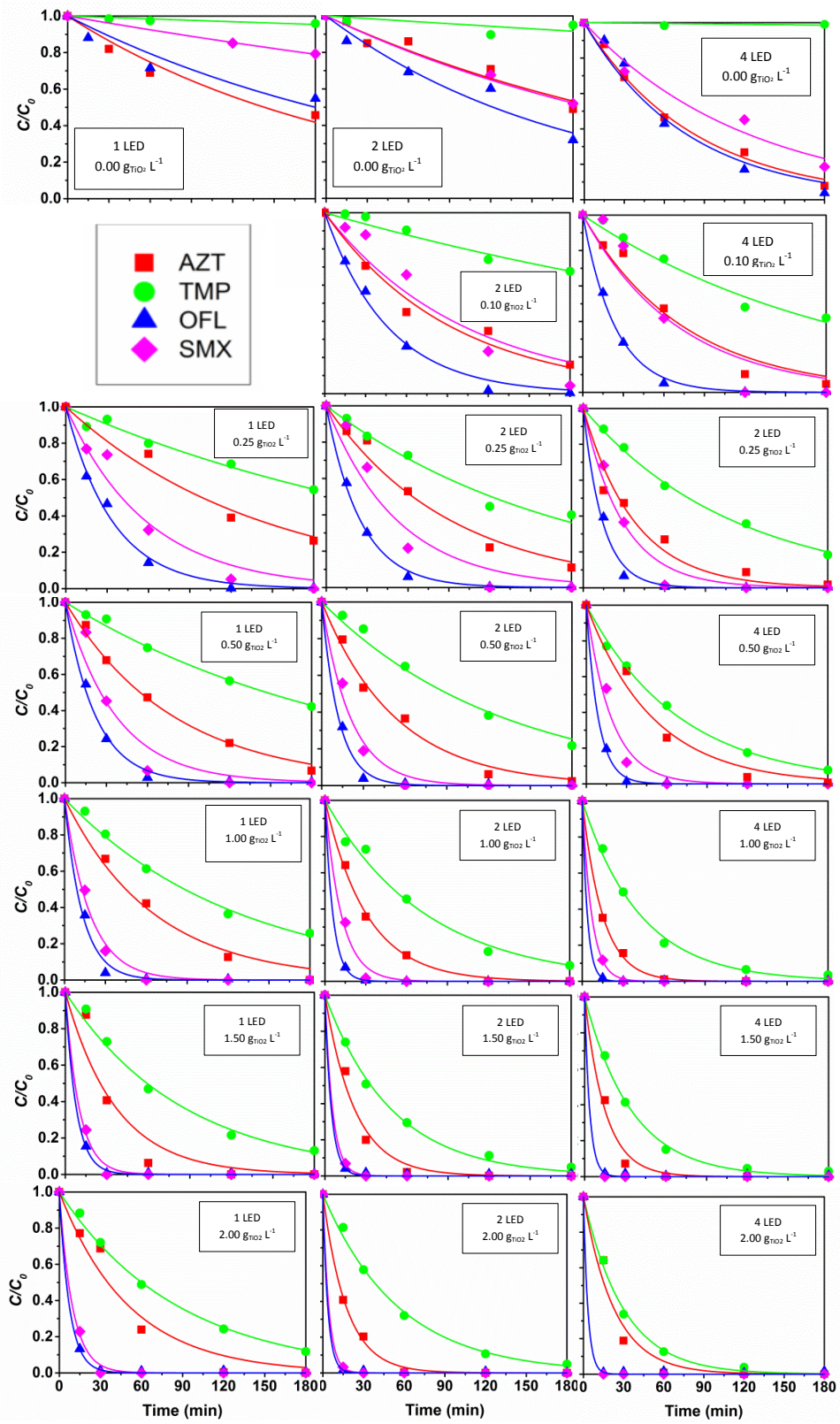

Figure 2.4. Removal efficiencies of AZT, TMP, OFL and SMX spiked in UWW (100 µg L^{-1}, with 0.05% MeOH), using different number of LEDs (1 – 4) and catalyst loads (0.00 – 2.00 g L^{-1}).

2.2.2 Radiation absorption-scattering model

The UVA-LEDs (lower cost and higher power efficiency than UVC- and UVB-LED (Ferreira et al. 2016)) present the main emission peak at 381 nm (**Figure 2.1b**), overlapping with the tail of the TiO_2 absorption spectrum (380 nm, (Malato et al. 2009)). The total emitted radiant energy (11.7 µJ) and its fraction (4.2 µJ) with photons having an energy higher than the bang gap of the photocatalyst (3.2 eV, (Malato et al. 2009)) is shown in **Figure 2.1b**.

According to the nature of the LED light (beam) and its viewing half angle (ca. ± 30°), only a part of the external reactor surface (4 cm diameter circle orthogonally projected on the cylindrical surface) is irradiated by the UVA light. The main ranges of irradiance (**Figure 2.1c**) are: 515-250 W m^{-2} (2 cm diameter red circle), 250-15 W m^{-2} (3 cm diameter orange circular crown) and 15-1 W m^{-2} (4 cm diameter yellow circular crown). The UV dose provided by a single LED in the red zone (area similar to a circle in a plane, ca. 3.14 cm^2) for an hour of light exposure is ca. 1,220 kJ m^{-2}. Since light uniformity also plays a key role in the efficiency of the process, systems based on LEDs must be properly designed in order to illuminate the entire reactor volume (Martín-Sómer et al. 2017).

Several studies have shown how important is the catalyst load, with low amounts permitting radiation losses due to the transparency of the solution, while an excess promoting screening effects due to the opacity of the solution, hampering the optimal irradiation of catalyst at the inner side of the reactor (Herrmann 1999; Li Puma and Brucato 2007; Rizzo et al. 2014b). Thus, to maximize the antibiotics' removal, it is recommended that all catalyst active sites are available, the photocatalytic efficiency being governed by the catalyst load, light irradiation and reactor geometry (Herrmann 1999). Optical thickness (τ, **Eq. 2.3**) considers all these three parameters. Since radiation field is not constant along the reactor, τ is estimated only for the central red parts of **Figure 2.1c** (irradiance of 515 W m^{-2}). Considering UVA radiation field and an average agglomeration size of TiO_2-P25 > 1 µm (conditions found in UWW) β is ca. 1,950 m^2 kg^{-1} (Salaices et al. 2002). Once calculated δ (0.005 m) and β, the values of τ for each catalyst load are reported in **Table 2.4**. According to Li Puma and Brucato (2007), for the scattering albedo of TiO_2 (ca. 0.74), radiation transmission factor is maximized at $\tau > 6$, meaning for the present configuration a catalyst load between 1.00 and 2.00 g L^{-1}.

2.2.3 Photocatalytic degradation of antibiotics in spiked UWW

The results obtained for the photocatalytic treatment of spiked UWW are shown in **Figures 2.3-2.5**. In the absence of MeOH (**Figure 2.3b-d** and **Figure 2.5**), the general resilience order (TMP ≈ AZT > SMX > OFL) was slightly different from that obtained by photolysis (**Figure 2.3a**). Moreover, it was generally observed that the degradation rates of all antibiotics increased linearly with the number of LEDs and catalyst load up to 1.00 g L^{-1}, either in the absence or presence of MeOH (**Figure 2.6**). The 4-LEDs configuration allowed the largest irradiated solution volume, since each LED irradiated a specific section of the reactor (**Figure 2.2c**). Moreover, the *k* values obtained when using 2 LEDs with 2.00 g L^{-1} of catalyst (**Figure 2.7b**) and 4 LEDs with 1.00 g L^{-1} of catalyst (**Figure 2.7c**) were similar for most antibiotics. These observations support the existence of a heterogeneous photocatalytic regime.

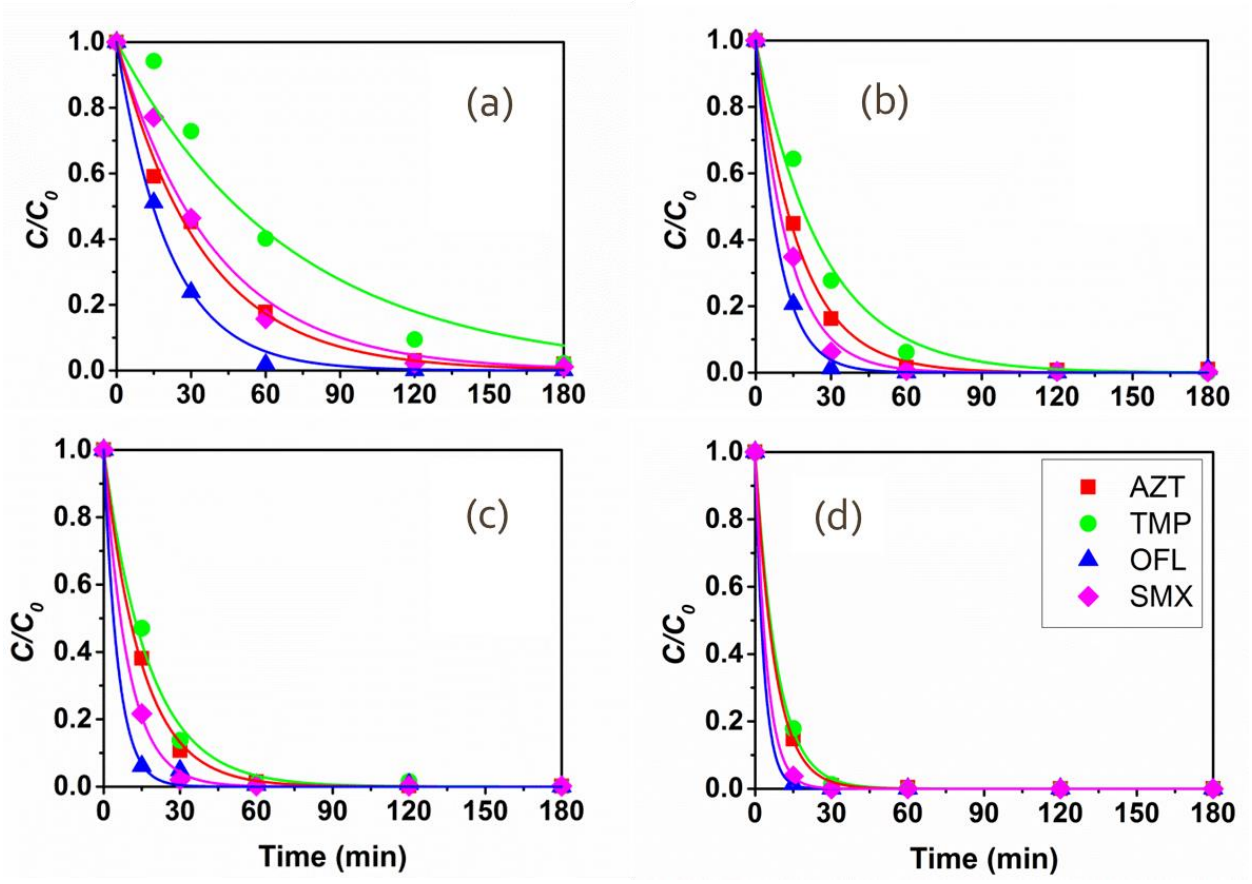

Figure 2.5. Removal efficiencies of AZT, TMP, OFL and SMX spiked in UWW (100 µg L^{-1} without MeOH) by photocatalysis using 0.10 (a), 0.25 (b), 0.50 (c) and 1.00 g L^{-1} (d) catalyst load (number of LEDs set at 4).

In all the photocatalytic tests performed using MeOH as radical scavenger, the *k* values determined for all the antibiotics were lower than those in the absence of MeOH, but the same order was observed for the degradation rates (**Figure 2.6**). TMP keeps being the most resilient compound and its *k* values were those mostly affected by the presence of the organic solvent, indicating a higher susceptibility to $HO^{\bullet}$ radicals than the other antibiotics under study. For instance, using 4 LEDs and 1.00 g L^{-1} of catalyst, k_{TMP} increased from 0.0235 min^{-1} (in the presence of MeOH) to 0.1171 min^{-1} (in the absence of MeOH) (**Figure 2.6a**).

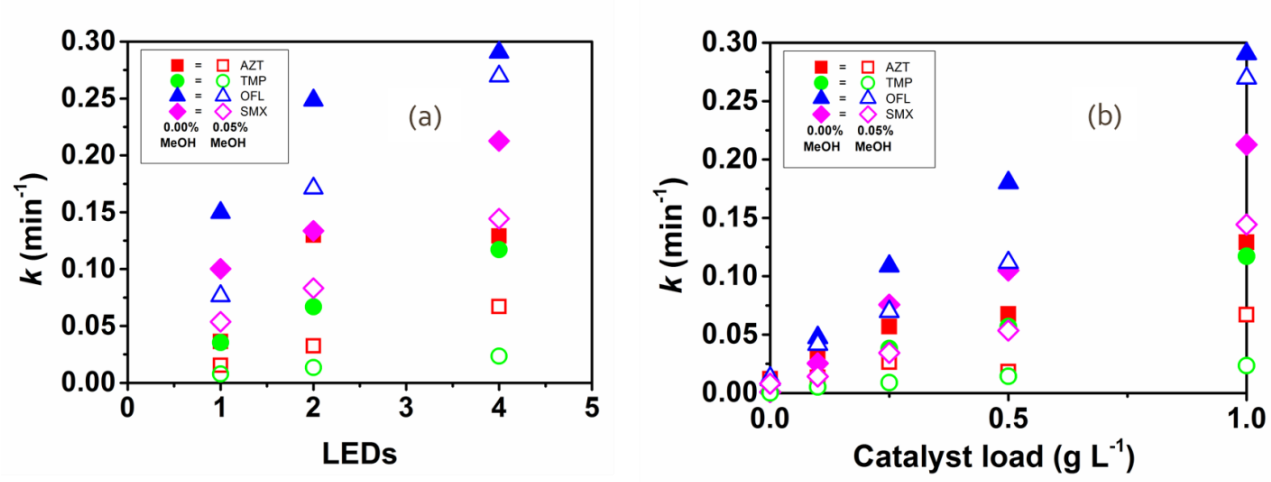

Figure 2.6. Apparent first-order reaction rate constant (*k*) of AZT, TMP, OFL and SMX spiked in UWW (100 µg L^{-1}, with (open symbols) and without methanol (solid symbols)) by photocatalysis: varying the number of LEDs and using a catalyst load set at 1.00 g L^{-1} (a); and using 4 LED and varying the catalyst loads (b).

A recent study on the influence of carrier solvent (Arlos et al. 2017) highlighted the influence of MeOH on the photocatalytic degradation of water micropollutants (including SMX and TMP).

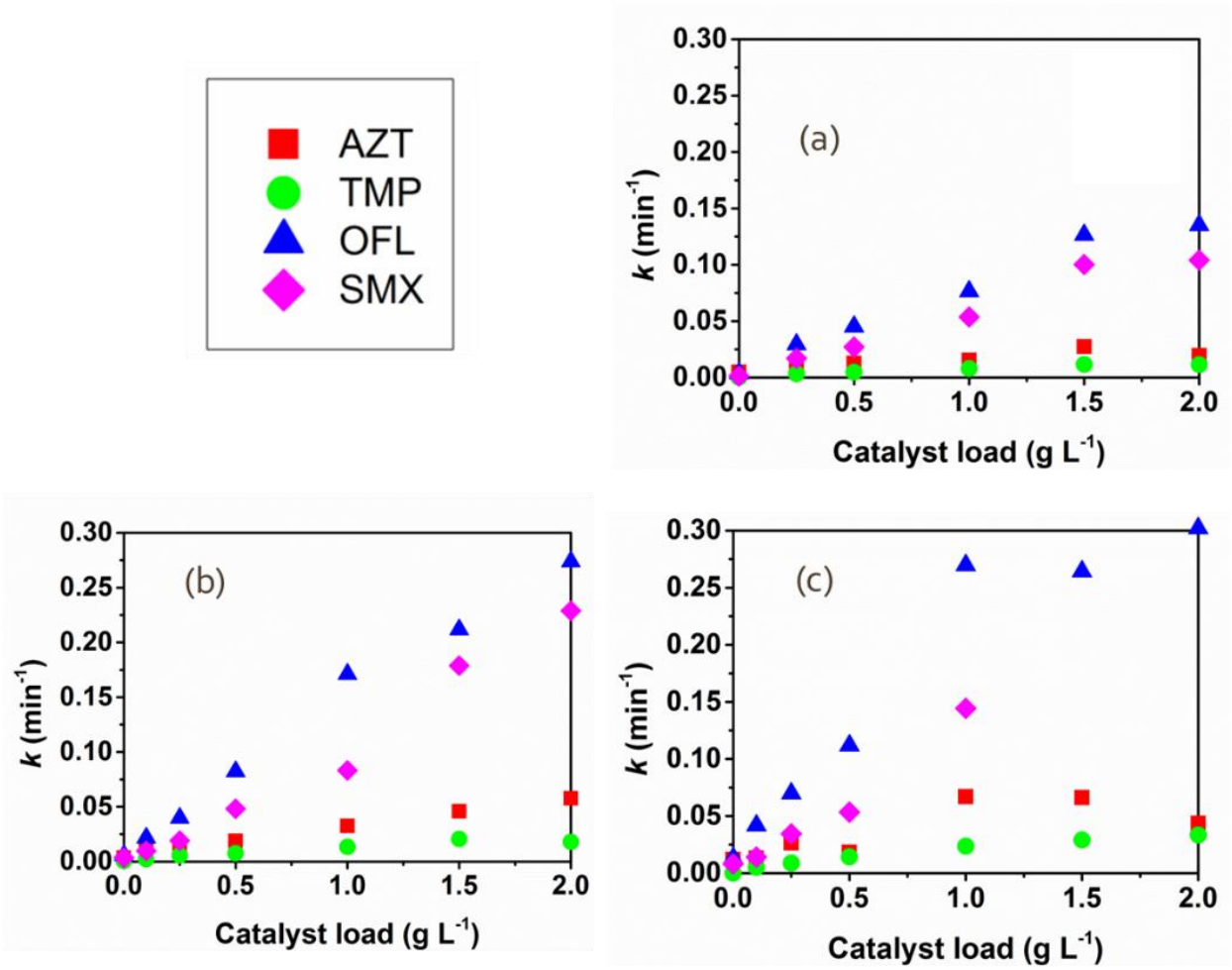

Figure 2.7. Apparent first-order reaction rate constant (*k*) of AZT, TMP, OFL and SMX spiked in UWW (100 µg L^{-1}, with 0.05% MeOH) by photocatalysis, as function of catalyst load, using 1 (a), 2 (b) and 4 (c) LEDs.

Regarding the photocatalytic degradation of OFL (1.00 g L^{-1} of catalyst), the difference between k_{OFL} in the presence and absence of MeOH is not markedly different in the case of 4 LEDs, compared to the results obtained with 1 and 2 LEDs (**Figure 2.6a**). Interestingly, Hapeshi and collaborators (2010) suggested that valence band holes are the primary photocatalytic oxidation pathway of OFL in ultrapure water.

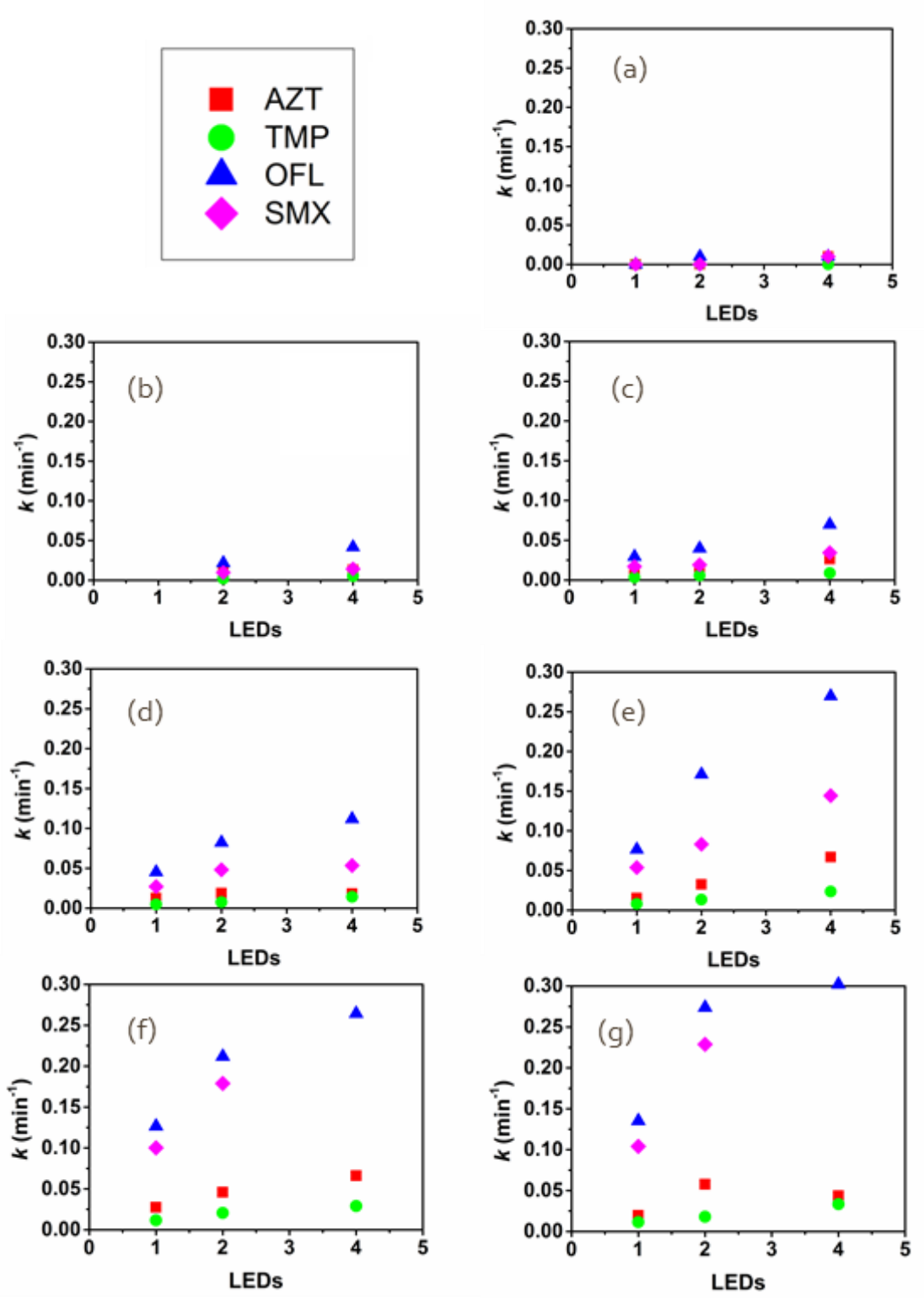

Figure 2.8. Apparent first-order reaction rate constant (*k*) of AZT, TMP, OFL and SMX spiked in UWW (100 µg L^{-1}, with 0.05% MeOH) by photocatalysis, as function of number of LEDs and catalyst loads of: 0.00 (a), 0.10 (b), 0.25 (c), 0.50 (d), 1.00 (e), 1.50 (f) and 2.00 g L^{-1} (g).

2.2.4 Photocatalytic degradation of antibiotics in non-spiked UWW

Three different sampling campaigns of secondary UWW were performed during the winter of 2017/2018 in a UWWTP located in Northern Portugal. The initial concentration of SMX was below the limit of quantification (LOQ) in all samples. Considering that CLI was always present in the UWW collected in this UWWTP, its concentration was quantified in the next experiments, together with AZT, TMP and OFL. The measured concentrations followed the general decreasing order: AZT > OFL > TMP > CLI, these concentrations being more variable for AZT (369-1686 ng L^{-1}) and OFL (105-648 ng L^{-1}).

The samples from the first campaign (UWW1, **Figure 2.9**) were used to compare the effect of 10 min photolysis with 10 min photocatalysis after adsorption in the dark for 24 h. Photolysis and adsorption had a similar performance in removing AZT, TMP and OFL, since photolysis led to abatements ranging from 33 ± 16% to 47 ± 3%, whereas the removal by adsorption varied between 41 ± 12% and 62 ± 9%. Both photolysis and adsorption steps had negligible effect over the CLI concentration. In contrast, the photocatalytic degradation of TMP, OFL and CLI was very fast, the concentrations reaching values below the LOQs in less than 10 min. In fact, only AZT could be quantified after the photocatalytic treatment, but at very low concentrations.

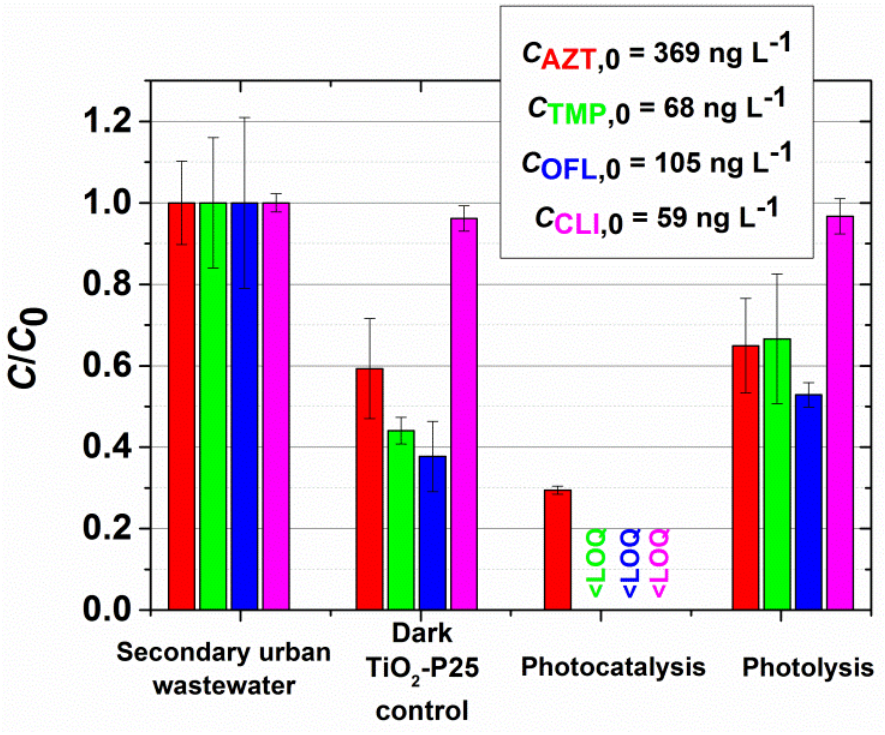

Figure 2.9. Normalized concentrations of AZT, TMP, OFL and CLI in UWW1 after 1 day of adsorption in the dark with TiO_2, and 10 min of photocatalytic and photolytic treatment.

The concentrations were nearly two times higher in the second sampling campaign (UWW2, **Figure 2.10a**), except for CLI which was quantified at levels similar to that found in UWW1. As in the first campaign, a remarkable adsorption (28 ± 2% for AZT, 62 ± 13% for TMP and 51 ± 7% for OFL) was found for all the antibiotics except for CLI (15 ± 1% only in UWW2). After treatment of UWW2 by photocatalysis, OFL and CLI were removed to levels below the LOQs, AZT and TMP being quantified at low concentrations after the photocatalytic treatment.

Higher concentrations of AZT and OFL were found in the third sampling campaign (UWW3, **Figure 2.10b**), an intermediate level of TMP and the same concentration of CLI. The average removals by adsorption in UWW3 were similar to those obtained in the other samples (36 ± 1% for AZT, 38 ± 1% for OFL and negligible in the case of CLI), with exception of TMP (21 ± 9%) which might be attributed to the sample heterogeneity. Once again, the photocatalytic treatment allowed to decrease the concentrations of OFL and CLI to levels below the LOQs, whereas AZT and TMP were quantified at low concentrations. The variations on the concentrations of these antibiotics during the photocatalytic treatment of UWW3 is represented in **Figure 2.10c** for AZT and OFL and **Figure 2.10d** for TMP and CLI. The required treatment time to reach the antibiotic concentration under the LOQ in UWW3 was 60 min and 15 min for AZT and TMP respectively, and 10 min for both OFL and CLI.

The degradation kinetics of AZT, TMP and OFL at actual concentrations in UWW (ng L^{-1} levels) were compared to those obtained in spiked UWW (100 μg L^{-1}) when the treatment was performed in the absence of MeOH. According to Malato and collaborators (2009), the rate constants of micropollutants usually increase with the initial substrate until reaching a steady-state (saturation level of Langmuir-Hinshelwood kinetic model). However, in the present study, this was observed only for k_{AZT} (ca. 100% increase). No relevant difference of k_{TMP} (ca. 10% decrease) and a significant decrease of k_{OFL} (ca. 20%) were found between non-spiked and spiked (absence of MeOH) tests (**Table 2.4**). In fact, AZT was also more resilient than TMP in another study using a UVA artificial lamp and 0.5 g L^{-1} of TiO_2 for the removal of emerging contaminants at real concentrations in UWW (Moreira et al. 2015). Moreover, the removal reported for OFL (84%) was also higher than that achieved for TMP (70%) in other study, after 8 h treatment using a compound parabolic collector and a very low amount of TiO_2 (0.02 g L^{-1}) in solar photocatalysis (Prieto-Rodriguez et al. 2012). AZT and TMP have been widely reported as recalcitrant compounds when using AOPs (Michael et al. 2012b), while quinolones are more susceptible to degradation than AZT and TMP, for instance by UVC irradiation of UWW (Kim et al. 2009).

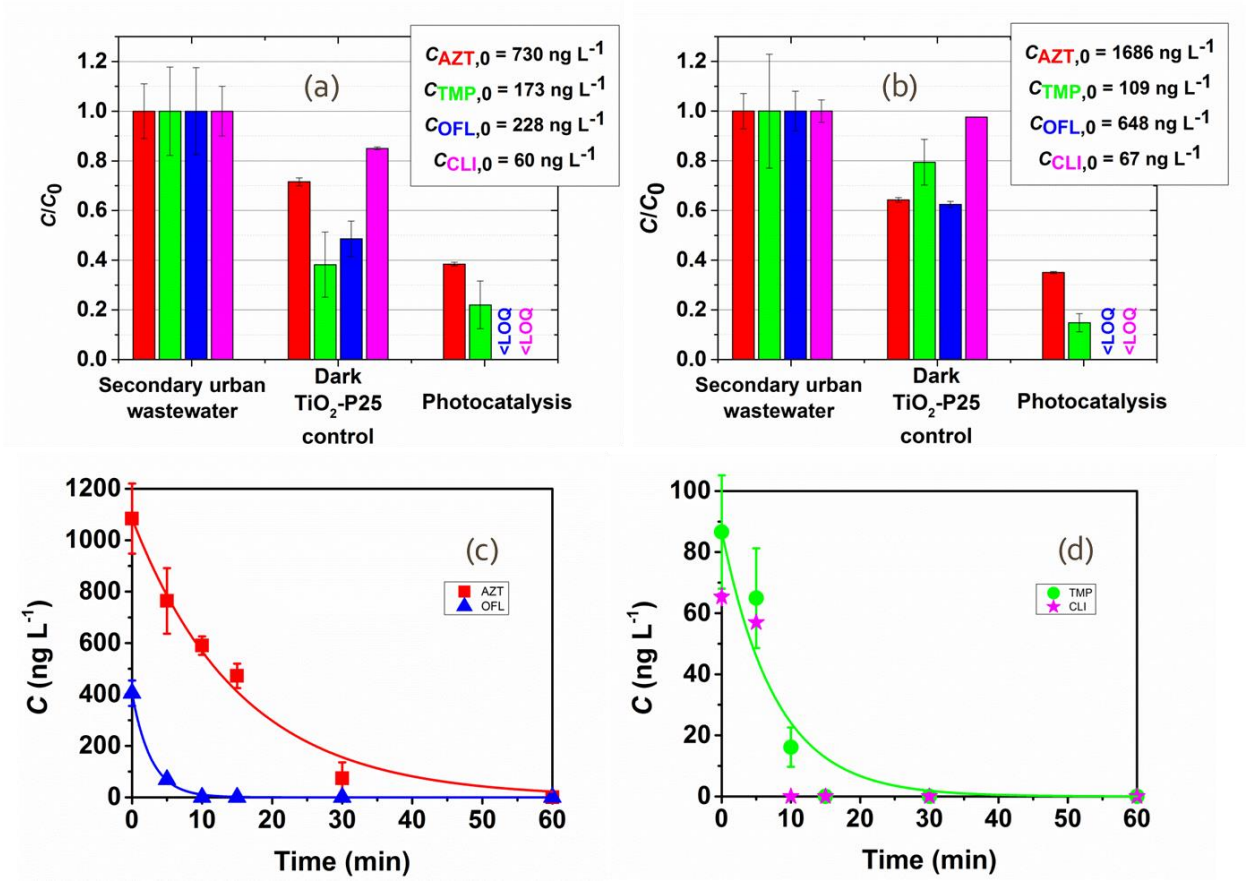

Figure 2.10. Normalized concentrations of AZT, OFL, TMP and CLI after adsorption in the dark (TiO_2, 1 day) and 10 min of photocatalytic treatment of UWW2 (a) and UWW3 (b). Evolution of concentrations of AZT and OFL (c), TMP and CLI (d) in UWW3 during photocatalytic treatment.

2.2.5 Disinfection, antibiotic resistance prevalence and bacterial regrowth

AOPs are promising processes for bacterial inactivation in UWW, although ARGs are detected after treatment, a fact that is worsened by bacterial regrowth and bacterial community disturbance (Dunlop et al. 2015; Alexander et al. 2016; Ferro et al. 2016; Sousa et al. 2017), thus increasing the risk of antibiotic resistance spread. Among the different AOPs, photo-Fenton, UV/H_2O_2 and heterogeneous photocatalysis (UV/TiO_2) have been tested for the inactivation of different bacterial groups (Rizzo et al. 2013b; Michael-Kordatou et al. 2018). However, the literature reports mainly the assessment of the efficiency of LEDs-driven TiO_2-photocatalysis on disinfection of UWW based on the monitoring of *E. coli* suspensions (Xiong and Hu 2013; Martín-Sómer et al. 2017). Recently, it was demonstrated that when using TiO_2 as photocatalyst in aqueous solution, a LED system was more efficient than traditional lamps if the same UV dose is applied for a shorter period but with higher intensity, leading to high *E. coli* inactivation rates

(Martín-Sómer et al. 2017), an additional advantage being the possibility of applying a periodic intense radiation (Xiong and Hu 2013).

In this study, the performance of 4 LEDs photolysis and 4 LEDs photocatalysis (using a catalyst load of 1.00 g L^{-1}) to reduce the counts of viable total heterotrophs, *E. coli* and enterococci and their antibiotic resistant counterparts in UWW samples, was assessed. CFUs were enumerated before and immediately after treatment, and after 3-day storage in the dark, at room temperature (**Figure 2.11**). Initial load of total heterotrophs, *E. coli* and enterococci in secondary UWW were 7.7 ± 0.2, 5.9 ± 0.4 and 5.7 ± 0.3 log (CFU / 100 mL), respectively. The percentage of SMX resistant heterotrophic bacteria and AZT resistant *E. coli* in the secondary UWW was 8.7 ± 2.9% and 1.9 ± 1.5%, respectively (**Table 2.5**). These values of sulfonamide resistant heterotrophs (Guo et al. 2013a; Novo et al. 2013) and AZT resistant *E. coli* (Ibekwe et al. 2016) are in agreement with previous studies. The percentage of OFL resistant enterococci was lower (1.5 ± 0.2%) (**Table 2.5**) than that reported by Michael and collaborators (2012a) (ca. 20%), probably because a 4 times higher OFL concentration (based on the epidemiological cut-off values (CLSI 2016)) was used in the culture media in the present study.

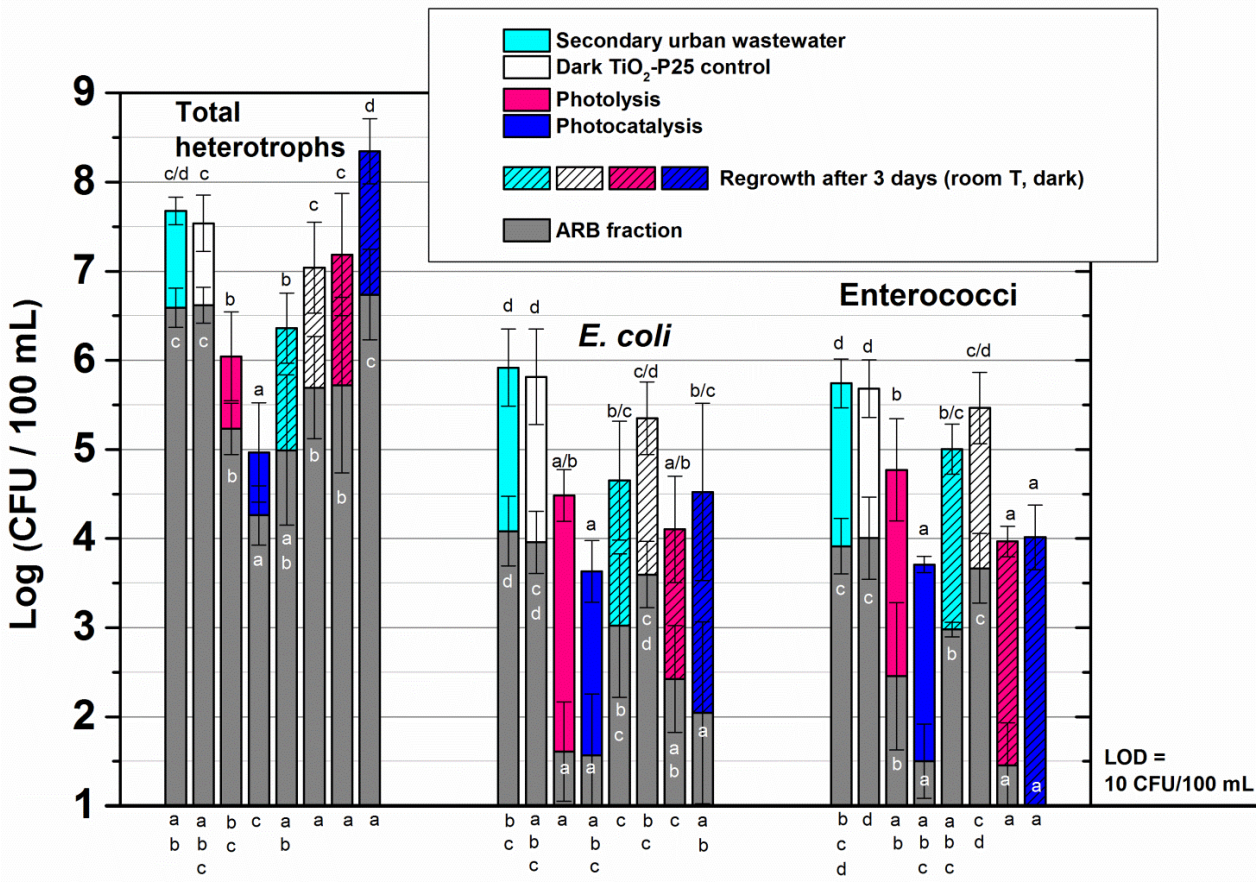

Figure 2.11. Total (coloured) and antibiotic resistant (grey) bacteria inactivation after 1 h photolysis/photocatalysis evaluated immediately (filled bars) and after 3-day storage in dark at room temperature (striped bars). The letters a, b, c, d and e indicate significantly ($p < 0.05$) different groups among the tested treatment conditions. The letters in black on the top of bars refer to total bacteria. The letters in white refer to the antibiotic resistant counterparts. The letters on the bottom of the graph refer to the percentage of resistant bacteria with respect to the total bacteria.

A reduction on the load of the analysed bacterial groups was observed for both photolytic and photocatalytic processes, with higher inactivation rates for photocatalysis (**Figure 2.11**, **Table 2.6**). The efficiency of photolysis on the bacterial load reduction of the studied bacteria followed the order: heterotrophs (1.6 ± 0.6 log reduction) > *E. coli* (1.4 ± 0.7 log reduction) > enterococci (1.0 ± 0.3 log reduction). Regarding antibiotic resistant groups, photolysis performance followed the order: *E. coli* (2.5 ± 0.2 log reduction) > enterococci (1.5 ± 0.6 log reduction) ≈ heterotrophs (1.4 ± 0.4 log reduction). Concerning the photocatalytic treatment, the following order was found: heterotrophs (2.7 ± 0.6 log reduction) > *E. coli* (2.3 ± 0.3 log reduction) > enterococci (2.0 ± 0.2 log reduction) and resistant groups (*E. coli* (2.5 ± 0.4 log reduction) ≈ enterococci

(2.4 ± 0.7 log reduction) > heterotrophs (2.3 ± 0.5 log reduction)). The bacterial loads of the control samples, with and without the addition of photocatalyst, were not observed to vary significantly.

Table 2.5. Percentage (%) of resistant bacteria in secondary UWW, in the dark TiO_2-P25 control, immediately after treatment (photolysis or photocatalysis) and after storage of the samples for 3 days at room temperature under the dark (starred treatments).

Treatment	Total heterotrophs		*E. coli*		Enterococci	
	Mean (%)	SD (%)	Mean (%)	SD (%)	Mean (%)	SD (%)
Secondary UWW	8.7	2.9	1.9	1.5	1.5	0.2
Dark TiO_2-P25 control	12.7	3.9	1.5	0.7	2.2	0.9
Photolysis	19.7	13.4	0.4	0.4	0.7	0.5
Photocatalysis	23.6	18.3	1.4	1.5	1.1	1.1
Secondary UWW*	7.3	6.7	2.5	0.8	1.0	0.5
Dark TiO_2-P25 control*	4.8	1.9	1.9	0.7	1.8	1.0
Photolysis*	4.6	3.5	2.3	1.1	0.4	0.4
Photocatalysis*	2.9	1.9	0.6	0.7	0.1	0.1

Because of the bacterial load variations, the percentage of ARB decreased after photolysis for *E. coli* (from 1.9 ± 1.5% to 0.4 ± 0.4%) and increased after photocatalysis for heterotrophs (from 8.7 ± 2.9% to 23.6 ± 18.3%) (**Figure 2.11**, **Table 2.5**). Other studies assessing the SMX resistant fraction of total heterotrophs after UVC irradiation (Guo et al. 2013a) and OFL resistant fraction of enterococci (Michael et al. 2012a) after solar photo-Fenton did not report variations with respect to the initial resistance percentage. Nevertheless, some authors observed faster inactivation of macrolide resistant *E. coli* than of susceptible *E. coli* counterparts in UWW treated by solar TiO_2 photocatalysis (Karaolia et al. 2018).

Despite the observed inactivation of the analysed microbial groups, it was hypothesized that at least some bacteria might have become transitorily unculturable, although maintaining the capacity to regrow, as reported before (Zhao et al. 2014; Fiorentino et al. 2015; Moreira et al. 2016, 2018). Regrowth is mainly attributed to survival and capacity to use available carbon sources generated during the oxidation of recalcitrant organic matter (Thayanukul et al. 2013; Zhao et al. 2014). When compared to the UWW immediately after the photolysis treatment, the loads of total heterotrophs increased (1.1 ± 0.9 log higher), and the loads of total enterococci

decreased (0.8 ± 0.5 log lower) after storage, whereas no significant changes in the abundance of total *E. coli* were found. Regarding antibiotic resistant counterparts, only enterococci showed a significant change (0.9 ± 0.6 log reduction) after storage. In the photocatalytic treated stored water, the loads of both the total heterotrophs and total *E. coli* were higher than immediately after the treatment (3.4 ± 0.7 and 0.7 ± 0.9 log higher, respectively), whereas no significant changes were observed for total enterococci. Regrowth of resistant heterotrophic bacteria was observed in the stored water treated by photocatalysis (2.5 ± 0.6 log increase), while no significant changes were found for resistant *E. coli* and resistant enterococci. Photocatalysis treated water seems to support higher regrowth than photolysis, suggesting that this treatment may increase the biodegradable organic matter more than photolysis (Thayanukul et al. 2013). In the non-treated controls, the abundance of all analysed microbial groups was maintained or decreased with storage.

Table 2.6. Log values (CFU / 100 mL) of total and resistant bacteria in secondary UWW, before and after each treatment. Starred treatments refer to the log values after the storage of the samples for 3 days at room temperature under the dark.

Treatment	Total heterotrophs		Resistant heterotrophs		*E. coli*		Resistant *E. coli*		Enterococci		Resistant Enterococci	
	Mean (Log)	SD (Log)	Mean (Log)	SD (Log)	Mean (Log)	SD (Log)	Mean (Log)	SD (Log)	Mean (Log)	SD (Log)	Mean (Log)	SD (Log)
Secondary UWW	7.68	0.16	6.59	0.22	5.92	0.43	4.08	0.39	5.74	0.27	3.91	0.31
Dark TiO_2-P25 control	7.54	0.32	6.62	0.20	5.82	0.53	3.96	0.35	5.68	0.32	4.00	0.46
Photolysis	6.05	0.50	5.23	0.29	4.49	0.29	1.61	0.56	4.77	0.58	2.45	0.83
Photocatalysis	4.97	0.56	4.26	0.33	3.63	0.35	1.57	0.69	3.71	0.09	1.50	0.42
Secondary UWW*	6.36	0.39	4.99	0.84	4.65	0.67	3.02	0.80	5.01	0.28	2.98	0.08
Dark TiO_2-P25 control*	7.04	0.51	5.69	0.57	5.35	0.41	3.60	0.37	5.47	0.40	3.67	0.39
Photolysis*	7.19	0.69	5.72	0.99	4.10	0.60	2.42	0.60	3.97	0.17	1.46	0.48
Photocatalysis*	8.35	0.36	6.74	0.51	4.52	1.00	2.04	1.02	4.01	0.36	<LOD	-

LOD = 10 CFU / 100 mL = 1 log (CFU / 100 mL)

Due to the variations pointed out above, when compared to secondary treated UWW, the stored UWW after photolysis showed lower loads of total *E. coli* (1.8 ± 0.4 log reduction) and total enterococci (1.8 ± 0.2 log reduction), with no significant reduction for total heterotrophs. Also the loads of the resistant bacterial groups were lower in the stored water than in the secondary treated UWW: enterococci (2.5 ± 0.2 log reduction) > *E. coli* (1.7 ± 0.3 log reduction) > heterotrophs (0.9 ± 0.9 log reduction). Similarly, in the stored UWW after photocatalysis only total enterococci and total *E. coli* were less abundant than in the original secondary UWW

(1.7 ± 0.4 and 1.4 ± 0.7 log reduction respectively), while total heterotrophs did not show significant changes. A similar trend was found for the antibiotic resistant groups, with lower loads of enterococci (3.0 ± 0.3 log reduction) and *E. coli* (2.0 ± 0.7 log reduction), and no significant changes in the load of heterotrophs.

Due to these variations, the percentage of OFL resistant enterococci in the stored treated wastewaters was significantly lower (photolysis: 0.4 ± 0.4%; photocatalysis: 0.1 ± 0.1%) than in the original secondary UWW (1.5 ± 0.2%) (**Figure 2.11**, **Table 2.5).** Fecal organisms, mainly enterococci, seem to be more vulnerable to disinfection (photolysis and photocatalysis) than total heterotrophs, probably due to the fact that they are at a lower abundance or because bacteria of this bacterial group are susceptible to permanent damage, as described in the literature (van Grieken et al. 2010; Laxma Reddy et al. 2017; Sousa et al. 2017).

2.3 Conclusion

The variability of antibiotic concentrations for different real UWW matrices coming from the same UWWTP constitutes no obstacle to their efficient degradation by TiO_2-heterogeneous photocatalysis using UVA-LEDs. Bacterial inactivation reached values of about 2 log-units, although this apparent removal was not enough to avoid bacterial regrowth of total heterotrophs to values close to those observed before treatment. The prevalence of antibiotic resistance after regrowth was similar (for total heterotrophs and *E. coli*) or lower (for enterococci) than in non-treated UWW, suggesting that resistant bacteria were not more fitted to regrow than their susceptible counterparts. Nevertheless, the microbiological risks associated with these effects in UWW treated by this and other AOPs are still a matter of concern that requires to be assessed. Even so, the results presented suggest the potential of UVA-LEDs photocatalysis to be successfully used as part of the tertiary treatment of UWW. The cost effectiveness in terms of energy consumption per volume of treated UWW, the design of new reactor configurations in what concerns to optimal light distribution, immobilization of the photocatalyst on adequate substrates, and the definition of conditions to minimize microbial regrowth, are critical aspects to consider for a successful implementation.

Chapter 3. Pilot scale photocatalytic membrane reactor

The present chapter describes the approach used for the development of the pilot scale photocatalytic membrane reactor (PMR). The LEDs tested in the previous chapter are up-scaled to be implemented in a pilot scale equipment employing photocatalytic membranes. In this way, TiO_2 is immobilized on ceramic membranes in order to avoid the disadvantages of slurry photocatalytic systems, such as catalyst recovery. Design and development of the technology were performed in collaboration with Adventech and the department of civil and environmental engineering of "Università degli Studi di Salerno". The potential of the developed PMR in the removal of antibiotics (fluoroquinolones, FQs), bacteria and antibiotic resistance genes (ARGs) from secondary urban wastewater is shown. The microbiological quality of the permeate is assessed also after 7 days-storage to check possible bacteria regrowth (collaboration with biotechnology school of Universidade Católica do Porto and LEPABE of FEUP). Presence of selected antibiotics is investigated in permeate and concentrate of PMR process (including relative control tests). Moreover, since the process is performed recirculating the concentrate, the percentage removal of the selected FQs is provided applying a global mass balance. A comparison of physical and chemical cleaning to recover the initial permeance of the membrane is also performed. Finally, the cost estimation of the PMR implementation in real scale urban wastewater treatment plant is provided. A possible publication of this work is under preparation.

3.1 Description of the apparatus

After the LEDs-driven photocatalytic experiments in batch mode, for removal of antibiotics and antibiotic resistant bacteria from secondary UWW, a photocatalytic LED-driven ultrafiltration (UF) ceramic membrane system is designed in an optic of scale up. The main steps were:

- Choice of the ceramic membrane: geometry, dimensions, material, nominal pore sizes;
- Proposal of different configurations and materials for housing system, sized as function of transmembrane pressure (TMPR);
- Choice of sealing and holder system;
- Choice of the pump function of maximum flow rate and TMPR;
- Selection of pipes water network, choice of elastic, rigid pipes and joint connections;
- Choice of UVA-LEDs configuration and cooling system;
- Photocatalyst immobilization into ceramic membrane by dip-coating method;
- Assembling customized pieces of photocatalytic membrane system;
- Preliminary/safety experiments with the cross-flow UF system in order to test the sealing system and monitoring the pressure loss in time with acquisition programs/PC interface.

Alumina multichannel cylindrical membranes (details in **Section 3.2.1**) are chosen as support of photocatalyst. The membrane housing is designed to allow filtration in cross-flow; however, dead-end flow mode is another possible application. Two configurations are taken into account for the membrane housing (1.5 L capacity):

- The first configuration involves a glass cylindrical body containing the membrane. UVA LEDs irradiates the glass reactor from outside. The maximum pressure admissible inside the reactor is 5 bar and sealing systems are composed by gaskets and screws (**Figure 3.1a**). This configuration was already proposed in several works (**Section 1.6.2**);
- The second configuration involves a metal cylindrical body containing the membrane and three glass pipes accommodating UVA-LEDs. The light irradiation is carried out inside the reactor. The maximum pressure admissible inside the reactor is 6 bar and sealing system involves O-rings, gaskets and screws (**Figure 3.1b**). This configuration was chosen to perform the experiments since it is the best alternative considering safety and efficiency criterion.

Hydraulic circuit (stainless steel pipes) was designed by eng. Sérgio Silva (Adventech) and assembled (**Figure 3.1c**). It involves pneumatic control valve actuators, two electromagnetic flowmeter and a pressure transducer. A high speed peristaltic pump (maximum 0.5 $m^3 h^{-1}$) was

chosen to reach maximum 8 bar. The whole pilot system is designed using the software AUTOCAD 2D and 3D. The system allows to work in dead-end and cross-flow mode (including the backwashing mode) through different actuators combinations. Two 50 L tanks (with ultrasonic water level sensor) feed the hydraulic circuit. The compressed air line (6 bar) is also linked to the housing of the membrane in order to create back-pulsing and remove the foulant material from the external surface of the membrane.

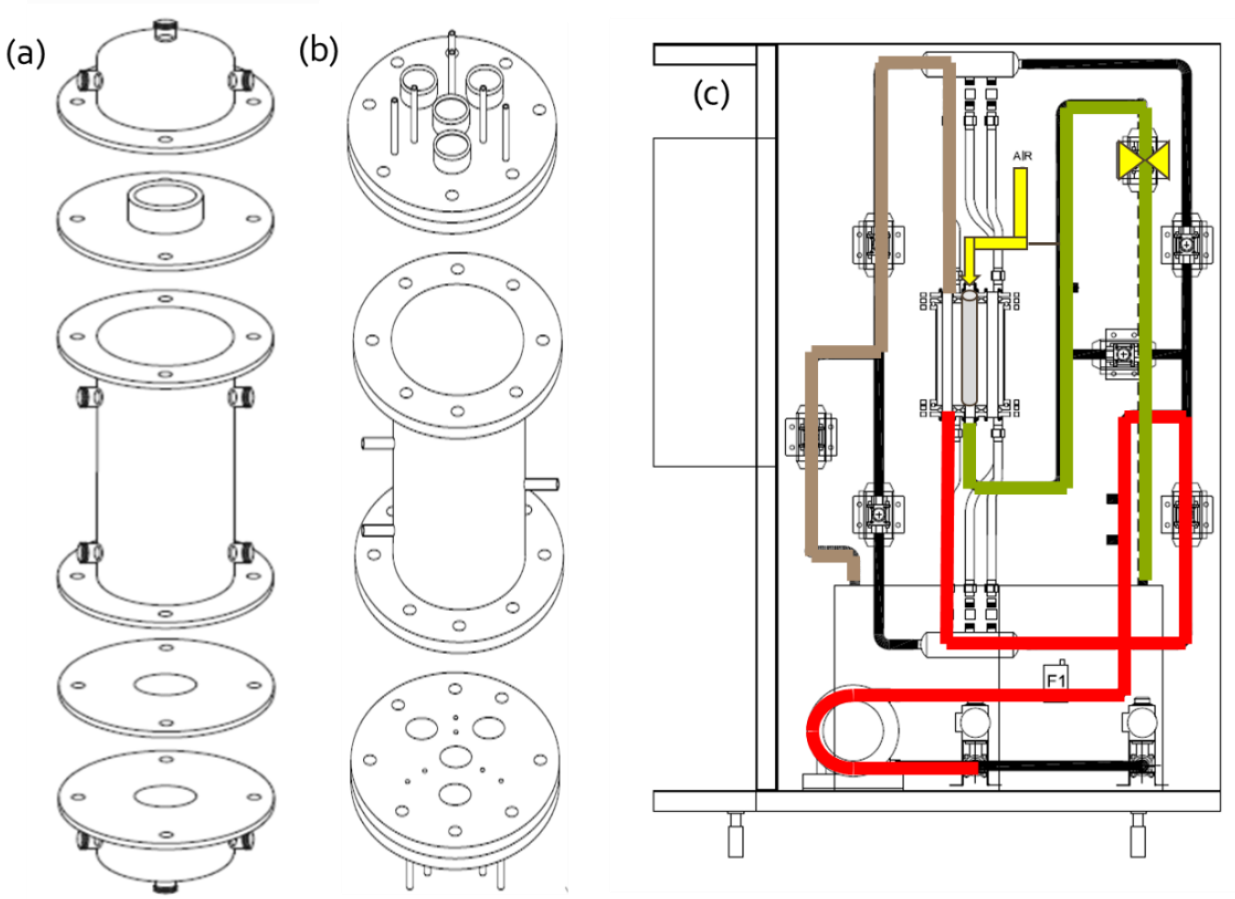

Figure 3.1. Schematic representation of membrane housing involving borosilicate (a) and stainless steel materials (b); PMR working in cross-flow mode (feed in red, concentrate in brown, permeate in green and backpulse system in yellow) (c).

Six UVA-LEDs (10 W) previously used in the lab scale tests (**Figure 3.2a**) and characterized in **Section 3.2.4** are fixed on aluminum heatsink and placed in the glass pipes of the reactor (**Figure 3.2b**). An innovative cooling system involving Peltier module was designed and assembled to cool down (convection) the LEDs by cold air (**Figure 3.2c**).

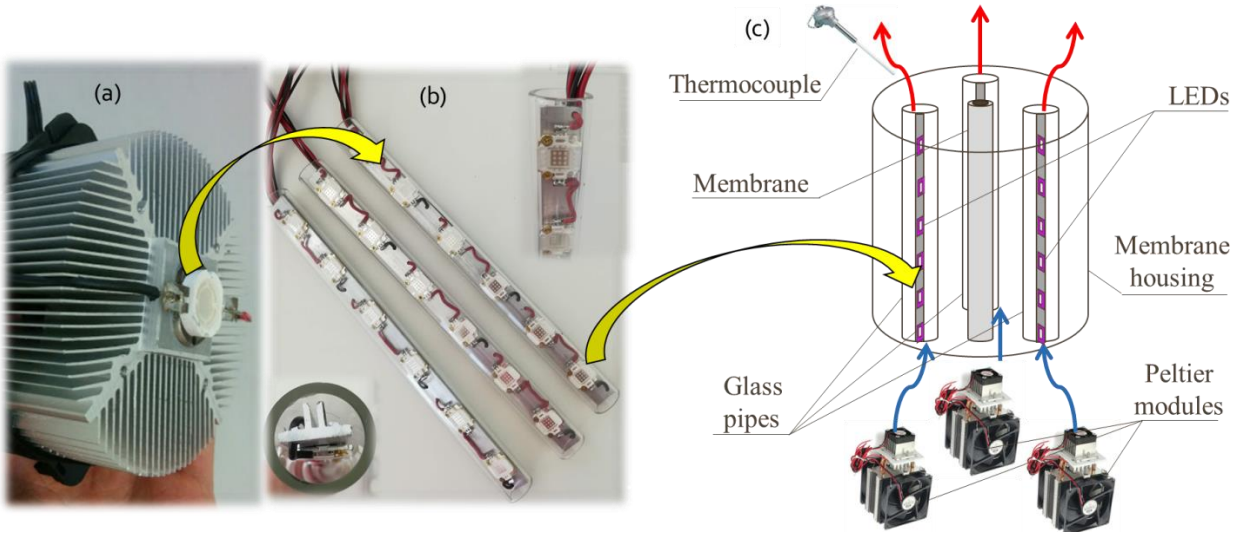

Figure 3.2. LED and heatsink/fan used in lab scale study (a); LEDs and heatsink accomodated in glass pipes (b); Ceramic membrane and LEDs configuration in the housing of PMR (c).

Commercial TiO_2-P25 (Degussa, Evonik) was immobilized into the ceramic membrane by the dip-coating method in order to form the active layers and to fix the catalyst on the rough membrane surface (details in **Section 3.2.3**).

The sealing of the housing and the hydraulic circuit were tested in cross flow filtration considering a maximum flow rate of 0.5 m^3 h^{-1} and a maximum pressure of 3 bar. No leaking occurs at the aforementioned conditions.

All the system (peristaltic pump, valves, back-pulsing, LEDs light intensity, cooling system) (**Figure 3.3a and b**) can be controlled in remote by programmable logic controller installed in the control panel (**Figure 3.3c**). Photocatalytic UF can be run in pressure control mode and flow-rate control mode. When the pressure is over 3 bar, a safety device stops the pump. However, in the case of glass outbreak, there is no critical risk: LEDs are ecofriendly (do not contain mercury or other warning materials) and the operator is protected (the eventual shot is screened by metal cylindrical body). Possible spread and release of the photocatalyst with the treated effluent is a concern that must be considered during the development of photocatalytic UF technologies. In the particular case of this PMR, the filtration occurs from the photocatalytic surface (external side) to raw surface (internal side) of the membrane; thus, the risk associated to release of photocatalyst in the permeate is reduced.

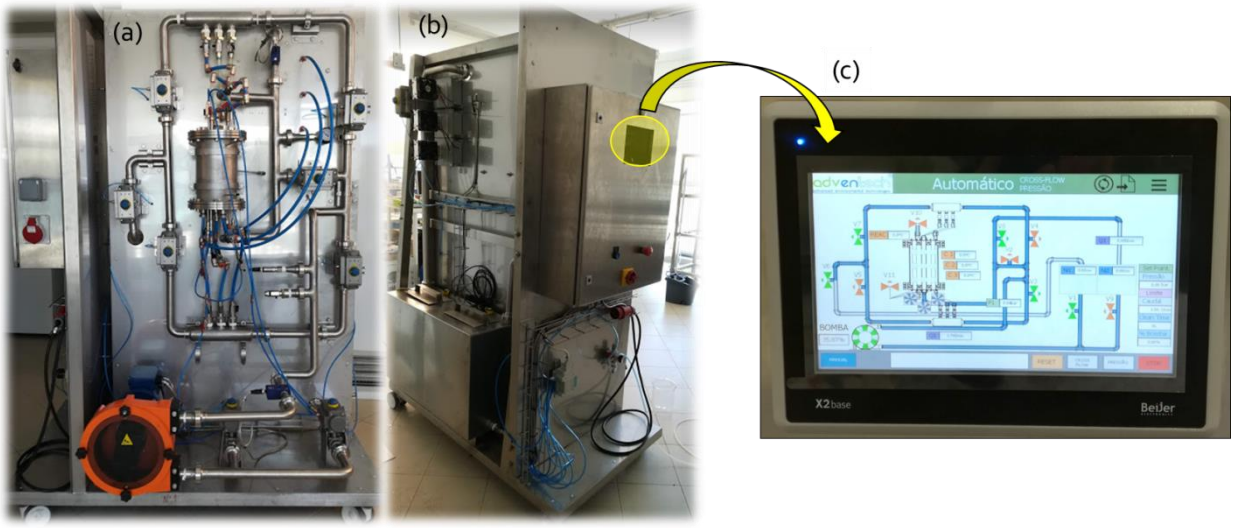

Figure 3.3. Front (a) and back (b) view of PMR; Touch screen panel showing process parameters (c).

3.2 Material and methods

3.2.1 Chemical and materials

Ofloxacin (OFL, CAS number 82419-36-1), ciprofloxacin (CIP, CAS number 85721-33-1) and enrofloxacin (ENR, CAS number 93106-60-6) were supplied by Sigma-Aldrich. Antibiotics were suspended in methanolic stock solution at concentration of 500 mg L^{-1}. Plate Count Agar (PCA) and Tryptone Bile X-Glucuronide Agar (TBX) used as culture media were purchased from Sigma-Aldrich. Multichannel tubular ceramic membranes with selective layer of α-Al_2O_3 (nominal pore size of 100 nm) were provided by Rauschert Distribution GmbH, Inopor®. Membranes are 305 mm length with 15 mm glazed ends. The external diameter is 25 mm and it presents 19 internal channel of 3.5 mm diameter. TiO_2-P25 (80% anatase, 20% rutile) was supplied by Evonik Degussa GmbH.

3.2.2 Wastewater characterization

The secondary effluent of an urban wastewater treatment plant (UWWTP) was collected from an UWWTP located in Northern Portugal. The wastewater characterization is performed with the help of dr. Cátia Graça (FEUP) and the results are presented in **Table 3.1**. The analytical methods used to characterize this urban wastewater (UWW) are detailed in **Section 3.2.8**.

Table 3.1. Secondary UWW characterization.

Component	Concentration (mg L^{-1})
Dissolved organic carbon	11.0 ± 0.8
Dissolved inorganic carbon	48.1 ± 1.4
Total suspended solids	16.8 ± 1.2
Na^+	13.8 ± 1.0
NH_4^+	13.3 ± 2.2
K^+	2.0 ± 0.2
Ca^{2+}	4.3 ± 0.3
Mg^{2+}	2.2 ± 0.1
Cl^-	89.9 ± 16.7
PO_4^{2-}	1.4 ± 1.2
NO_3^{2-}	0.9 ± 0.4
SO_4^{2-}	41.6 ± 4.4

3.2.3 Membrane development

TiO_2-P25 was immobilized on the external surface of the membrane using a dip-coating procedure (Athanasekou et al. 2014). Briefly, the catalyst was placed in a graduated cylinder containing distilled water (50 g L^{-1}). Both ends of the membrane were sealed with parafilm and the membrane was coated two times in the prepared solution. Down/up velocity and dip time were respectively 50 mm min^{-1} and 30 s. After each coating step, the membrane was dried at 120 °C for 1 h and finally treated at 200 °C for 3 h.

3.2.4 Experimental setup

The PMR is described above (**Section 1.6.2).** The raw/coated membrane is assembled in the stainless steel housing accommodating LEDs (**Figure 3.4a**). Each LED (working at 9 W) presents an emission peak at 372 nm and a total irradiance of 20 W m^{-2} (**Figure 3.4b**). The emission spectrum and the irradiance were obtained at 4 cm (distance between the membrane and the LEDs) using a spectrometer (Ocean Optics USB2000+) with cosine corrector and *Spectra Suite* software.

The system involving assembled housing and hydraulic circuit is set up to work in cross-flow configuration, setting the transmembrane pressure at 1 bar, transducer, flowmeter and pump being connected to a programmable logic controller. The feed passes through the housing and part of the water is forced (due to the pressure) to pass through the external surface of the

membrane, flowing out from the internal channels (**Figure 3.4c**). The concentrate is recirculated, while the permeate is collected for further analysis. Before starting the filtration, secondary UWW (15 L) is recirculated in the feed/concentrate circuit for 15 min. Standard physical cleaning (backwash and backpulse) and chemical cleaning with H_2O_2 at 30% v/v (only inside the membrane) are used after each test to recover the original permeance of the membrane. After chemical cleaning, the membrane is washed with distilled water until H_2O_2 is not detected (according to the colorimetric method using titanium IV oxysulfate; DIN 38402H15).

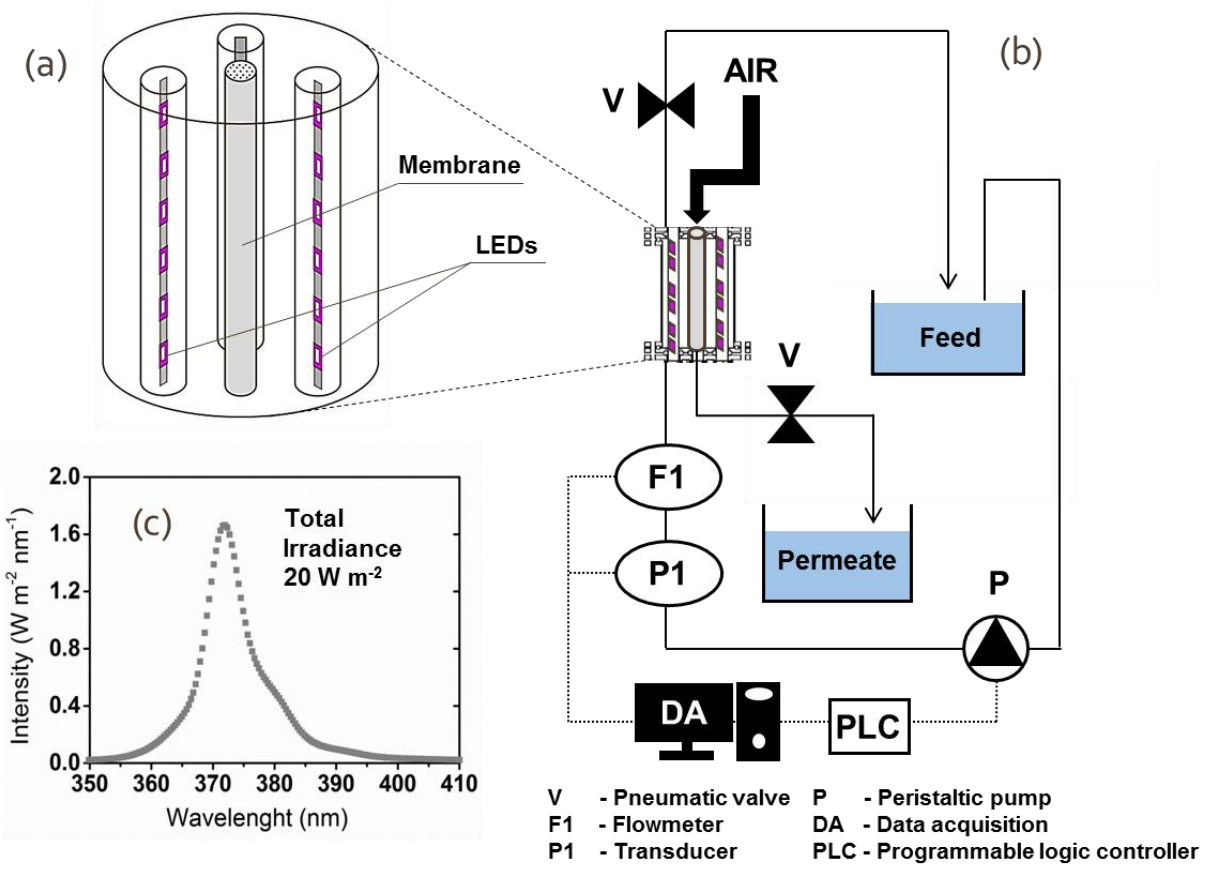

Figure 3.4. Ceramic membrane and LEDs configuration in the housing (a); photocatalytic membrane reactor working in cross-flow mode (b); light spectra of the LEDs (c).

3.2.5 Bacteria and gene retention

Secondary UWW was filtered using the raw membrane without LEDs. All the produced permeate (6 L) was collected in sterile bottles. 4 L were used for bacteria/gene quantifications, while 2 L were stored for 7 days in the dark at room temperature (24 °C) to assess possible bacterial

regrowth, simulating a wastewater storage scenario before its reuse. The tests were performed in duplicate.

3.2.6 Degradation and adsorption of antibiotics

A volume of 3 mL of antibiotic stock solution was spiked in an empty 1 L flask and dried using low nitrogen flow. After all the methanol was evaporated, the flask was filled with 1 L of secondary UWW, gently mixed and sonicated for 3 min. All the content was added in the feed tank containing the remaining 14 L of secondary UWW. Filtration took place using the raw membrane without light (UF) or with light (UF+UVA), and the TiO_2 coated membrane without light (TiO_2-UF) or with light (TiO_2-UF+UVA).

Before the filtration started, 2 mL of feed were collected. During filtration, 2 mL permeate samples were collected at time 0, 10, 20, 30, 60, 120, 180 and 240 min. After the collection of the last permeate sample, 2 mL of concentrate samples were also collected. All the samples were collected in duplicate.

The concentration of the three antibiotics in the permeate during the sampling time, and in the concentrate after 4 h of treatment, was normalized with respect to the initial feed concentration (100 µg L^{-1}). Moreover, the removal percentage of the antibiotics (removal (%)) at the end of the process (with respect to the initial mass of antibiotics introduced into the system) was expressed according to the mass balance given by **Eq. (3.1)**:

$$Removal\ (\%) = \left(1 - \frac{C_{conc,240}\, V_{conc,240} + C_{perm,240}\, V_{perm,240}}{C_{feed,0}\, V_{feed,0}}\right) \times 100 \qquad (\boldsymbol{Eq.3.1})$$

where $C_{conc,240}$, $C_{perm,240}$, and $C_{feed,0}$ are the concentrations of antibiotics in the concentrate at time 240 min, permeate at time 240 min, and feed at time 0 min. $V_{conc,240}$, $V_{perm,240}$, and $V_{feed,0}$ represent the respective volume of wastewater.

The methodology to calculate the final mass of the antibiotics in the permeate tank at time 240 min ($C_{perm,240}\, V_{perm,240}$) is an estimation according to the **Eq. (3.2)**:

$$C_{perm,240}\, V_{perm,240} = \sum_{i=0}^{240} C_{perm,i}\, V_{perm,i} \qquad (\boldsymbol{Eq.3.2})$$

where $C_{perm,i}$ represents the antibiotics concentration in the permeate flow at generic time i and $V_{perm,i}$ is the volume at generic time i, estimated using the permeate flow (**Figure 3.5**).

3.2.7 Bacterial count and gene quantification

Secondary UWW and the permeate (including the stored samples) were analysed in terms of total heterotrophs and total coliforms. Bacterial groups were enumerated according to the membrane filtration method using PCA (for total heterotrophs) and TBX agar (for total coliforms). Cellulose nitrate filters (0.22 µm porosity, Biotech, Germany) were used to retain bacteria present in the samples or serial diluted samples (triplicates). The filters were placed on PCA and TBX medium and respectively incubated at 30 °C and 37 °C for 24 h. The results are expressed in terms of log (CFU / 100 mL), the limit of quantification (LOQ) being 1 log (CFU / 100 mL) for all the bacterial groups.

Molecular biology assays were applied on secondary UWW and permeate (fresh and stored samples) in order to quantify 16S rRNA and *intI1* genes. The samples were filtered through polycarbonate membranes (0.22 µm porosity, Whatman, UK) and PowerWater was used as DNA extraction kit. Power SYBR green and KAPA SYBR were used as master mix for *intI1* and 16S rRNA, respectively. Gene quantification is performed using standard curve method in qPCR system (Life Technologies, Carlsbad). The results are given in log (copy number / 100 mL), considering the LOQ of 2 log (copy number / 100 mL) for *intI1* and 3 log (copy number / 100 mL) for 16S rRNA. DNA extraction and qPCR assays were performed by Joana Silva (Universidade Catòlica Portuguesa).

3.2.8 Analytical methods

Ion chromatography analyses were performed in a Metrohm 881 Compact IC Pro apparatus, equipped with a Metrosep C4 Cationic Exchange Column (250 mm × 4.0 mm) for quantification of cations and a Metrosep A Supp 7 Anionic Exchange Column (250 mm × 4.0 mm) for quantification of anions. The dissolved organic carbon (DOC) and inorganic carbon (DIC) contents were determined using a Shimadzu TOC-L analyzer.

OFL, CIP and ENR concentrations were monitored with the help of dr. Cátia Graça and dr. Rita Ribeiro (FEUP) by ultra-high-performance liquid chromatography (UHPLC, Nexera - Shimadzu) in an equipment with two pumps (LC-30AD), autosampler (SIL-30AC), oven (CTO-20AC), degasser (DGU-20A5) and fluorescence detector (RF-20AXS). Chromatographic separation was optimized using a Kinetex™ 1.7 µm XB-C18 100 Å column (100 × 2.1 mm i.d.) supplied by Phenomenex, Inc. (California, USA), set at 40 °C. The mobile phase consisted of 0.1% aqueous formic acid (A) and methanol (B) with a flow rate of 0.3 mL min^{-1} and the following gradient mode regarding (A): 25% for 0.5 min, a linear gradient from 25 to 65% in 9 min (held for 0.5 min), a linear gradient from 65 to 25% in 0.5 min, and an equilibration time of 7.5 min,

totalizing a run time of 18 min. The autosampler temperature was kept at 15 °C and the injection volume was 30 μL. The excitation and emission wavelengths of the fluorescence detector were set as 290 and 460 nm, respectively.

3.3 Results and discussion

3.3.1 Permeate production of raw and photocatalytic membrane

Operating conditions (Choi et al. 2005; Guerra et al. 2012) and cleaning procedures (with/without use of chemical) (Shi et al. 2014) represent common tools to deal with fouling phenomena. However, a pre-treatment of the feed wastewater also makes difference in fouling mechanism (Winter et al. 2016). For instance, before the UF process, an additional pre-treatment can be implemented to minimize the biopolymers concentration in the effluent and at the same time remove micropollutants (Zheng et al. 2014). Coagulation, adsorption, UV and advanced oxidation technologies (H_2O_2/UV, O_3) as pre-treatment to UF processes in UWW reclamation (Lehman and Liu 2009; Jeong et al. 2014; Filloux et al. 2016; Winter et al. 2016; Hamid et al. 2017) were successfully applied to reduce the membrane fouling.

In the present study, the production of the permeate during UF of secondary UWW was affected by fouling, the permeance decreasing from ca. 612 to 14 L m^{-2} h^{-1} bar^{-1} after 4 h of the filtration process. A drastic decrease of permeance was observed during the first hour (from 612 to 50 L m^{-2} h^{-1} bar^{-1}), followed by a flux stabilization around 14 L m^{-2} h^{-1} bar^{-1}. A 5 h backwash step (5 L min^{-1} using distilled water) combined with backpulse (10 sec frequency at 3 bar pressure) did not restore completely the initial permeance of the membrane. The first physical cleaning step (second cycle in **Figure 3.5a**) partially restored the initial permeance, while the second physical cleaning step had no effect (third cycle in **Figure 3.5a**). Due to the inefficiency of the physical cleaning tested, the internal channels of the membrane were filled with H_2O_2 (30% v/v) and left to react overnight. The H_2O_2 chemical cleaning restored almost all the initial permeance (556 L m^{-2} h^{-1} bar^{-1}) and permitted to have similar permeate production from the second to the third ultrafiltration cycles (**Figure 3.5b**).

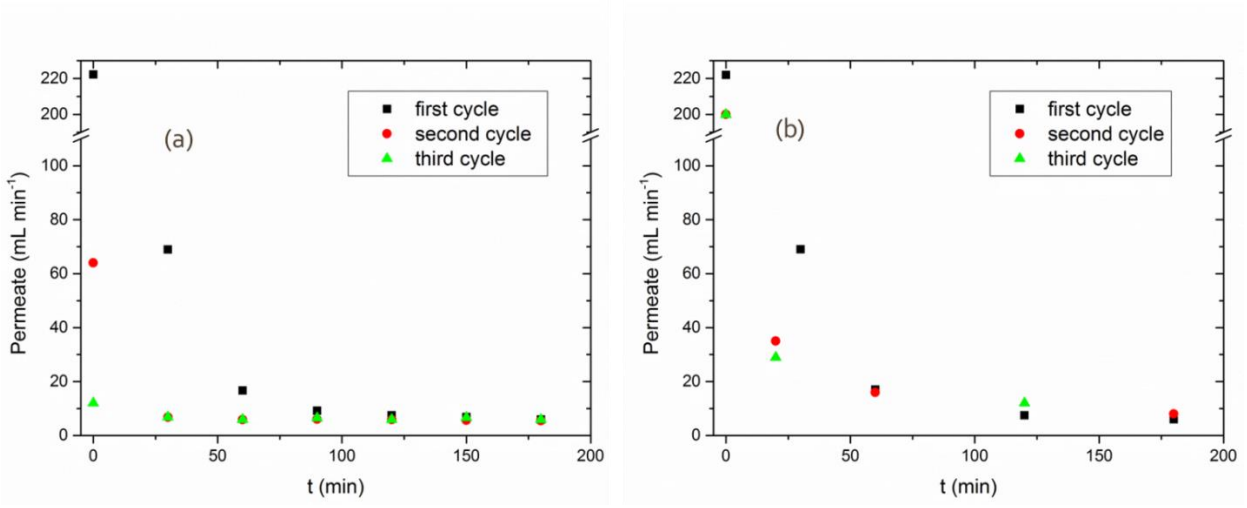

Figure 3.5. Permeate flow during ultrafiltration (1 bar transmembrane pressure) of secondary UWW. Between each UF cycle a cleaning step was performed. Effect of physical cleaning (a) and chemical cleaning (b) on recovering the initial permeance.

Generally, as more catalyst is deposited on the membrane, the higher is the photocatalytic efficiency in the degradation of pollutants present in the wastewater, until a certain amount of photocatalyst. However, the deposition of photocatalyst on the surface of the membrane decreases the initial pore size, affecting negatively the permeance property. A compromise between the photocatalytic performance and permeate production is needed when designing an efficient PMR process. A good immobilization technique should avoid the heterogeneous coverage and possible leaching of the catalyst during filtration. Some authors focused the research on the development of TiO_2 layers that do not compromise the permeance of the original membrane (Athanasekou et al. 2012; Romanos et al. 2013). In particular, chemical vapour layer-by-layer deposition of TiO_2 on alumina membrane did not compromise the initial permeance of the ceramic membrane as the conventional nanoparticle growth chemical vapour deposition method (Athanasekou et al. 2012). In the present study, a simple and up-scalable technique (dip-coating) of photocatalyst deposition was used to immobilize TiO_2-P25 on the external side of the membrane. After catalyst immobilization, the initial permeance did not decrease. It can be attributed to the fact that photocatalyst deposition (diameter smaller than the pore size of the membrane) did not occluded the original pores. In a different study, carbonaceous modified TiO_2 (due to its high hydrophilicity and low particle size) improved the permeance of a photocatalytic membrane with respect to the raw membrane (Moustakas et al. 2014).

3.3.2 Disinfection efficiency and genes removal

The efficiency of alumina membrane to retain bacteria and genes present in secondary UWW was evaluated. CFU of total heterotrophs and total coliforms and copy number of 16S rRNA and *intI1* were quantified before and after the UF process. Moreover, secondary UWW and permeate samples were stored during 7 days in dark at room temperature and the selected bacteria and genes were quantified again. Conventional cultivable methods are worldwide used to easily and quickly check the microbial characteristic of a water, including permeate samples (Arnal et al. 2004). Molecular biology is a powerful tool applied on water samples to quantify specific genes. It gives an idea of real bacterial load, both cultivable and not cultivable groups being considered. In particular, 16S rRNA is an indicator of bacteria presence (live and dead), while *intI1* is related to the horizontal gene transfer.

Concerning cultivable bacteria (**Figure 3.6**), secondary UWW exhibits an initial load of total heterotrophs and total coliforms of 6.9 ± 0.1 and 5.7 ± 0.2 (CFU / 100 mL), respectively. However, these selected bacterial groups were not quantifiable in the permeate samples (< LOQ). The bacterial load of secondary UWW (without filtration) was lower after the storage during 7 days than that found for freshly collected UWW. Total heterotrophs and total coliforms decreased to 5.6 ± 0.3 and 5.2 ± 0.7 log (CFU / 100 mL), respectively. On the other hand, stored permeate showed no bacterial regrowth, the load of all the selected bacterial groups being under the LOQs. It is worth to mention that the DOC of permeate is almost the same of secondary UWW (**Table 3.1**), carbon sources being available for possible bacterial regrowth. Therefore, despite the permeate presents an ideal condition for bacterial regrowth, it seems that the permeate did not contain enough cells for bacterial fission.

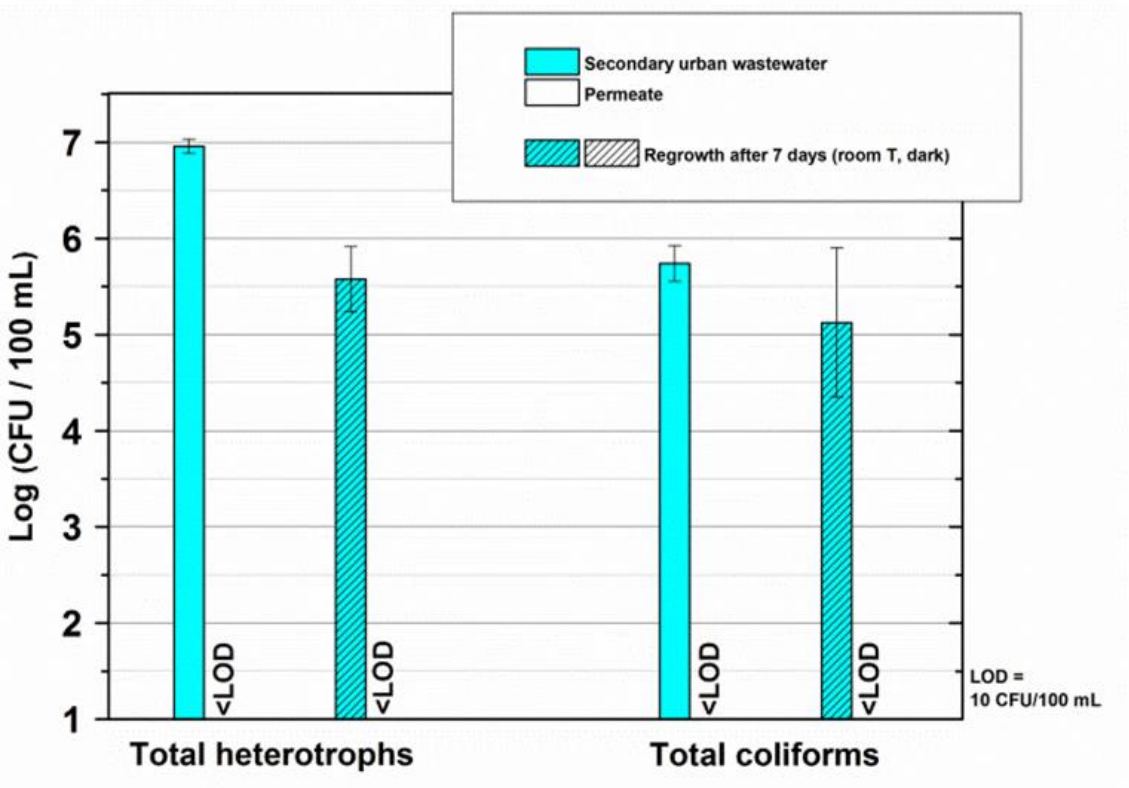

Figure 3.6. Total heterotrophs and total coliforms abundance before/after ultrafiltration process.

Regarding the genes (**Figure 3.7**), initial abundance of 16S rRNA and *intI1* in secondary UWW was 8.9 ± 0.1 and 7.5 ± 0.2 log (gene copy number / 100 mL). Permeate analysis revealed the presence of both genes, but 16S rRNA and *intI1* were reduced to 4.2 ± 0.1 and 2.6 ± 0.1 log (gene copy number / 100 mL), respectively. In another ultrafiltration study, using a 50 nm pore size membrane, both genes were also present in the permeate (Ren et al. 2018). Moreover, in the present study, 16S rRNA after water storage slightly decreased to 3.9 ± 0.1 log (gene copy number / 100 mL), showing no bacterial regrowth of uncultivable bacterial groups. Furthermore, *intI1* decreased to values under LOQ, preventing the horizontal gene transfer risk.

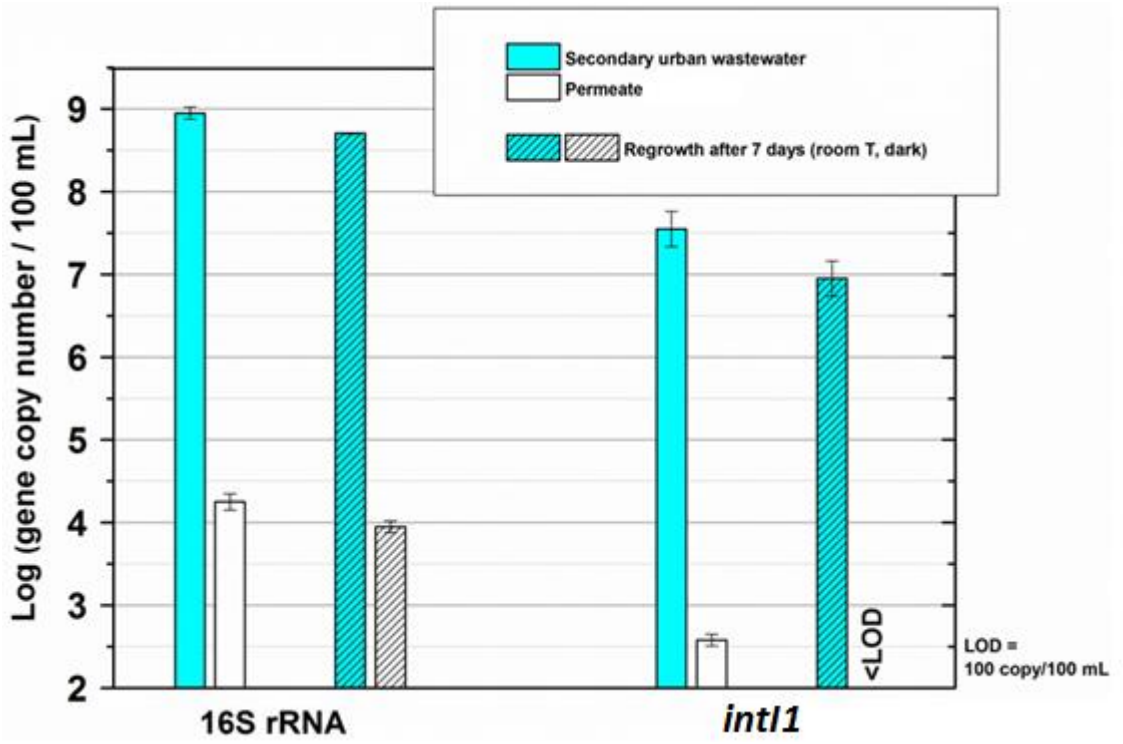

Figure 3.7. 16S rRNA and *intI1* abundance before/after ultrafiltration process.

These results demonstrate the efficiency of the UF system for wastewater disinfection. However, organic micropollutants are not expected to be retained by this membrane and, thus, the immobilization of the TiO_2-P25 photocatalyst is investigated in the next section as strategy to oxidize these pollutants.

3.3.3 Antibiotics quantification in the permeate and global mass removal

The concentrate destination of pressure-driven processes is an important issue to manage with caution. Some authors studied the application of the Fenton process (Miralles-Cuevas et al. 2017) and ozonation (Liu et al. 2014; Mendret et al. 2019) to treat the concentrate resulting from nanofiltration, showing the feasibility of these processes. In the present study, the concentration of FQs in the concentrate was the same or lower than in the initial feed (**Figure 3.8**).

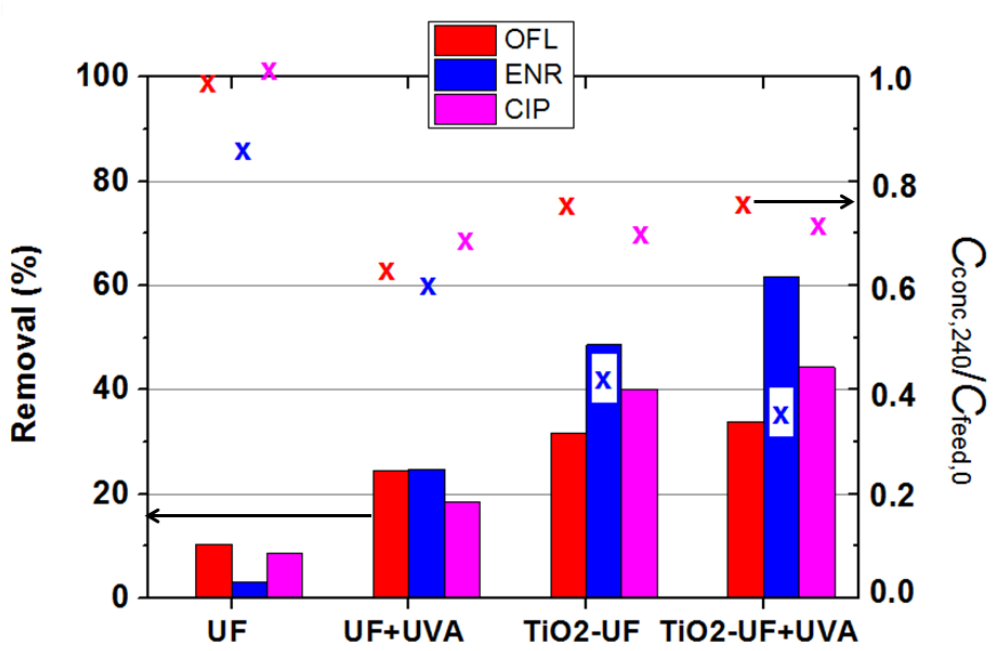

Figure 3.8. Removal of the three antibiotics after 4 h of photocatalytic ultrafiltration process and relative controls considering a global mass balance (bars). Normalized concentration of antibiotics in the concentrate after 4 h (crosses).

Regarding UF and TiO_2-UF, a possible explanation for the results shown in **Figure 3.8**, is given by some adsorption of the antibiotics on the membrane (especially ENR). Adsorption of pharmaceuticals on polyamide nanofiltration (Dolar et al. 2013a) and ceramic UF membranes (Espíndola et al. 2019) was already reported in the literature. Other study showed higher concentration of OFL in the permeate of UF than in the secondary UWW fed to the system (ca. 10% increase); however, the authors attributed the result to the analytical variance (Urtiaga et al. 2013). According to Kim and collaborators (2018), hydrophilic CECs as FQs ($Log_{KOW} < 2.6$) are unlikely adsorbed onto polymeric membranes in filtration processes. However, ligand exchange reaction between $AlOH_2^+$ and carboxyl group of OFL can be one of the main mechanisms through which OFL at zwitterionic phase (pH at ca. 7) binds to Al_2O_3 (Goyne et al. 2005). On the other hand, desorption of micropollutants can also take place, for instance as consequence of competitive adsorption-desorption with dissolved organic matter (DOM) (Aschermann et al. 2019). Likewise, micropollutants interacting with non-adsorbable DOM can be maintained in solution after adsorption treatment processes (Mailler et al. 2016). In the present study, according to the mass balance done (**Eq. 3.1**), final mass removal by membrane adsorption was less than 10% for the three single antibiotics in UF (**Figure 3.8**), but these differences are not significant since these results are affected by some uncertainty due to the estimates employed in the mass balance.

Regarding the UF+UVA experiment (**Figure 3.8**), higher removals were obtained for OFL and ENR (25%) than for CIP (18%); however, it is worth to say that CIP can be a transformation by-product of ENR photolysis, meaning that some CIP might be formed from ENR (Babić et al. 2013). FQs are present in UWW under zwitterionic form and they can absorb light wavelengths between 230-350 nm (Ge et al. 2010; Dolar et al. 2013b). They have short half-life under solar radiation compared to other antibiotics groups (macrolides and sulphonamides), singlet oxygen being an effective reactive oxygen species (ROS) for degradation of most FQs. In wastewater treatment, DOM competes with FQs in photon absorption, the photolytic degradation of FQs being slower than in distilled water (Ge et al. 2010; Hapeshi et al. 2010; Wammer et al. 2013). In the present work, considering no light absorption from FQs, some indirect photolysis takes place (UF+UVA vs. UF in **Figure 3.8**). This output is in accordance with the previous results obtained in slurry (Chapter 2), where ca. 90% of OFL degradation in secondary UWW was achieved after 3 h of UVA-LEDs photolysis (Biancullo et al. 2019). Moreover, partial degradation of ENR under UV-Vis radiation was already reported in another study (Lu et al. 2013).

FQs adsorption on the photocatalyst (32%, 40% and 48% for OFL, CIP and ENR, respectively) presents higher mass removals than UVA photolysis (**Figure 3.8**). Adsorption of CIP and OFL on slurry TiO_2-P25 was already reported in literature (Van Wieren et al. 2012; Eckert et al. 2015), spiked (Diao et al. 2017) and non-spiked tests (Sousa et al. 2012) showing ca. 10% adsorption of CIP and OFL on TiO_2-P25. In another study, adsorption on TiO_2 immobilized over glass spheres also contributed to ca. 10% CIP removal in 1 h (Xing et al. 2018).

Regarding the photocatalytic UF treatment (TiO_2-UF+UVA), and according to the global mass balance, ENR removal (62%) was higher with respect to the other FQs tested (33% and 43% for OFL and CIP, respectively) (**Figure 3.8**). Moreover, OFL, ENR and CIP concentrations in the permeate collected during the TiO_2 photocatalytic UF treatment (TiO_2-UF+UVA), as well as the respective control tests (UF+UVA and TiO_2-UF), were normalized with respect to the permeate concentrations determined for UF at each respective treatment time (**Figure 3.9**). The concentrations of FQs in the permeate increase when employing ultrafiltration with the TiO_2-coated membrane without (TiO_2-UF) and with radiation (TiO_2-UF+UVA), after some period reaching some stabilization in most of cases. However, the antibiotics removal by photocatalysis does not seem to be really efficient at the employed conditions, considering the results of control tests (i.e., the adsorption on the TiO_2 coated membrane and indirect photolysis, **Figure 3.8** and **Figure 3.9**). Adsorption of effluent organic matter on the immobilized photocatalyst may have compromised the photocatalytic activity. Several studies in the literature for the photocatalytic

degradation of CIP, ENR and OFL with TiO_2-based systems different than membranes (Lu et al. 2013, 2014; Sood et al. 2016; Diao et al. 2017) reported partial degradation (60-65%) for all the three FQs after 1 h treatment, even when studying OFL and CIP in secondary UWW (Sousa et al. 2012). Thus, the operating conditions and membrane cleaning procedure should be optimized in future works, in order to exploit the advantages of this PMR for UWW treatment, i.e. simultaneous disinfection and degradation of organic micropollutants.

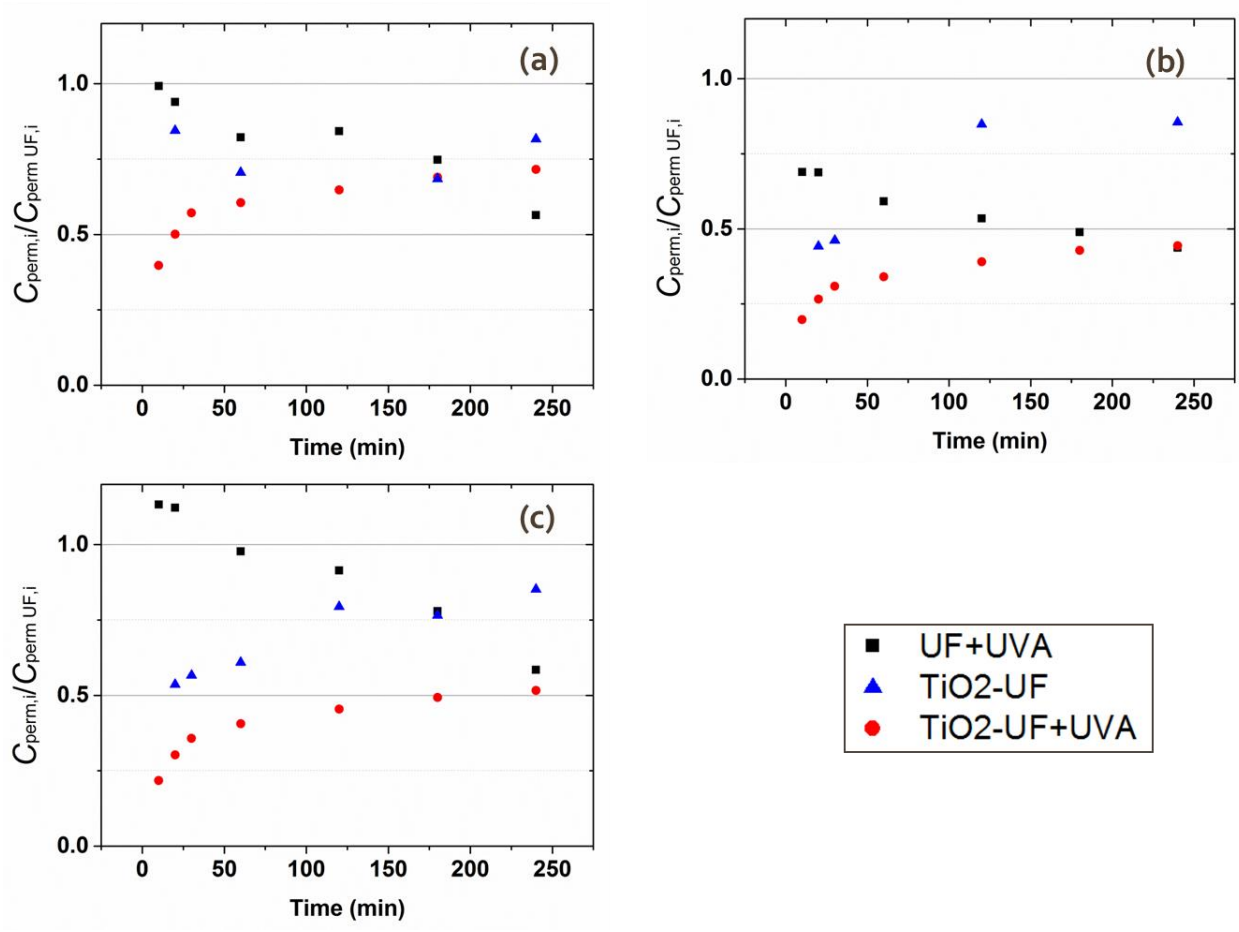

Figure 3.9. Concentration of OFL (a), ENR (b) and CIP (c) in the permeate during ultrafiltration using raw membrane with light (UF+UVA) and TiO_2 coated-membrane without (TiO_2-UF) or with light (TiO_2-UF +UVA) normalized with respect to the concentration in UF permeate.

3.3.4 Economic viability of the new solution and its market acceptability

Capital expenditure (CAPEX) and operational expenditure (OPEX) represent, respectively, the development cost of technology and the operating cost during its lifespan. OPEX of conventional tertiary treatment (i.e. chlorination and UV radiation) and AOPs have already been estimated in

the literature (Benotti et al. 2009; Jordá et al. 2011; De la Cruz et al. 2013; Zhuang et al. 2015). As already mentioned before, conventional tertiary treatments have low efficiency in the removal of CECs and in the control of antibiotic resistance from UWW, the OPEX resulting low in comparison with the more efficient AOPs. Considering standard operational conditions, costs for chlorination (chlorine dose of 40 mg L^{-1}, 1 h contact time) and UV radiation (500 mJ cm^{-2} UV dose) have been estimated as 0.5 € and 0.6 € per 100 m^3 of UWW. On the other hand, Fenton (Zhuang et al. 2015) and solar photo-Fenton processes (Jordá et al. 2011) (both using Fe^{2+}/H_2O_2 ratios of 1/10 at pH 3) are found more expensive processes due to the cost related to the reagents. In particular, the proposed OPEX (related to the treatment of 100 m^3 of UWW) is in the range of 13.7-73.9 €. Another study considering the feasibility of UV/H_2O_2 process reports its OPEX between 126-179.8 €, residence time (10-60 sec) and H_2O_2 dose (20-50 mg L^{-1}) being the main parameters affecting the cost of the process (De la Cruz et al. 2013). OPEX of heterogeneous photocatalysis should consider also the cost of catalyst separation. An interesting study on PMR (slurry) reports the cost related to the removal of pharmaceuticals from river water. An OPEX of 86 € is found to treat efficiently 100 m^3 of water using UVC lamps and low catalyst concentration (0.05 g L^{-1}) (Benotti et al. 2009).

The pilot PMR developed in the framework of this thesis has the potential to host more than one tubular membrane (1 m long, 0.078 m^2); however, only one short membrane (0.3 m, 0.024 m^2) was used for the experimental work conducted in this PhD thesis. At this condition, the pilot has a CAPEX of 16,000 €. In particular, hydraulic circuit (including the wheels structure), PLC and metal housing (including LEDs and membrane) have costs of 3,000, 5,000 and 1,500 €, respectively. The probes (pressure transducer, flowmeters, level sensors), the pneumatic valves (including air compressed system) and the peristaltic pump have a total cost of 1,500, 2,000 and 3,000 €, respectively. Considering the target of treating 100 m^3 in one day, more membranes have to be implemented in the pilot unit. Assuming a constant permeance of photocatalytic UF membranes around 350 L m^{-2} h^{-1} bar^{-1} (50% of original value) during the day, at least 12 m^2 of filtrating surface (corresponding to 154 membranes) are needed to satisfy the target treating volume. Considering that one up-scaled membrane housing contains 38 membranes (**Figure 3.10a**), four big housings should be implemented in the real scale scenario. The up-scaled housing involves a central metal cylinder (0.4 m diameter and 1 meter long) with six sight glasses and two holed flanges on bottom and top extremities (**Figure 3.10a**). LEDs (ten in arrays) inside the glass pipes constitute the internal source of light, while the LEDs arrays situated out of the sight glasses are external source of light. **Figure 3.10b** shows the plane section of the membranes and LEDs. This configuration should be able to guarantee enough radiation uniformity on the photocatalytic membranes (central and perimetric ones). The total number of LEDs for a single

big housing is six hundred. The LEDs should be set at low power (<10 W) to increase the feasibility of the treatment process. A bigger hydraulic circuit including four pumps and bigger tanks, should be used to feed the four big housings. Its total cost is estimated to be four times higher than the pilot scale circuit (12,000 €). CAPEX of PMR implemented in real scenario is the sum of cost related to a big hydraulic circuit, four pumps (12,000 €), a PLC (5.000 €), 150 membranes (300 € each), 2,400 LEDs (5 € each) and four big housings (5,000 € each). Finally, CAPEX is estimated as 106,000 €.

Considering the cost of energy equal to 0.20 € kW^{-1} h^{-1}, daily OPEX is the sum of LEDs radiation and pumping cost, estimated as 115.2 € (576 kW h consumption) and 0.6 € (3 kW h consumption), respectively. In the previous calculation, LEDs and pumps are assumed to work 24 h daily. The pumping energy is estimated according to Athanasekou and collaborators (2015). OPEX of UF PMR (involving immobilized doped catalyst) treating dye solutions are already proposed in literature (Athanasekou et al. 2012, 2014, 2015; Athanasiou et al. 2016). The OPEX related to treat 100 m^3 of a solution of dyes ranges between 6-24 €. However, the studies do not take into account the fouling generated from UWW filtration (suspended solids and organic matter).

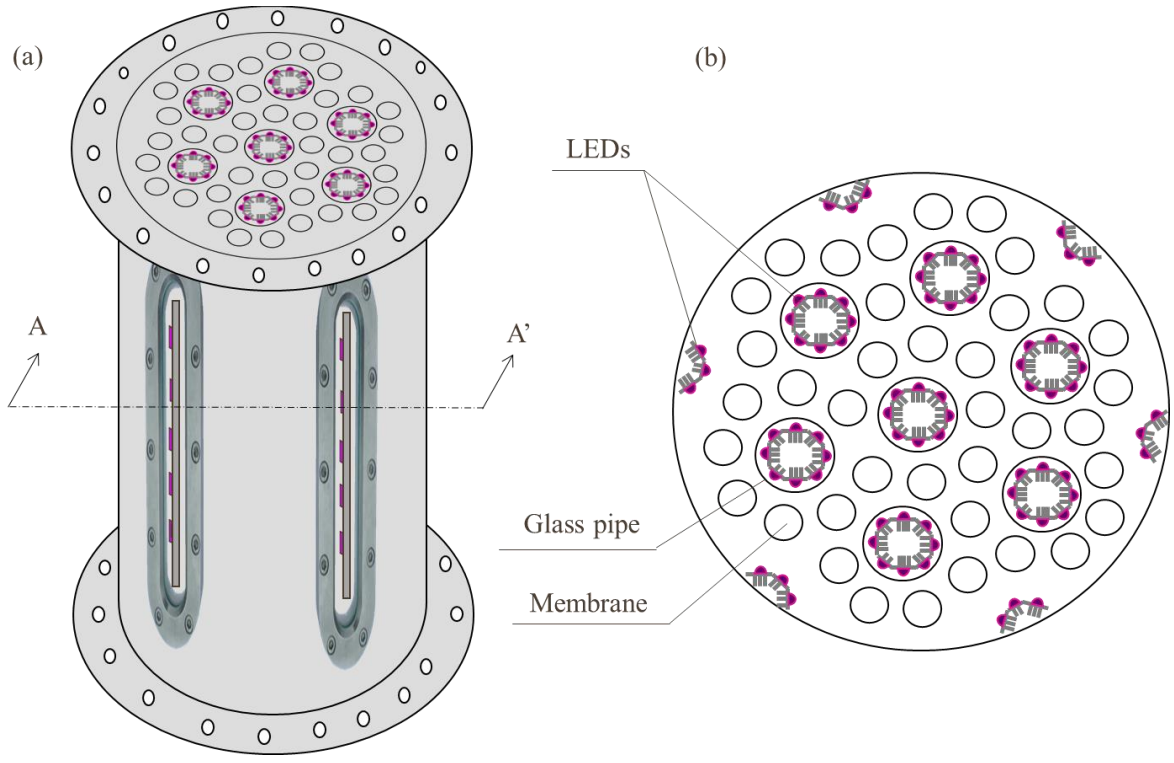

Figure 3.10. Real scale membrane housing involving 38 photocatalytic membranes and 600 LEDs (a). Cross section view of PMR (b).

3.4 Conclusion

PMRs are a compact technology with the potential to produce microbiologically safe and low content micropollutants effluent from UWW in limited space. Despite the already known effect of UF process on bacteria retention, the fouling due to the presence of solids and DOM decreased the production of permeate from secondary UWW. The risk of horizontal gene transfer is minimized considering the abundance of *intI1* in permeate and stored permeate. Moreover, the presence of 16S rRNA in the permeate did not create concerns, since the abundance of the mentioned gene slightly decreased after permeate storage (no bacterial regrowth). However, the presence of FQs in the permeate requires further process optimization. Moreover, for a full scale application of the PMR technology as tertiary treatment of UWW, the fouling should be better mitigated.

Chapter 4. Main conclusions and future work

In this chapter the main achievements of the lab scale batch and pilot scale tests are summarized, as well as the possible future work is proposed.

4.1 Final remarks

Advanced oxidation processes (AOPs) have high potential in water decontamination but some of them, as photocatalysis, do not still find application in large scale urban wastewater (UWW) treatment.

In the present PhD thesis, optimization of the light condition through innovative light sources (i.e. UVA-LEDs) favored the feasibility of heterogeneous photocatalysis in antibiotics removal from UWW, the optical thickness being one of the most important parameters to consider in the slurry configuration. Despite photocatalysis showed interesting results for the removal of selected antibiotics (especially ofloxacin), the microbiological risk in treated water was considered a threat. According to the results of the lab scale batch tests, at optimal operational conditions (1 g L^{-1} catalyst load and 4 LEDs), complete inactivation of selected bacterial groups was not reached even after 1 h treatment. Moreover, the risk of bacterial regrowth, especially for total heterotrophs, during the storage of treated water needs to be minimized. However, the antibiotic resistant bacteria was not considered alarming, since lower regrowth was observed than for the total bacteria.

Physical separation involving ultrafiltration membranes (100 nm pore size) demonstrated to be an excellent approach to retain bacteria and genes using low transmembrane pressure (ca. 1 bar), the microbiological regrowth in the permeate being mitigated. In particular, total heterotrophs and total coliforms were not detected in the produced permeate, whereas the presence of some non-cultivable bacteria was not excluded, 16S rRNA and *intI1* being detected at low concentrations. Moreover, the microbiological quality of the stored treated water did not create preoccupation, 16S rRNA being stable and *intI1* decreasing under the limit of quantification.

The developed pilot scale photocatalytic membrane reactor (PMR) consisting of UVA-LEDs and TiO_2 coated membranes guarantees that the photocatalyst is not released with the treated water, as in the case of the lab scale batch tests with slurry configuration. However, regarding the degradation of the selected antibiotics, despite the catalyst immobilized configuration is known to be less efficient than catalyst suspension configuration, better results were expected. In fact, the adsorption of antibiotics on the TiO_2 coated membrane together with the degradation through indirect photolysis (resulting from control tests) seem to play the major role in the removal of the selected antibiotics, rather than degradation by photocatalysis. Another limitation of the developed PMR is related to the permeance reduction due to fouling. For this reason, a cleaning procedure involving H_2O_2 was needed to restore the initial permeance of the membrane after each test.

The filtration surface used in the pilot scale reactor corresponds to ca. 0.02 m^2. However, a bigger housing was designed in order to reach 3.00 m^2 filtering surface area. Four of the aforementioned housings have the potential to treat 100 m^3 d^{-1} of secondary UWW with rough estimated operational expenditure in line with other AOPs (between 100-200 € per 100 m^3). However, the capacity and the cost refers to an optimized process dealing effectively with the fouling phenomena. Thus, the operating conditions and fouling mitigation strategies should be optimized in order to exploit the advantages of this PMR for UWW treatment and possible reuse.

4.2 Future works

Before UVA-LEDs driven-PMRs using immobilized catalyst are implemented at full scale, several technical and scientific issues should be addressed. The technical issues concern fouling phenomena and operational expenditure. On the other hand, scientific issues are related with photocatalytic efficiency and quality of the effluent.

Currently, it is difficult to decide which cleaning procedure is the most appropriate to restore the original permeance of the clogged membranes. In the present study, chemical cleaning with H_2O_2 showed higher efficiency than air backpulse and backwash. However, the long cleaning time (i.e. 12 h) is not feasible in real scale applications. Moreover, in pressure control mode, the cleaning procedure should start when a certain minimum permeate flux is reached (i.e. 20% of the maximum value). The application of a conventional pretreatment (i.e. microfiltration, coagulation) before photocatalytic ultrafiltration should be also investigated. In fact, despite the fact that an additional treatment seems to increase the overall cost of the process, fouling phenomena decreases and the use of cleaning procedures are reduced.

It is worth to mention that also cross flow velocity is an important parameter mitigating the fouling. However, the hydraulic regime in PMRs involving immobilized catalysts is different with respect to standard ultrafiltration. The available studies on PMRs show a gap of knowledge on the effect of turbulence on the fouling reduction, a laminar hydraulic regime being preferred to minimize the catalyst detachment from the membrane.

Moreover, the energy consumption related to the use of UVA-LEDs in the developed PMR has a critical weight on the overall energy requirement of the equipment. However, the UVA-LEDs system is designed to work at variable irradiance. Depending on the turbidity of the UWW, different irradiance should be tested in order to optimize the cost related to the light source. The use of photocatalysts absorbing visible light could be another option towards lower operational expenditure. However, the cost related to produce such non-commercial photocatalysts and its immobilization on the membranes can result in an overcharge of the capital expenditure.

The UVA-LEDs/TiO_2-P25 batch/slurry configuration showed higher removal of antibiotics that the tested catalyst immobilized process (PMR). In order to improve the photocatalytic efficiency of the PMR, more than two dip-coating cycles are advised to guarantee enough mass of photocatalyst on the coated membrane. At the same time, the permeance of each new prepared photocatalytic membrane should be checked, the original pore size expecting to decrease after each dip-coating step.

Depending on the specific site, UWW presents a diversity of contaminants of emerging concern (including antibiotics) and microbiological community. However, the concentrations of antibiotics present in UWW are often several order lower than that spiked in UWW for pilot scale studies. Therefore, the efficiency of PMRs in the removal of antibiotics at real concentrations should be also tested (i.e. without any spike of the UWW).

Another gap of knowledge concerns the toxicological study of permeate from PMRs involving the immobilized photocatalyst. In fact, possible transformed-products more hazardous than parent compounds can be generated during the photocatalytic process. Therefore several bioassays (i.e. toxicity, phytotoxicity) should be applied to the effluent of the PMR before the large scale technology implementation and possible water reuse in agriculture.

References

Abellàn MN, **Giménez J**, **Esplugas S**. Photocatalytic degradation of antibiotics: The case of sulfamethoxazole and trimethoprim. *Catal Today* 144: 131–136, 2009.

Abellán MNN, **Bayarri B**, **Giménez J**, **Costa J**. Photocatalytic degradation of sulfamethoxazole in aqueous suspension of TiO_2. *Appl Catal B Environ* 74: 233–241, 2007.

Acero JL, **Benitez FJ**, **Real FJ**, **Teva F**. Coupling of adsorption, coagulation, and ultrafiltration processes for the removal of emerging contaminants in a secondary effluent. *Chem Eng J* 210: 1–8, 2012.

Alexander J, **Knopp G**, **Dötsch A**, **Wieland A**, **Schwartz T**. Ozone treatment of conditioned wastewater selects antibiotic resistance genes, opportunistic bacteria, and induce strong population shifts. *Sci Total Environ* 559: 103–112, 2016.

Andrade LH, **Mendes FDS**, **Espindola JC**, **Amaral MCS**. Reuse of dairy wastewater treated by membrane bioreactor and nanofiltration: Technical and economic feasibility. *Brazilian J Chem Eng* 32: 735–747, 2015.

Arévalo J, **Ruiz LM**, **Parada-Albarracìn DM**, **Gonzàlez-Pérez J**, **Pérez B**, **Moreno B**, **Gómez MA**. Wastewater reuse after treatment by MBR. Microfiltration or ultrafiltration? *Desalination* 299: 22–27, 2012.

Árki P, **Hecker C**, **Tomandl G**, **Joseph Y**. Streaming potential properties of ceramic nanofiltration membranes – Importance of surface charge on the ion rejection. *Sep Purif Technol* 212: 660–669, 2019.

Arlos MJ, **Liang R**, **Li LCM**, **Fong C**, **Zhou NY**, **Ptacek CJ**, **Andrews SA**, **Servos MR**. Influence of methanol when used as a water-miscible carrier of pharmaceuticals in TiO_2 photocatalytic degradation experiments. *J Environ Chem Eng* 5: 4497–4504, 2017.

Arnal JM, **Sancho M**, **Verdú G**, **Lora J**, **Marín JF**, **Cháfer J**. Selection of the most suitable ultrafiltration membrane for water disinfection in developing countries. *Desalination* 168: 265–270, 2004.

Aschermann G, **Neubert L**, **Zietzschmann F**, **Jekel M**. Impact of different DOM size fractions on the desorption of organic micropollutants from activated carbon. *Water Res* 161: 161–170, 2019.

Athanasekou C, **Pedrosa M**, **Tsoufis T**, **Pastrana-Martínez LM**, **Romanos G**, **Favvas E**, **Katsaros F**, **Mitropoulos A**, **Psycharis V**, **Silva AMT**. Comparison of self-standing and supported graphene oxide membranes prepared by simple filtration: Gas and vapor separation, pore structure and stability. *J Memb Sci* 522: 303–315, 2017.

Athanasekou CP, **Morales-Torres S**, **Likodimos V**, **Romanos GE**, **Pastrana-Martinez LM**, **Falaras P**, **Dionysiou DD**, **Faria JL**, **Figueiredo JL**, **Silva AMT**. Prototype composite membranes of partially

reduced graphene oxide/TiO_2 for photocatalytic ultrafiltration water treatment under visible light. *Appl Catal B Environ* 158–159: 361–372, 2014.

Athanasekou CP, **Moustakas NG**, **Morales-Torres S**, **Pastrana-Martínez LM**, **Figueiredo JL**, **Faria JL**, **Silva AMT**, **Dona-Rodriguez JM**, **Romanos GE**, **Falaras P**. Ceramic photocatalytic membranes for water filtration under UV and visible light. *Appl Catal B Environ* 178: 12–19, 2015.

Athanasekou CP, **Romanos GE**, **Katsaros FK**, **Kordatos K**, **Likodimos V**, **Falaras P**. Very efficient composite titania membranes in hybrid ultrafiltration/photocatalysis water treatment processes. *J Memb Sci* 392–393: 192–203, 2012.

Athanasiou DA, **Romanos GE**, **Falaras P**. Design and optimization of a photocatalytic reactor for water purification combining optical fiber and membrane technologies. *Chem Eng J* 305: 92–103, 2016.

Autin O, **Hart J**, **Jarvis P**, **MacAdam J**, **Parsons SA**, **Jefferson B**. Environmental Comparison of UV/TiO_2 and UV/H_2O_2 processes in an annular photoreactor for removal of micropollutants: Influence of water parameters on metaldehyde removal, quantum yields and energy consumption. *Appl Catal B Environ* 139: 268–275, 2013.

Babić S, **Periša M**, **Škorić I**. Photolytic degradation of norfloxacin, enrofloxacin and ciprofloxacin in various aqueous media. *Chemosphere* 91: 1635–1642, 2013.

Barbero N, **Vione D**. Why Dyes Should Not Be Used to Test the Photocatalytic Activity of Semiconductor Oxides. *Environ Sci Technol* 50: 2130–2131, 2016.

Barbosa MO, **Moreira NFF**, **Ribeiro AR**, **Pereira MFR**. Occurrence and removal of organic micropollutants: An overview of the watch list of EU Decision 2015/495. *Water Res* 94: 257–279, 2016.

Becerra-Castro C, **Macedo G**, **Silva AMT**, **Manaia CM**, **Nunes OC**. Proteobacteria become predominant during regrowth after water disinfection. *Sci Total Environ* 573: 313–323, 2016.

Benito A, **Garcia G**, **Gonzalez-Olmos R**. Fouling reduction by UV-based pretreatment in hollow fiber ultrafiltration membranes for urban wastewater reuse. *J Memb Sci* 536: 141–147, 2017.

Benotti MJ, **Stanford BD**, **Wert EC**, **Snyder SA**. Evaluation of a photocatalytic reactor membrane pilot system for the removal of pharmaceuticals and endocrine disrupting compounds from water. *Water Res* 43: 1513–1522, 2009.

Bernabeu A, **Vercher RF**, **Santos-juanes L**, **Simón PJ**, **Lardín C**, **Martínez MA**, **Vicente JA**, **González R**, **Llosá C**, **Arques A**, **Amat AM**. Solar photocatalysis as a tertiary treatment to remove emerging pollutants from wastewater treatment plant effluents. *Catal Today* 161: 235–240, 2011.

Biancullo F, **Moreira NFF**, **Ribeiro AR**, **Manaia CM**, **Faria JL**, **Nunes OC**, **Castro-Silva SM**, **Silva AMT**. Heterogeneous photocatalysis using UVA-LEDs for the removal of antibiotics and antibiotic

resistant bacteria from urban wastewater treatment plant effluents. *Chem Eng J* 367: 304–313, 2019.

Byrne C, **Subramanian G**, **Pillai SC**. Recent advances in photocatalysis for environmental applications. *J Environ Chem Eng* : 3531–3555, 2018.

Cai Q, **Hu J**. Decomposition of sulfamethoxazole and trimethoprim by continuous UVA/LED/TiO_2 photocatalysis: Decomposition pathways, residual antibacterial activity and toxicity. *J Hazard Mater* 323: 527–536, 2017.

California code of regulations. Water Recycling criteria, 2000.

Carvalho IT, **Santos L**. Antibiotics in the aquatic environments: A review of the European scenario. *Environ Int* 94: 736–757, 2016.

Chiu TY, **James AE**. Sustainable flux enhancement in non-circular ceramic membranes on wastewater using the Fenton process. *J Memb Sci* 279: 347–353, 2006.

Choi H, **Antoniou MG**, **de la Cruz AA**, **Stathatos E**, **Dionysiou DD**. Photocatalytic TiO_2 films and membranes for the development of efficient wastewater treatment and reuse systems. *Desalination* 202: 199–206, 2007.

Choi H, **Zhang K**, **Dionysiou DD**, **Oerther DB**, **Sorial GA**. Effect of permeate flux and tangential flow on membrane fouling for wastewater treatment. *Sep Purif Technol* 45: 68–78, 2005.

Christou A, **Agüera A**, **Bayona JM**, **Cytryn E**, **Fotopoulos V**, **Manaia CM**, **Michael C**, **Revitt M**, **Schroder P**, **Fatta-Kassinos D**. The potential implications of reclaimed wastewater reuse for irrigation on the agricultural environment: The knowns and unknowns of the fate of antibiotics and antibiotic resistant bacteria and resistance genes - A review. *Water Res* 123: 448–467, 2017a.

Christou A, **Karaolia P**, **Hapeshi E**, **Michael C**, **Fatta-Kassinos D**. Long-term wastewater irrigation of vegetables in real agricultural systems: Concentration of pharmaceuticals in soil, uptake and bioaccumulation in tomato fruits and human health risk assessment. *Water Res* 109: 24–34, 2017b.

CLSI. M100S Performance Standards for Antimicrobial Susceptibility Testing, 2016.

De la Cruz N, **Esquius L**, **Grandjean D**, **Magnet A**, **Tungler A**, **de Alencastro LF**, **Pulgarín C**. Degradation of emergent contaminants by UV, UV/H_2O_2 and neutral photo-Fenton at pilot scale in a domestic wastewater treatment plant. *Water Res* 47: 5836–5845, 2013.

Delgado Diaz S, **Vera Peña L**, **González Cabrera E**, **Martínez Soto M**, **Vera Cabezas LM**, **Bravo Sánchez LR**. Effect of previous coagulation in direct ultrafiltration of primary settled municipal wastewater. *Desalination* 304: 41–48, 2012.

Diao Z-H, **Xu X-R**, **Jiang D**, **Liu J-J**, **Kong L-J**, **Li G**, **Zuo L-Z**, **Wu Q-H**. Simultaneous photocatalytic

Cr(VI) reduction and ciprofloxacin oxidation over TiO_2/Fe^0 composite under aerobic conditions: Performance, durability, pathway and mechanism. *Chem Eng J* 315: 167–176, 2017.

Dilaver M, **Hocaoğlu SM**, **Soydemir G**, **Dursun M**, **Keskinler B**, **Koyuncu İ**, **Ağtaş M**. Hot wastewater recovery by using ceramic membrane ultrafiltration and its reusability in textile industry. *J Clean Prod* 171: 220–233, 2018.

Directive. COMMISSION IMPLEMENTING DECISION (EU) 2015/495 of 20 March 2015 establishing a watch list of substances for Union-wide monitoring in the field of water policy pursuant to Directive 2008/105/EC of the European Parliament and of the Council [Online]. *Off JEur Union* L78: 40–43, 2015. https://eur-lex.europa.eu/legal-content/EN/TXT/PDF/?uri=CELEX:32015D0495&from=EN [8 Jul. 2018].

Directive. COMMISSION IMPLEMENTING DECISION (EU) 2018/840 of 5 June 2018 establishing a watch list of substances for Union-wide monitoring in the field of water policy pursuant to Directive 2008/105/EC of the European Parliament and of the Council and repealing Comm. *Off JEur Union* L141: 9–12, 2018.

Dolar D, **Košutić K**, **Ašperger D**. Influence of Adsorption of Pharmaceuticals onto RO/NF Membranes on Their Removal from Water. *Water, Air, Soil Pollut* 224: 1–13, 2013a.

Dolar D, **Košutić K**, **Periša M**, **Babić S**. Photolysis of enrofloxacin and removal of its photodegradation products from water by reverse osmosis and nanofiltration membranes. *Sep Purif Technol* 115: 1–8, 2013b.

Dunlop PSM, **Byrne JA**, **Manga N**, **Eggins BR**. The photocatalytic removal of bacterial pollutants from drinking water. *J Photochem Photobiol A Chem* 148: 355–363, 2002.

Dunlop PSM, **Ciavola M**, **Rizzo L**, **Mcdowell DA**, **Byrne JA**. Effect of photocatalysis on the transfer of antibiotic resistance genes in urban wastewater. *Catal Today* 240: 55–60, 2015.

Eckert H, **Bobeth M**, **Teixeira S**, **Kühn K**, **Cuniberti G**. Modeling of photocatalytic degradation of organic components in water by nanoparticle suspension. *Chem Eng J* 261: 67–75, 2015.

Eggen RIL, **Hollender J**, **Joss A**, **Scha M**, **Stamm C**. Reducing the Discharge of Micropollutants in the Aquatic Environment: The Benefits of Upgrading Wastewater Treatment Plants. *Environ Sci Technol* 48: 7683–7689, 2014.

Espíndola JC, **Szymański K**, **Cristóvão RO**, **Mendes A**, **Vilar VJP**, **Mozia S**. Performance of hybrid systems coupling advanced oxidation processes and ultrafiltration for oxytetracycline removal. *Catal Today* 328: 274–280, 2019.

European innovation partnership on water. Strategic implementation plan, 2012.

Even-Ezra I, **Beliavski M**, **Tarre S**, **Dosoretz C**, **Green M**. Chemical versus biological pretreatment for

membrane filtration of domestic wastewater. *Desalination* 272: 85–89, 2011.

Falaras P, Romanos G, Aloupogiannis P. Photocatalytic Purification Device, European Patent, EP2409954 (A1) , 2012.

Fatta-Kassinos D, **Vasquez MI**, **Kümmerer K**. Transformation products of pharmaceuticals in surface waters and wastewater formed during photolysis and advanced oxidation processes - Degradation, elucidation of byproducts and assessment of their biological potency. *Chemosphere* 85: 693–709, 2011.

Ferreira LC, **Lucas MS**, **Fernandes JR**, **Tavares PB**. Photocatalytic oxidation of Reactive Black 5 with UV-A LEDs. *J Environ Chem Eng* 4: 109–114, 2016.

Ferro G, **Fiorentino A**, **Alferez MC**, **Polo-Lòpez MI**, **Rizzo L**, **Fernàndez-Ibànez P**. Urban wastewater disinfection for agricultural reuse: Effect of solar driven AOPs in the inactivation of a multidrug resistant *E. coli* strain. *Appl Catal B Environ* 178: 65–73, 2015.

Ferro G, **Guarino F**, **Castiglione S**, **Rizzo L**. Antibiotic resistance spread potential in urban wastewater effluents disinfected by UV/H_2O_2 process. *Sci Total Environ* 560–561: 29–35, 2016.

Filloux E, **Gernjak W**, **Gallard H**, **Croue JP**. Investigating the relative contribution of colloidal and soluble fractions of secondary effluent organic matter to the irreversible fouling of MF and UF hollow fibre membranes. *Sep Purif Technol* 170: 109–115, 2016.

Fiorentino A, **Ferro G**, **Alferez MC**, **Polo-López MI**, **Fernández-Ibañez P**, **Rizzo L**. Inactivation and regrowth of multidrug resistant bacteria in urban wastewater after disinfection by solar-driven and chlorination processes. *J Photochem Photobiol B Biol* 148: 43–50, 2015.

Fischer K, **Grimm M**, **Meyers J**, **Dietrich C**, **Gläser R**, **Schulze A**. Photoactive micro filtration membranes via directed synthesis of TiO_2 nanoparticles on the polymer surface for removal of drugs from water. *J Memb Sci* 478: 49–57, 2015a.

Fischer K, **Kuhnert M**, **Glaser R**, **Schulze A**. Photocatalytic degradation and toxicity evaluation of diclofenac by nanotubular titanium dioxide – PES. *RSC Adv* 5: 16340–16348, 2015b.

Ganiyu SO, **Van Hullebusch ED**, **Cretin M**, **Esposito G**, **Oturan MA**. Coupling of membrane filtration and advanced oxidation processes for removal of pharmaceutical residues: A critical review. *Sep Purif Technol* 156: 891–914, 2015.

Garcia-Ivars J, **Durá-María J**, **Moscardó-Carreño C**, **Carbonell-Alcaina C**, **Alcaina-Miranda MI**, **Iborra-Clar MI**. Rejection of trace pharmaceutically active compounds present in municipal wastewaters using ceramic fine ultrafiltration membranes: Effect of feed solution pH and fouling phenomena. *Sep Purif Technol* 175: 58–71, 2017.

Ge L, **Chen J**, **Wei X**, **Zhang S**, **Qiao X**, **Cai X**, **Xie Q**. Aquatic Photochemistry of Fluoroquinolone

Antibiotics: Kinetics, Pathways, and Multivariate Effects of Main Water Constituents. *Environ Sci Technol* 44: 2400–2405, 2010.

Giannakis S, **Gamarra Vives FA**, **Grandjean D**, **Magnet A**, **De Alencastro LF**, **Pulgarin C**. Effect of advanced oxidation processes on the micropollutants and the effluent organic matter contained in municipal wastewater previously treated by three different secondary methods. *Water Res* 84: 295–306, 2015.

Goyne KW, **Chorover J**, **Kubicki JD**, **Zimmerman AR**, **Brantley SL**. Sorption of the antibiotic ofloxacin to mesoporous and nonporous alumina and silica. *J Colloid Interface Sci* 283: 160–170, 2005.

Guerra K, **Pellegrino J**, **Drewes JE**. Impact of operating conditions on permeate flux and process economics for cross flow ceramic membrane ultrafiltration of surface water. *Sep Purif Technol* 87: 47–53, 2012.

Guo M-T, **Yuan Q-B**, **Yang J**. Distinguishing Effects of Ultraviolet Exposure and Chlorination on the Horizontal Transfer of Antibiotic Resistance Genes in Municipal Wastewater. *Env Sci Pollut Res* 49: 5771–5778, 2015.

Guo M-T, **Yuan Q-B**, **Yang J**. Microbial selectivity of UV treatment on antibiotic-resistant heterotrophic bacteria in secondary effluents of a municipal wastewater treatment plant. *Water Res* 47: 6388–6394, 2013a.

Guo M-T, **Yuan Q-B**, **Yang J**. Ultraviolet reduction of erythromycin and tetracycline resistant heterotrophic bacteria and their resistance genes in municipal wastewater. *Chemosphere* 93: 2864–2868, 2013b.

Hamid K, **Sanciolo P**, **Gray S**, **Duke M**, **Muthukumaran S**. Impact of ozonation and biological activated carbon filtration on ceramic membrane fouling. *Water Res* 126: 308–318, 2017.

Hanamoto S, **Nakada N**, **Yamashita N**, **Tanaka H**. Modeling the Photochemical Attenuation of Down-the-Drain Chemicals during River Transport by Stochastic Methods and Field Measurements of Pharmaceuticals and Personal Care Products. *Environ Sci Technol* 47: 13571−13577, 2013.

Hapeshi E, **Achilleos A**, **Vasquez MI**, **Michael C**, **Xekoukoulotakis NP**, **Mantzavinos D**, **Kassinos D**. Drugs degrading photocatalytically: Kinetics and mechanisms of ofloxacin and atenolol removal on titania suspensions. *Water Res* 44: 1737–1746, 2010.

Hatat-Fraile M, **Liang R**, **Servos MR**, **Zhou YN**. Concurrent photocatalytic and filtration processes using doped TiO_2 coated quartz fiber membranes in a photocatalytic membrane reactor. *Chem Eng J* 330: 531–540, 2017.

Herrmann J. Heterogeneous photocatalysis: fundamentals and applications to the removal of various types of aqueous pollutants. *Catal Today* 53: 115–129, 1999.

Ho DP, **Vigneswaran S**, **Ngo HH**. Photocatalysis-membrane hybrid system for organic removal from biologically treated sewage effluent. *Sep Purif Technol* 68: 145–152, 2009.

Huertas RM, **Fraga MC**, **Crespo JG**, **Pereira VJ**. Sol-gel membrane modification for enhanced photocatalytic activity. *Sep Purif Technol* 180: 69–81, 2017.

Ibekwe AM, **Murinda SE**, **DebRoy C**, **Reddy GB**. Potential pathogens, antimicrobial patterns and genotypic diversity of *Escherichia coli* isolates in constructed wetlands treating swine wastewater. *FEMS Microbiol Ecol* 92: 1–14, 2016.

Issaoui M, **Limousy L**. Low-cost ceramic membranes: Synthesis, classifications, and applications. *Comptes Rendus Chim* 22: 175–187, 2019.

Jallouli N, **Pastrana-Martínez LM**, **Ribeiro AR**, **Moreira NFF**, **Faria JL**, **Hentati O**, **Silva AMT**, **Ksibi M**. Heterogeneous photocatalytic degradation of ibuprofen in ultrapure water, municipal and pharmaceutical industry wastewaters using a TiO_2/UV-LED system. *Chem Eng J* 334: 976–984, 2018.

Jeong K, **Lee D**, **Kim D**, **Ko S**. Effects of ozonation and coagulation on effluent organic matter characteristics and ultrafiltration membrane fouling. *J Environ Sci* 26: 1325–1331, 2014.

Ji J, **Liu F**, **Hashim NA**, **Abed MRM**, **Li K**. Poly(vinylidene fluoride) (PVDF) membranes for fluid separation. *React Funct Polym* 86: 134–153, 2015.

Jiang L, **Zhang X**, **Choo K-H**. Submerged microfiltration-catalysis hybrid reactor treatment: Photocatalytic inactivation of bacteria in secondary wastewater effluent. *Sep Purif Technol* 198: 87–92, 2018.

Jordá LSJ, **Martín MMB**, **Gómez EO**, **Reina AC**, **Sánchez IMR**, **López JLC**, **Pérez JAS**. Economic evaluation of the photo-Fenton process. Mineralization level and reaction time: The keys for increasing plant efficiency. *J Hazard Mater* 186: 1924–1929, 2011.

Kang G, **Cao Y**. Application and modification of poly(vinylidene fluoride) (PVDF) membranes – A review. *J Memb Sci* 463: 145–165, 2014.

Kappel C, **Kemperman AJB**, **Temmink H**, **Zwijnenburg A**, **Rijnaarts HHM**, **Nijmeijer K**. Impacts of NF concentrate recirculation on membrane performance in an integrated MBR and NF membrane process for wastewater treatment. *J Memb Sci* 453: 359–368, 2014.

Karaolia P, **Michael-Kordatou I**, **Hapeshi E**, **Drosou C**, **Bertakis Y**, **Christofilos D**, **Armatas GS**, **Sygellou L**, **Schwartz T**, **Xekoukoulotakis NP**, **Fatta-Kassinos D**. Removal of antibiotics, antibiotic-resistant bacteria and their associated genes by graphene-based TiO_2 composite photocatalysts under solar radiation in urban wastewaters. *Appl Catal B Environ* 224: 810–824, 2018.

Karkman A, **Do TT**, **Walsh F**, **Virta MPJ**. Antibiotic-Resistance Genes in Waste Water. *Trends*

Microbiol 26: 220–228, 2018.

Kaur A, **Umar A**, **Anderson WA**, **Kansal SK**. Facile synthesis of CdS/TiO_2 nanocomposite and their catalytic activity for ofloxacin degradation under visible illumination. *J Photochem Photobiol A Chem* 360: 34–43, 2018.

Kim HY, **Kim T-H**, **Yu S**. Photolytic degradation of sulfamethoxazole and trimethoprim using UV-A, UV-C and vacuum-UV (VUV). *J Environ Sci Heal Part A* 50: 292–300, 2015.

Kim I, **Yamashita N**, **Tanaka H**. Performance of UV and UV/H_2O_2 processes for the removal of pharmaceuticals detected in secondary effluent of a sewage treatment plant in Japan. *J Hazard Mater* 166: 1134–1140, 2009.

Kim J, **Davies SHR**, **Baumann MJ**, **Tarabara V V**, **Masten SJ**. Effect of ozone dosage and hydrodynamic conditions on the permeate flux in a hybrid ozonation-ceramic ultrafiltration system treating natural waters. *J Memb Sci* 311: 165–172, 2008.

Kim S, **Chu KH**, **Al-Hamadani YAJ**, **Park CM**, **Jang M**, **Kim D-H**, **Yu M**, **Heo J**, **Yoon Y**. Removal of contaminants of emerging concern by membranes in water and wastewater: A review. *Chem Eng J* 335: 896–914, 2018.

Klamerth N, **Miranda N**, **Malato S**, **Agüera A**, **Fernández-Alba AR**, **Maldonado MI**, **Coronado JM**. Degradation of emerging contaminants at low concentrations in MWTPs effluents with mild solar photo-Fenton and TiO_2. *Catal Today* 144: 124–130, 2009.

Laxma Reddy PV, **Kavitha B**, **Kumar Reddy PA**, **Kim K-H**. TiO_2-based photocatalytic disinfection of microbes in aqueous media: A review. *Environ Res* 154: 296–303, 2017.

Lee S-A, **Choo K-H**, **Lee C-H**, **Lee H-I**, **Hyeon T**, **Choi W**, **Kwon H-H**. Use of Ultrafiltration Membranes for the Separation of TiO_2 Photocatalysts in Drinking Water Treatment. *Ind Eng Chem Res* 40: 1712–1719, 2002.

Lee S, **Ihara M**, **Yamashita N**, **Tanaka H**. Improvement of virus removal by pilot-scale coagulation-ultrafiltration process for wastewater reclamation: Effect of optimization of pH in secondary effluent. *Water Res* 114: 23–30, 2017.

Lee Y, **Von Gunten U**. Advances in predicting organic contaminant abatement during ozonation of municipal wastewater effluent: reaction kinetics, transformation products, and changes of biological effects. *Environ Sci Water Res Technol* 2: 421–442, 2014.

Lehman SG, **Liu L**. Application of ceramic membranes with pre-ozonation for treatment of secondary wastewater effluent. *Water Res* 43: 2020–2028, 2009.

Li Puma G, **Brucato A**. Dimensionless analysis of slurry photocatalytic reactors using two-flux and six-

flux radiation absorption-scattering models. *Catal Today* 122: 78–90, 2007.

Li Puma G, **Khor JN**, **Brucato A**. Modeling of an Annular Photocatalytic Reactor for Water Purification: Oxidation of Pesticides. *Environ Sci Technol* 38: 3737–3745, 2004.

Li Puma G, **Puddu V**, **Tsang HK**, **Gora A**, **Toepfer B**. Photocatalytic oxidation of multicomponent mixtures of estrogens (estrone (E1), 17β-estradiol (E2), 17α-ethynylestradiol (EE2) and estriol (E3)) under UVA and UVC radiation: Photon absorption, quantum yields and rate constants independent of photon absorption. *Appl Catal B, Environ* 99: 388–397, 2010.

Li W, **Guo C**, **Su B**, **Xu J**. Photodegradation of four fluoroquinolone compounds by titanium dioxide under simulated solar light irradiation. *J Chem Technol Biotechnol* 87: 643–650, 2012.

Li W, **Ling G**, **Lei F**, **Li N**, **Peng W**, **Li K**, **Lu H**, **Hang F**, **Zhang Y**. Ceramic membrane fouling and cleaning during ultrafiltration of limed sugarcane juice. *Sep Purif Technol* 190: 9–24, 2018.

Liu L, **Liu Z**, **Bai H**, **Sun DD**. Concurrent filtration and solar photocatalytic disinfection/degradation using high-performance Ag/TiO_2 nanofiber membrane. *Water Res* 46: 1101–1112, 2012.

Liu P, **Zhang H**, **Feng Y**, **Yang F**, **Zhang J**. Removal of trace antibiotics from wastewater: A systematic study of nanofiltration combined with ozone-based advanced oxidation processes. *Chem Eng J* 240: 211–220, 2014.

Liu S-S, **Qu H-M**, **Yang D**, **Hu H**, **Liu W-L**, **Qiu Z-G**, **Hou A-M**, **Guo J**, **Li J-W**, **Shen Z-Q**, **Jin M**. Chlorine disinfection increases both intracellular and extracellular antibiotic resistance genes in a full-scale wastewater treatment plant. *Water Res* 136: 131–136, 2018.

Liu Y, **He X**, **Duan X**, **Fu Y**, **Dionysiou DD**. Photochemical degradation of oxytetracycline: Influence of pH and role of carbonate radical. *Chem Eng J* 276: 113–121, 2015.

Lu Z, **Chen F**, **He M**, **Song M**, **Ma Z**, **Shi W**, **Yan Y**, **Lan J**, **Li F**, **Xiao P**. Microwave synthesis of a novel magnetic imprinted TiO_2 photocatalyst with excellent transparency for selective photodegradation of enrofloxacin hydrochloride residues solution. *Chem Eng J* 249: 15–26, 2014.

Lu Z, **Zhou W**, **Huo P**, **Luo Y**, **He M**, **Pan J**, **Li C**, **Yan Y**. Performance of a novel TiO_2 photocatalyst based on the magnetic floating fly-ash cenospheres for the purpose of treating waste by waste. *Chem Eng J* 225: 34–42, 2013.

Mailler R, **Gasperi J**, **Coquet Y**, **Derome C**, **Buleté A**, **Vulliet E**, **Bressy A**, **Varrault G**, **Chebbo G**, **Rocher V**. Removal of emerging micropollutants from wastewater by activated carbon adsorption: Experimental study of different activated carbons and factors influencing the adsorption of micropollutants in wastewater. *J Environ Chem Eng* 4: 1102–1109, 2016.

Malato S, **Fernández-Ibáñez P**, **Maldonado MI**, **Blanco J**, **Gernjak W**. Decontamination and

disinfection of water by solar photocatalysis: Recent overview and trends. *Catal Today* 147: 1–59, 2009.

Manaia CM, **Rocha J**, **Scaccia N**, **Marano R**, **Radu E**, **Biancullo F**, **Cerqueira F**, **Fortunato G**, **Iakovides I**, **Zammit I**, **Kampouris I**, **Vaz-Moreira I**, **Nunes OC**. Antibiotic resistance in wastewater treatment plants: Tackling the black box. *Environ Int* 115: 312–324, 2018.

Martín-Sómer M, **Pablos C**, **van Grieken R**, **Marugán J**. Influence of Light Distribution on The Performance of Photocatalytic Reactors: LED vs Mercury Lamps. *Appl Catal B Environ* 215: 1–7, 2017.

Marugán J, **Grieken R Van**, **Pablos C**, **Satuf ML**, **Cassano AE**, **Alfano OM**. Rigorous kinetic modelling with explicit radiation absorption effects of the photocatalytic inactivation of bacteria in water using suspended titanium dioxide. *Appl Catal B Environ* 102: 404–416, 2011.

Matafonova G, **Batoev V**. Recent advances in application of UV light-emitting diodes for degrading organic pollutants in water through advanced oxidation processes: A review. *Water Res* 132: 177–189, 2018.

Mendret J, **Azais A**, **Favier T**, **Brosillon S**. Urban wastewater reuse using a coupling between nanofiltration and ozonation: Techno-economic assessment. *Chem Eng Res Des* 145: 19–28, 2019.

Michael-Kordatou I, **Iacovou M**, **Frontistis Z**, **Hapeshi E**, **Dionysiou DD**, **Fatta-Kassinos D**. Erythromycin oxidation and ERY-resistant *Escherichia coli* inactivation in urban wastewater by sulfate radical-based oxidation process under UV-C irradiation. *Water Res* 85: 346–358, 2015.

Michael-Kordatou I, **Karaolia P**, **Fatta-Kassinos D**. The role of operating parameters and oxidative damage mechanisms of Advanced Chemical Oxidation Processes in the combat against antibiotic-resistant bacteria and resistance genes present in urban wastewater. *Water Res* 129: 208–230, 2018.

Michael I, **Hapeshi E**, **Michael C**, **Varela AR**, **Kyriakou S**, **Manaia CM**, **Fatta-Kassinos D**. Solar photo-Fenton process on the abatement of antibiotics at a pilot scale: Degradation kinetics, ecotoxicity and phytotoxicity assessment and removal of antibiotic resistant enterococci. *Water Res* 46: 5621–5634, 2012a.

Michael I, **Rizzo L**, **Mcardell CS**, **Manaia CM**, **Merlin C**, **Schwartz T**, **Dagot C**, **Fatta-Kassinos D**. Urban wastewater treatment plants as hotspots for the release of antibiotics in the environment: A review. *Water Res* 47: 957–995, 2012b.

Miralles-Cuevas S, **Oller I**, **Agüera A**, **Sánchez Pérez JA**, **Malato S**. Strategies for reducing cost by using solar photo-Fenton treatment combined with nanofiltration to remove microcontaminants in real municipal effluents: Toxicity and economic assessment. *Chem Eng J* 318: 161–170, 2017.

Miranda-García N, **Suárez S**, **Sánchez B**, **Coronado JM**, **Malato S**, **Maldonado MI**. Photocatalytic degradation of emerging contaminants in municipal wastewater treatment plant effluents using immobilized TiO_2 in a solar pilot plant. *Appl Catal B Environ* 103: 294–301, 2011.

Molinari R, **Lavorato C**, **Argurio P**. Recent progress of photocatalytic membrane reactors in water treatment and in synthesis of organic compounds. A review. *Catal Today* 281: 144–164, 2017.

Morawski AW, **Mozia S**. Humic acids removal in a photocatalytic membrane reactor with a ceramic UF membrane. *Chem Eng J* 305: 19–27, 2016.

Moreira NFF, **Narciso-da-Rocha C**, **M. Inmaculada Polo-López**, **Pastrana-Martínez LM**, **Faria JL**, **Manaia CM**, **Fernández-Ibáñez P**, **Nunes OC**, **Adrián M.T. Silva**. Solar treatment (H_2O_2, TiO_2-P25 and GO-TiO_2 photocatalysis, photo-Fenton) of organic micropollutants, human pathogen indicators, antibiotic resistant bacteria and related genes in urban wastewater. *Water Res* 135: 195–206, 2018.

Moreira NFF, **Orge CA**, **Ribeiro AR**, **Faria JL**, **Nunes OC**, **Pereira MFR**, **Silva AMT**. Fast mineralization and detoxification of amoxicillin and diclofenac by photocatalytic ozonation and application to an urban wastewater. *Water Res* 87: 87–96, 2015.

Moreira NFF, **Sousa JM**, **Macedo G**, **Ribeiro AR**, **Barreiros L**, **Pedrosa M**, **Faria JL**, **Pereira MFR**, **Castro-Silva S**, **Segundo MA**, **Manaia CM**, **Nunes OC**, **Silva AMT**. Photocatalytic ozonation of urban wastewater and surface water using immobilized TiO_2 with LEDs: Micropollutants, antibiotic resistance genes and estrogenic activity. *Water Res* 94: 10–22, 2016.

Moustakas NG, **Katsaros FK**, **Kontos AG**, **Romanos GE**, **Dionysiou DD**, **Falaras P**. Visible light active TiO_2 photocatalytic filtration membranes with improved permeability and low energy consumption. *Catal Today* 224: 56–69, 2014.

Mozia S, **Darowna D**, **Szymański K**, **Grondzewska S**, **Borchert K**, **Wróbel R**, **Morawski AW**. Performance of two photocatalytic membrane reactors for treatment of primary and secondary effluents. *Catal Today* 236: 135–145, 2014.

Mozia S, **Darowna D**, **Wróbel R**, **Morawski AW**. A study on the stability of polyethersulfone ultrafiltration membranes in a photocatalytic membrane reactor. *J Memb Sci* 495: 176–186, 2015.

Mozia S, **Morawski AW**, **Toyoda M**, **Tsumura T**. Effect of process parameters on photodegradation of Acid Yellow 36 in a hybrid photocatalysis–membrane distillation system. *Chem Eng J* 150: 152–159, 2009.

Mozia S, **Toyoda M**, **Inagaki M**, **Tryba B**, **Morawski AW**. Application of carbon-coated TiO_2 for decomposition of methylene blue in a photocatalytic membrane reactor. *J Hazard Mater* 140: 369–375, 2007.

Murić A, **Petrinić I**, **Christensen ML**. Comparison of ceramic and polymeric ultrafiltration membranes for treating wastewater from metalworking industry. *Chem Eng J* 255: 403–410, 2014.

Naraginti S, **Yu Y-Y**, **Fang Z**, **Yong Y-C**. Visible light degradation of macrolide antibiotic azithromycin by novel ZrO2/Ag@TiO_2 nanorod composite: Transformation pathways and toxicity evaluation. *Process*

Saf Environ Prot 125: 39–49, 2019.

Novo A, **Andre S**, **Viana P**, **Nunes OC**, **Manaia M**. Antibiotic resistance, antimicrobial residues and bacterial community composition in urban wastewater. *Water Res* 47: 1875–1887, 2013.

Papageorgiou SK, **Katsaros FK**, **Favvas EP**, **Romanos GE**, **Athanasekou CP**, **Beltsios KG**, **Tzialla OI**, **Falaras P**. Alginate fibers as photocatalyst immobilizing agents applied in hybrid photocatalytic/ultrafiltration water treatment processes. *Water Res* 46: 1858–1872, 2012.

Pastrana-Martínez LM, **Morales-Torres S**, **Figueiredo JL**, **Faria JL**, **Silva a MT**. Graphene oxide based ultrafiltration membranes for photocatalytic degradation of organic pollutants in salty water. *Water Res* 77: 179–190, 2015.

Pastrana-Martinez LM, **Morales-Torres S**, **Likodimos V**, **Figueiredo JL**, **Faria JL**, **Falaras P**, **Silva AMT**. Advanced nanostructured photocatalysts based on reduced graphene oxide-TiO_2 composites for degradation of diphenhydramine pharmaceutical and methyl orange dye. *Appl Catal B Environ* 123–124: 241–256, 2012.

Prieto-Rodriguez L, **Miralles-Cuevas S**, **Oller I**, **Agüera A**, **Puma GL**, **Malato S**. Treatment of emerging contaminants in wastewater treatment plants (WWTP) effluents by solar photocatalysis using low TiO_2 concentrations. *J Hazard Mater* 211–212: 131–137, 2012.

Ramasundaram S, **Na H**, **Guen K**, **Lee J**, **Jin K**, **Won S**. Titanium dioxide nanofibers integrated stainless steel filter for photocatalytic degradation of pharmaceutical compounds. *J Hazard Mater* 258–259: 124–132, 2013.

Ren S, **Boo C**, **Guo N**, **Wang S**, **Elimelech M**, **Wang Y**. Photocatalytic Reactive Ultrafiltration Membrane for Removal of Antibiotic Resistant Bacteria and Antibiotic Resistance Genes from Wastewater Effluent. *Environ Sci Technol* 52: 8666–8673, 2018.

Ribeiro AR, **Moreira NFF**, **Li Puma G**, **Silva AMT**. Impact of water matrix on the removal of micropollutants by advanced oxidation technologies. *Chem. Eng. J.* 363: 155–173, 2019.

Ribeiro AR, **Nunes OC**, **Pereira MFR**, **Silva AMT**. An overview on the advanced oxidation processes applied for the treatment of water pollutants defined in the recently launched Directive 2013/39/EU. *Environ Int* 75: 33–51, 2015a.

Ribeiro AR, **Pedrosa M**, **Moreira NFF**, **Pereira MFR**, **Silva AMT**. Environmental friendly method for urban wastewater monitoring of micropollutants defined in the Directive 2013/39/EU and Decision 2015/495/EU. *J Chromatogr A* 1418: 140–149, 2015b.

Richardson SD, **Ternes TA**. Water Analysis: Emerging Contaminants and Current Issues. *Anal Chem* 90: 398–428, 2018.

Rizzo L, **Ferro G**, **Manaia CM**. Wastewater Disinfection by Solar Heterogeneous Photocatalysis: Effect on Tetracycline Resistant/Sensitive *Enterococcus* strains. *Glob NEST J* 16: 455–462, 2014a.

Rizzo L, **Fiorentino A**, **Anselmo A**. Effect of solar radiation on multidrug resistant *E. coli* strains and antibiotic mixture photodegradation in wastewater polluted stream. *Sci Total Environ* 427–428: 263–268, 2012.

Rizzo L, **Fiorentino A**, **Anselmo A**. Advanced treatment of urban wastewater by UV radiation: Effect on antibiotics and antibiotic-resistant *E. coli* strains. *Chemosphere* 92: 171–176, 2013a.

Rizzo L, **Malato S**, **Antakyali D**, **Beretsou VG**, **Đolić MB**, **Gernjak W**, **Heath E**, **Ivancev-Tumbas I**, **Karaolia P**, **Lado Ribeiro AR**, **Mascolo G**, **McArdell CS**, **Schaar H**, **Silva AMT**, **Fatta-Kassinos D**. Consolidated vs new advanced treatment methods for the removal of contaminants of emerging concern from urban wastewater. *Sci Total Environ* 655: 986–1008, 2019.

Rizzo L, **Manaia C**, **Merlin C**, **Schwartz T**, **Dagot C**, **Ploy MC**, **Michael I**, **Fatta-Kassinos D**. Urban wastewater treatment plants as hotspots for antibiotic resistant bacteria and genes spread into the environment: A review. *Sci Total Env* 447: 345–360, 2013b.

Rizzo L, **Della Sala A**, **Fiorentino A**, **Li Puma G**. Disinfection of urban wastewater by solar driven and UV lamp - TiO_2 photocatalysis: Effect on a multi drug resistant *Escherichia coli* strain. *Water Res* 53: 145–152, 2014b.

Rizzo L, **Sannino D**, **Vaiano V**, **Sacco O**, **Scarpa A**, **Pietrogiacomi D**. Effect of solar simulated N-doped TiO_2 photocatalysis on the inactivation and antibiotic resistance of an *E. coli* strain in biologically treated urban wastewater. *Appl Catal B Environ* 144: 369–378, 2014c.

Rodríguez EM, **Márquez G**, **Tena M**, **Álvarez PM**, **Beltrán FJ**. Determination of main species involved in the first steps of TiO_2 photocatalytic degradation of organics with the use of scavengers: The case of ofloxacin. *Appl Catal B Environ* 178: 44–53, 2015.

Romanos GE, **Athanasekou CP**, **Katsaros FK**, **Kanellopoulos NK**, **Dionysiou DD**, **Likodimos V**, **Falaras P**. Double-side active TiO_2-modified nanofiltration membranes in continuous flow photocatalytic reactors for effective water purification. *J Hazard Mater* 211–212: 304–316, 2012.

Romanos GE, **Athanasekou CP**, **Likodimos V**, **Aloupogiannis P**, **Falaras P**. Hybrid Ultrafiltration/Photocatalytic Membranes for Efficient Water Treatment. *Ind Eng Chem Res* 52: 13938–13947, 2013.

Ryan CC, **Tan DT**, **Arnold WA**. Direct and indirect photolysis of sulfamethoxazole and trimethoprim in wastewater treatment plant effluent. *Water Res* 45: 1280–1286, 2010.

Salaices M, **Serrano B**, **De Lasa HI**. Experimental evaluation of photon absorption in an aqueous TiO_2 slurry reactor. *Chem Eng J* 90: 219–229, 2002.

Satuf ML, **Brandi RJ**, **Cassano AE**, **Alfano OM**. Experimental Method to Evaluate the Optical Properties of Aqueous Titanium Dioxide Suspensions. *Ind Eng Chem Res* 44: 6643–6649, 2005.

Sayadi MH, **Sobhani S**, **Shekari H**. Photocatalytic degradation of azithromycin using GO@Fe_3O_4/ZnO/SnO_2 nanocomposites. *J Clean Prod* 232: 127–136, 2019.

Shaham-Waldmann N, **Paz Y**. Away from TiO_2: A critical minireview on the developing of new photocatalysts for degradation of contaminants in water. *Mater Sci Semicond Process* 42: 72–80, 2016.

Shi X, **Tal G**, **Hankins NP**, **Gitis V**. Fouling and cleaning of ultrafiltration membranes: A review. *J Water Process Eng* 1: 121–138, 2014.

Sirtori C, **Agu A**, **Gernjak W**, **Malato S**. Effect of water-matrix composition on Trimethoprim solar photodegradation kinetics and pathways. *Water Res* 44: 2735–2744, 2010.

Sood S, **Mehta SK**, **Sinha ASK**, **Kansal SK**. Bi_2O_3/TiO_2 heterostructures: Synthesis, characterization and their application in solar light mediated photocatalyzed degradation of an antibiotic, ofloxacin. *Chem Eng J* 290: 45–52, 2016.

Sousa JCG, **Ribeiro AR**, **Barbosa MO**, **Pereira MFR**, **Silva AMT**. A review on environmental monitoring of water organic pollutants identified by EU guidelines. *J Hazard Mater* 344: 146–162, 2018.

Sousa JM, **Pedrosa M**, **Becerra-Castro C**, **Castro-silva S**, **Pereira MFR**, **Silva AMT**, **Nunes OC**, **Manaia CM**. Ozonation and UV254 nm radiation for the removal of microorganisms and antibiotic resistance genes from urban wastewater. *J Hazard Mater* 323: 434–441, 2017.

Sousa MA, **Gonçalves C**, **Vilar VJP**, **Boaventura RAR**, **Alpendurada MF**. Suspended TiO_2-assisted photocatalytic degradation of emerging contaminants in a municipal WWTP effluent using a solar pilot plant with CPCs. *Chem Eng J* 198–199: 301–309, 2012.

Szymański K, **Morawski AW**, **Mozia S**. Effectiveness of treatment of secondary effluent from a municipal wastewater treatment plant in a photocatalytic membrane reactor and hybrid UV/H_2O_2 – ultrafiltration system. *Chem Eng Process - Process Intensif* 125: 318–324, 2018.

Thayanukul P, **Kurisu F**, **Kasuga I**, **Furumai H**. Evaluation of microbial regrowth potential by assimilable organic carbon in various reclaimed water and distribution systems. *Water Res* 47: 225–232, 2013.

Tong L, **Eichhorn P**, **Pérez S**, **Wang Y**, **Barceló D**. Photodegradation of azithromycin in various aqueous systems under simulated and natural solar radiation: Kinetics and identification of photoproducts. *Chemosphere* 83: 340–348, 2011.

Tsai T-M, **Chang H-H**, **Chang K-C**, **Liu Y-L**, **Tseng C-C**. A comparative study of the bactericidal effect of photocatalytic oxidation by TiO_2 on antibiotic-resistant and antibiotic-sensitive bacteria. *J Chem*

Technol Biotechnol 85: 1642–1653, 2010.

Urtiaga AM, **Pérez G**, **Ibáñez R**, **Ortiz I**. Removal of pharmaceuticals from a WWTP secondary effluent by ultrafiltration/reverse osmosis followed by electrochemical oxidation of the RO concentrate. *Desalination* 331: 26–34, 2013.

Vaiano V, **Sacco O**, **Sannino D**, **Ciambelli P**. Photocatalytic removal of spiramycin from wastewater under visible light with N-doped TiO_2 photocatalysts. *Chem Eng J* 261: 3–8, 2015.

Venieri D, **Bikouvaraki M**, **Binas V**, **Zachopoulos A**, **Kiriakidis G**, **Mantzavinos D**. Solar photocatalysis as disinfection technique: Inactivation of *Klebsiella pneumoniae* in sewage and investigation of changes in antibiotic resistance profile. *J Environ Manage* 195: 140–147, 2017.

Verlicchi P, **Al Aukidy M**, **Zambello E**. Occurrence of pharmaceutical compounds in urban wastewater: Removal, mass load and environmental risk after a secondary treatment-A review. *Sci Total Environ* 429: 123–155, 2012.

Vione D, **Feitosa-Felizzola J**, **Minero C**, **Chiron S**. Phototransformation of selected human-used macrolides in surface water: Kinetics, model predictions and degradation pathways. *Water Res* 43: 1959–1967, 2009.

Wammer KH, **Korte AR**, **Lundeen RA**, **Sundberg JE**, **Mcneill K**, **Arnold WA**. Direct photochemistry of three fluoroquinolone antibacterials: Norfloxacin, ofloxacin, and enrofloxacin. *Water Res* 47: 439–448, 2013.

Wang Q, **Li P**, **Zhang Z, Jiang C**, **Zuojiao K**, **Liu J**, **Wang Y**. Kinetics and mechanism insights into the photodegradation of tetracycline hydrochloride and ofloxacin mixed antibiotics with the flower-like $BiOCl/TiO_2$ heterojunction. *J Photochem Photobiol A Chem* 378: 114–124, 2019a.

Wang G, **Wang D**, **Dong X**, **Zhang X**, **Ma H**. Sodium persulfate based PVDF membrane for concurrent advanced oxidation and ultrafiltration of ofloxacin in water. *Chem Eng J* 315: 509–515, 2017.

Wang X, **Ma B**, **Bai Y**, **Lan H**, **Liu H**, **Qu J**. The effects of hydrogen peroxide pre-oxidation on ultrafiltration membrane biofouling alleviation in drinking water treatment. *J Environ Sci* 73: 117–126, 2018.

Wang Y-H, **Wu Y-H**, **Tong X**, **Yu T**, **Peng L**, **Bai Y**, **Zhao X-H**, **Huo Z-Y**, **Ikuno N**, **Hu H-Y**. Chlorine disinfection significantly aggravated the biofouling of reverse osmosis membrane used for municipal wastewater reclamation. *Water Res* 154: 246–257, 2019b.

van Grieken R, **Marugán J**, **Pablos C**, **Furones L**, **López A**. Comparison between the photocatalytic inactivation of Gram-positive *E. faecalis* and Gram-negative *E. coli* faecal contamination indicator microorganisms. *Appl Catal B Environ* 100: 212–220, 2010.

van Wieren EM, **Seymour MD**, **Peterson JW**. Interaction of the fluoroquinolone antibiotic, ofloxacin, with titanium oxide nanoparticles in water: Adsorption and breakdown. *Sci Total Environ* 441: 1–9, 2012.

WHO. Guidelines for the safe use of wastewater in agriculture, 2006.

Winter J, **Uhl W**, **Bérubé P**. Integrated oxidation membrane filtration process e NOM rejection and membrane fouling. *Water Res* 104: 418–424, 2016.

Xie R, **Meng X**, **Sun P**, **Niu J**, **Jiang W**, **Bottomley L**, **Li D**, **Chen Y**, **Crittenden J**. Electrochemical oxidation of ofloxacin using a TiO_2-based SnO_2-Sb/polytetrafluoroethylene resin-PbO_2 electrode: Reaction kinetics and mass transfer impact. *Appl Catal B Environ* 203: 515–525, 2017.

Xing X, **Du Z**, **Zhuang J**, **Wang D**. Removal of ciprofloxacin from water by nitrogen doped TiO_2 immobilized on glass spheres: Rapid screening of degradation products. *J Photochem Photobiol A Chem* 359: 23–32, 2018.

Xiong P, **Hu J**. Inactivation/reactivation of antibiotic-resistant bacteria by a novel UVA/LED/TiO_2 system. *Water Res* 47: 4547–4555, 2013.

Xiong P, **Hu J**. Decomposition of acetaminophen (Ace) using TiO_2/UVA/LED system. *Catal Today* 282: 48–56, 2017.

Yan S, **Yao B**, **Lian L**, **Lu X**, **Snyder SA**, **Li R**, **Song W**. Development of Fluorescence Surrogates to Predict the Photochemical Transformation of Pharmaceuticals in Wastewater Effluents. *Environ Sci Technol* 51: 2738–2747, 2017.

Yu W, **Graham NJD**, **Fowler GD**. Coagulation and oxidation for controlling ultrafiltration membrane fouling in drinking water treatment: Application of ozone at low dose in submerged membrane tank. *Water Res* 95: 1–10, 2016.

Zhang H, **Quan X**, **Chen S**, **Zhao H**, **Zhao Y**. Fabrication of photocatalytic membrane and evaluation its efficiency in removal of organic pollutants from water. *Sep Purif Technol* 50: 147–155, 2006.

Zhang X, **Fan L**, **Roddick FA**. Effect of feedwater pre-treatment using UV/H_2O_2 for mitigating the fouling of a ceramic MF membrane caused by soluble algal organic matter. *J Memb Sci* 493: 683–689, 2015.

Zhao X, **Hu H-Y**, **Yu T**, **Su C**, **Jiang H**, **Liu S**. Effect of different molecular weight organic components on the increase of microbial growth potential of secondary effluent by ozonation. *J Environ Sci* 26: 2190–2197, 2014.

Zhao Y-X, **Li P**, **Li R-H**, **Li X-Y**. Direct filtration for the treatment of the coagulated domestic sewage using flat-sheet ceramic membranes. *Chemosphere* 223: 383–390, 2019.

Zheng J, **Su C**, **Zhou J**, **Xu L**, **Qian Y**, **Chen H**. Effects and mechanisms of ultraviolet, chlorination, and ozone disinfection on antibiotic resistance genes in secondary effluents of municipal wastewater treatment plants. *Chem Eng J* 317: 309–316, 2017.

Zheng X, **Ernst M**, **Jekel M**. Identification and quantification of major organic foulants in treated domestic wastewater affecting filterability in dead-end ultrafiltration. *Water Res* 43: 238–244, 2009.

Zheng X, **Khan MT**, **Croué JP**. Contribution of effluent organic matter (EfOM) to ultrafiltration (UF) membrane fouling: Isolation, characterization, and fouling effect of EfOM fractions. *Water Res* 65: 414–424, 2014.

Zhuang Y, **Ren H**, **Geng J**, **Zhang Y**. Inactivation of antibiotic resistance genes in municipal wastewater by chlorination, ultraviolet, and ozonation disinfection. *Env Sci Pollut Res* 22: 7037–7044, 2015.

List of publications

Biancullo F, Moreira NFF, Ribeiro AR, Manaia CM, Faria JL, Nunes OC, Castro-Silva SM, Silva AMT. Heterogeneous photocatalysis using UVA-LEDs for the removal of antibiotics and antibiotic resistant bacteria from urban wastewater treatment plant effluents. Chem Eng J 367: 304–313, 2019.

Manaia CM, Rocha J, Scaccia N, Marano R, Radu E, **Biancullo F**, Cerqueira F, Fortunato G, Iakovides I, Zammit I, Kampouris I, Vaz-Moreira I, Nunes OC. Antibiotic resistance in wastewater treatment plants: Tackling the black box. Environ Int 115: 312–324, 2018.

Biancullo F, Graca C, Silva J, Ribeiro AR, Manaia CM, Faria JL, Nunes OC, Castro-Silva SM, Silva AMT. Photocatalytic ultrafiltration membrane reactor using UVA-LEDs for the removal of fluoroquinolones, bacteria and antibiotic resistance genes from urban wastewater. In preparation.

Other outputs

Biancullo F, Moreira NFF, Ribeiro AR, Faria JL, Castro-Silva SM, Silva AMT. Removal of Organic Micropollutants in Urban Wastewater by using UV-LEDs – Heterogeneous Photocatalysis. Poster at EMEC18, 26-29 November 2017, Porto (Portugal).

Biancullo F, Moreira NFF, Ribeiro AR, Faria JL, Castro-Silva SM, Nunes OC, Silva AMT. UVA-LEDs Heterogeneous Photocatalysis for Removal of Antibiotics and Antibiotic Resistant Bacteria in Municipal Wastewater. Poster at SPEA10, 04-08 June 2018, Almeria (Spain).

Biancullo F, Moreira NFF, Ribeiro AR, Castro-Silva SM, Nunes OC, Faria JL, Silva AMT. Antibiotics and Antibiotic Resistant Bacteria Removal in Urban Wastewater by Heterogeneous Photocatalysis using UVA-LEDs. Oral presentation at XENOWAC II, 10-12 October 2018, Limassol (Cyprus). Awarded as best science communication in science slam contest.